Nonlinear Effects in Elastic Rayleigh Waves

Thesis by

Russina Sgoureva-Philippakos

In Partial Fulfillment of the Requirements

for the Degree of

Doctor of Philosophy

California Institute of Technology

Pasadena, California

1998

(Submitted May 19, 1998)

Acknowledgements

This thesis would not have been possible without Professor Whitham's guidance and support. I am indebted to him for introducing me to the problem of nonlinear Rayleigh waves, and for the insightful suggestions and encouraging supervision, which helped me immensely during the research and preparation of this thesis.

I am greatful to my colleagues Michael Louie, Philip Love, and Mark Meloon for their valuable assistance in the typesetting of this document.

Finally, I would like to thank the faculty, staff, and students of the Applied Mathematics Department for providing me with a very stimulating and supportive academic environment during my graduate and undergraduate studies at Caltech.

Abstract

The propagation of nonlinear surface elastic waves, or Rayleigh waves, is studied in the case of a harmonic elastic material. In the linear theory Rayleigh waves are non-dispersive, and linear profiles of any shape are acceptable. When nonlinear effects are taken into consideration, special restrictions on the permissible wave profiles need to be imposed. Parker and Talbot investigated the possibility of steady-shape profiles within the second-order approximation of the Rayleigh problem. They established numerically the existence of several families of periodic Rayleigh waves of a permanent form, which may move at phase speeds that differ from the linear Rayleigh wave velocity or at speeds that equal the Rayleigh wave velocity. The distinguishing feature of the Parker-Talbot numerical solutions is that plots of the surface horizontal displacement have singularities which resemble finite corners.

The goal of our work has been to gain an understanding of the Rayleigh wave solution structure, particularly in the context of the second-order theory. We propose that there exist infinite families of steady-profile periodic solutions moving at speeds equal to or differing from the linear Rayleigh wave velocity. We present various examples of such solutions, and discuss a simple numerical procedure for generating any member of the infinite families of solutions. The nature of the singularities of the presented numerical profiles is examined, and empirical evidence is provided that the surface horizontal displacements display fractional singularity behavior rather than the corner-like behaviour of the corresponding Parker-Talbot profiles. The numerical approach is then modified to accommodate the proposed singular behavior.

We use a solvability condition of a Fredholm type to perform a local study of the surface displacement singularities of Rayleigh waves on an infinite interval.

The hypothesis of the existence of fractional singularities in the surface horizontal displacement is tested using two different approximations of the solvability condition. We show that within the second-order theory the steady-profile Rayleigh waves can have only one type of fractional singularity behavior, whether they move at the linear Rayleigh wave velocity or not.

Contents

List of Figures

List of Tables

Chapter 1 Introduction

The Rayleigh waves considered here are waves which propagate along the free surface of an elastic half-space. They are characterized by a high level of energy concentration in the surface layer of the elastic material, and by a rapid exponential decay of the elastic disturbances as one moves away from the free surface of the solid.

One of the most important applications of Rayleigh waves is in modeling earthquakes, since surface elastic waves represent one of the most destructive high-energy components of seismic disturbances. Rayleigh waves are also of important use in determining the location of various geophysical phenomena, such as earthquakes and underground nuclear explosions, as well as in nondestructive testing of the constituent properties of the Earth. Until recently, nonlinear effects were not generally included in seismic wave propagation studies. However, new laboratory and experimental observations of seismic wave propagation, such as the ones discussed in [1], reveal the importance of nonlinear effects in Rayleigh waves.

The study of nonlinear Rayleigh waves has also become increasingly important in the development of surface acoustic wave devices used for signal processing. This particular application was prompted by the nonlinear signal processing capabilities of such devices, for example parametric amplification, convolution, etc.

Nonlinear Rayleigh waves represent a very intriguing physical system due to the complex structure of the boundary value problem which describes them. The governing partial differential equations are coupled and highly nonlinear, and so are the boundary conditions. In the linear version of the problem the differential equations uncouple to a set of two stretched Laplace equations, while the boundary conditions remain coupled. The resulting linear horizontal and vertical displacements $\xi(x, y)$

and $\eta(x, y)$ can be shown to be of the following form:

$$\begin{aligned} \xi(x, y) &= \frac{1}{1-\sigma^2}\big\{E(x, py) - \sigma^2 E(x, sy)\big\}, \\ \eta(x, y) &= \frac{1}{1-\sigma^2}\big\{-pN(x, py) + \frac{\sigma^2}{s}N(x, sy)\big\}, \end{aligned} \tag{1.1}$$

where $E(x, y)$ and $N(x, y)$ are conjugate harmonic functions, and p, s and σ are constants which depend on the properties of the elastic media, as well as on the velocity of the linear Rayleigh waves. The derivation of (1.1), using the linear differential equations and boundary conditions, is discussed in Section 2.2.2. Notably, it turns out that the linear Rayleigh wave problem has only non-dispersive solutions which propagate with constant velocity $c = c_R$. The velocity c_R is the only physically acceptable real positive solution of an algebraic equation, and it only depends on the elastic properties of the solid material.

Several aspects of the presented formulas for $\xi(x, y)$ and $\eta(x, y)$ deserve further consideration. Each of the elastic displacements ξ and η is expressed in terms of a linear combination of the same function stretched in two different ways in y. Due to the presence of two different stretchings and to the complex structure of the nonlinear Rayleigh wave equations, any analysis performed using (1.1) with $y > 0$ ends up being very complicated. However, these formulas simplify significantly on the surface of the elastic material when $y = 0$. This suggests that a possible way to tackle the nonlinear boundary value problem is to reduce it to a set of equations valid on the surface of the half-space by getting rid of the dependence on y.

This approach was first used by Kalyanasundaram et al. in [11], where the method of multiple scales was applied to the Rayleigh wave problem for an isotropic material. By imposing a solvability condition on the second-order equations, Kalyanasundaram et al. obtained an infinite set of coupled first-order PDEs for the evolution of the Fourier coefficients of a periodic profile. They used the resulting equations to study the evolution of the first two or three harmonics of a periodic Rayleigh wave.

Parker and Talbot in [16] were the first to use a solvability condition type of argument in a detailed study of steady-profile periodic Rayleigh waves. Zabolotskaya et al. [20] later derived the coupled-amplitude evolution equations using the Hamiltonian formalism, while in his later publications Parker et al. [15], [17], as well as Ionov [7], [8], employed Fourier transforms along with a solvability condition to the same end.

It is also very significant that the functions $E(x,y)$ and $N(x,y)$ in (1.1) are related to the surface horizontal displacament $\xi(x,0) = \xi_0(x)$ through the following Poisson-type formula:

$$E(x,y) + iN(x,y) = \frac{1}{\pi i} \int_{-\infty}^{\infty} \frac{\xi_0(w)}{w - (x+iy)}\, dw, \tag{1.2}$$

with $E(x,0) = \xi_0(x)$. This relation implies that as long as the $\xi_0(x)$ profile is known, the full linear Rayleigh wave solution can be reconstructed within the entire elastic material. Therefore, each linear Rayleigh wave solution is uniquely determined by its horizontal surface displacement. Linear theory does not impose any restrictions on the shapes of the displacements $\xi_0(x)$, and therefore any linear Rayleigh wave profile is acceptable. Since linear surface elastic waves are also non-dispersive, any displacement profile will travel at $c = c_R$ without distortion or attenuation. Thus, within the realms of linear theory, Rayleigh waves of any possible shape are allowed to exist.

This does not prove to be the case when nonlinear effects are taken into consideration. When steady shape profiles are considered, Parker et al. in [15], [16], and [17], show that the second-order equations dictate that only linear displacements of certain special shapes can be used as first-order terms in a perturbation expansion of the nonlinear solutions.

The most detailed study of steady-profile Rayleigh waves was performed by Parker and Talbot in [16], and it contributed greatly to the understanding of the

importance of nonlinear effects in modeling Rayleigh waves. They considered steady-profile solutions in a Fourier series form and obtained an infinite system of quadratic equations for the Fourier coefficients of the considered profiles. Their analysis showed the existence of steady-profile solutions which may move with phase speeds different from the linear Rayleigh wave velocity, as well as those which propagate at the Rayleigh wave velocity. Parker and Talbot went on to solve numerically truncated forms of the infinite systems for the Fourier coefficients. They determined four different steady-profile solutions. Two of these numerical solutions have speeds different from c_R, and the other two have speeds equal to the linear Rayleigh wave velocity. Plots of the surface displacements $\xi(x,0)$ of the Parker-Talbot solutions are given on Figures 1.1 through 1.4. The plots were generated using all of the Fourier coefficients given in [16] for each of the numerical solutions.

The most intriguing feature of the Parker-Talbot numerical solutions is the presence of horizontal displacement singularities which resemble finite angles in the plots of $\xi(x,0)$. The nature of these singularities, as well as the possibility of the existence of additional solutions to the Rayleigh wave problem, have not been explored until now.

The motivation for our work has therefore been to gain an understanding of the Rayleigh wave solutions structure, particularly in the context of second-order elasticity theory. To this end, we proceed in Chapter 2 to reformulate the full nonlinear equations describing the propagation of Rayleigh waves in an isotropic harmonic material. A solvability condition for the resulting equations is determined using a Fredholm alternative type of argument.

Assuming small-amplitude steady-state displacements, the second-order formulation of the Rayleigh problem is derived. Then we use the solvability condition for the full problem to obtain a restriction on the corresponding linear profiles, which can be used as first-order terms in small-amplitude expansions of the steady-profile Rayleigh waves. In the periodic case the consistency condition is used to derive in-

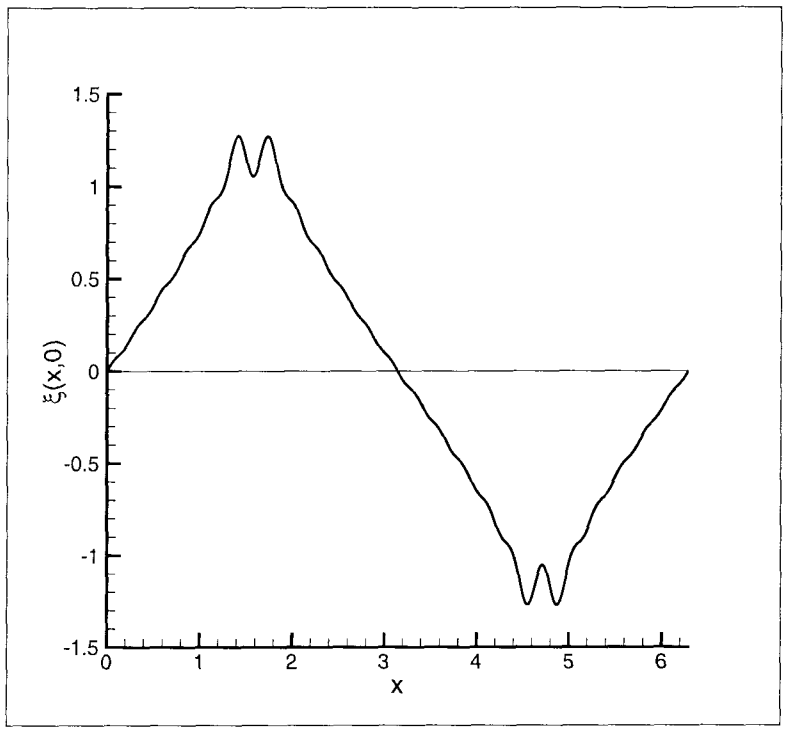

Figure 1.1: The horizontal displacement $\xi(x, 0)$ of the Parker-Talbot numerical solution 1 for $c = c_R$ with 12 Fourier modes.

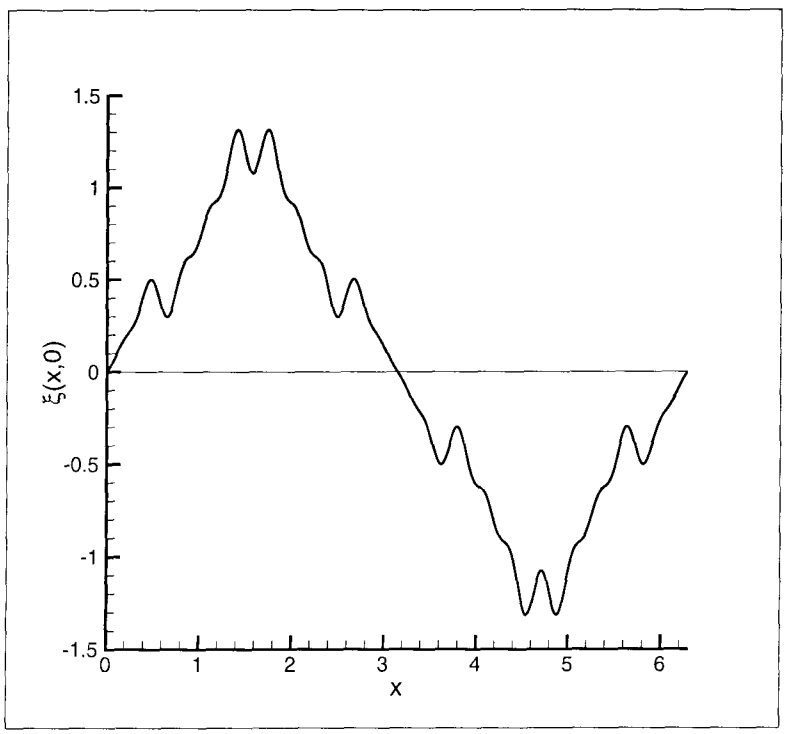

Figure 1.2: The horizontal displacement $\xi(x, 0)$ of the Parker-Talbot numerical solution 2 for $c = c_R$ with 12 Fourier modes.

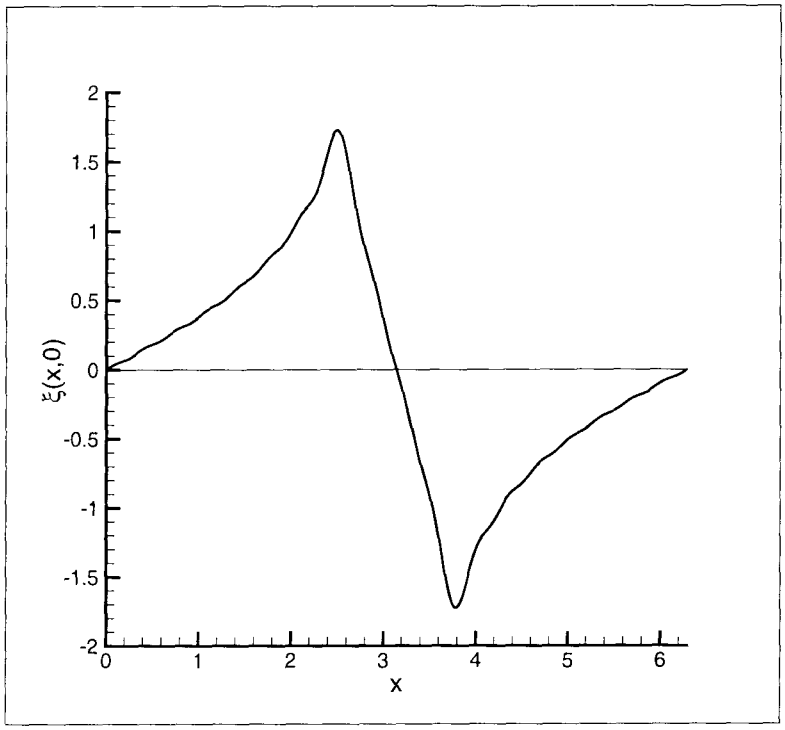

Figure 1.3: The horizontal displacement $\xi(x,0)$ of the Parker-Talbot numerical solution 1 for $c \neq c_R$ with 18 Fourier modes.

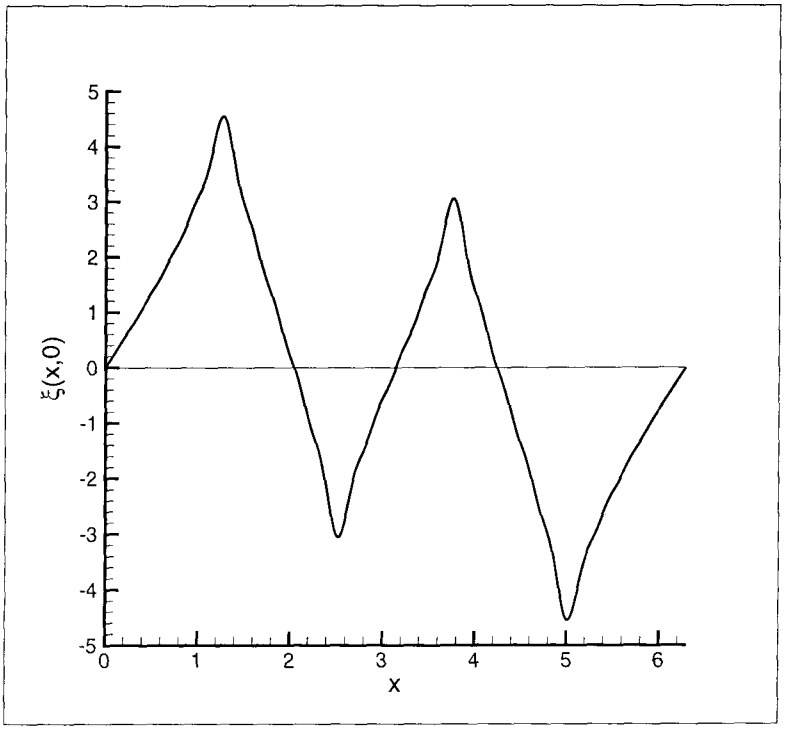

Figure 1.4: The horizontal displacement $\xi(x,0)$ of the Parker-Talbot numerical solution 2 for $c \neq c_R$ with 25 Fourier modes.

finite quadratic systems for the Fourier coefficients of the prescribed linear Rayleigh wave profiles. We then discuss two approximations for the infinite systems proposed by G.B. Whitham.

The infinite systems for the Fourier coefficients of the linear elastic displacements are studied numerically in Chapter 3 using the Newton-Raphson method with specially constructed initial guesses. We propose that there exist infinite families of solutions to the systems, and we present various examples of such solutions in the case of $c = c_R$ and $c \neq c_R$. In both cases we examine the nature of the singularities of the surface profiles of the numerical solutions, and provide empirical evidence showing that they display fractional singularity behavior. The computational scheme is modified to accommodate the proposed singular behavior, and improved numerical solutions to the Rayleigh wave problem are presented.

In Chapter 4 we examine the second-order Rayleigh wave problem on an infinite interval. The solvability condition derived in Chapter 2 is used in a local study of the surface displacement singularities. The possibility of the existence of fractional singularities in the surface horizontal displacement is studied using two different approximations of the solvability condition. The resulting equations are solved for the fractional singularity power, which is then compared with its corresponding numerically predicted values. It is shown that within the second-order theory the fractional singularities for $c = c_R$ and $c \neq c_R$ are of the same form.

Chapter 2 Basic Equations

2.1 The Full Nonlinear Rayleigh Wave Equations

The equations describing the propagation of Rayleigh waves are derived from the variational principle

$$\delta \int_{-\infty}^{\infty} \int_{0}^{\infty} \int_{0}^{\infty} \{ \frac{1}{2} \rho \, (\xi_t + \eta_t)^2 - W(\xi, \eta) \} \, dx \, dy \, dt = 0, \tag{2.1}$$

where $\xi(x, y, t)$ and $\eta(x, y, t)$ are the horizontal and vertical displacements from the coordinates x and y in the unstrained material, while ρ is the density of the half-space. $W(\xi, \eta)$ is the strain-energy density, chosen to correspond to the isotropic harmonic elastic material proposed by F. John in [9], given by

$$W(\xi, \eta) = \frac{1}{2}(\lambda + 2\mu)(w_1 - 2)^2 + 2\mu(w_1 - w_2 - 1), \tag{2.2}$$

where λ and μ are Lamé's constants, and $w_1(x, y, t)$ and $w_2(x, y, t)$ are defined by the following equations:

$$\begin{aligned} w_1(\xi, \eta) &= \sqrt{(2 + \xi_x + \eta_y)^2 + (\xi_y - \eta_x)^2}, \\ w_2(\xi, \eta) &= \begin{vmatrix} 1 + \xi_x & \xi_y \\ \eta_x & 1 + \eta_y \end{vmatrix}. \end{aligned} \tag{2.3}$$

The corresponding equations of motion from (2.1) are

$$\begin{aligned}\rho\,\xi_{tt} &= \frac{\partial\,\tau_{11}}{\partial x} + \frac{\partial\,\tau_{21}}{\partial y} = \frac{\partial}{\partial x}\left(\frac{\partial W}{\partial \xi_x}\right) + \frac{\partial}{\partial y}\left(\frac{\partial W}{\partial \xi_y}\right),\\ \rho\,\eta_{tt} &= \frac{\partial\,\tau_{12}}{\partial x} + \frac{\partial\,\tau_{22}}{\partial y} = \frac{\partial}{\partial x}\left(\frac{\partial W}{\partial \eta_x}\right) + \frac{\partial}{\partial y}\left(\frac{\partial W}{\partial \eta_y}\right),\end{aligned} \tag{2.4}$$

where in the middle expressions we have related the terms on the right to the stress components τ_{ij}. The expressions for w_1 and w_2 in (2.3) make it natural to introduce the physically significant quantities

$$D = \xi_x + \eta_y, \quad C = \xi_y - \eta_x, \quad J = \xi_x\eta_y - \xi_y\eta_x, \tag{2.5}$$

so that

$$w_1(\xi,\eta) = \sqrt{(2+D)^2 + C^2}, \quad w_2(\xi,\eta) = 1 + D + J. \tag{2.6}$$

Then (2.2), (2.4) and (2.6) give

$$\begin{aligned}\rho\,\xi_{tt} = \frac{\partial}{\partial x}\Big[(\lambda+2\mu)D + 2(\lambda+\mu)\big(1 - \frac{(2+D)}{\sqrt{(2+D)^2+C^2}}\big) - 2\mu\eta_y\Big] +\\ + \frac{\partial}{\partial y}\Big[\mu C + (\lambda+\mu)\big(C - \frac{2C}{\sqrt{(2+D)^2+C^2}}\big) + 2\mu\eta_x\Big],\end{aligned} \tag{2.7}$$

$$\begin{aligned}\rho\,\eta_{tt} = -\frac{\partial}{\partial x}\Big[\mu C + (\lambda+\mu)\big(C - \frac{2C}{\sqrt{(2+D)^2+C^2}}\big) - 2\mu\xi_y\Big] +\\ + \frac{\partial}{\partial y}\Big[(\lambda+2\mu)D + 2(\lambda+\mu)\big(1 - \frac{(2+D)}{\sqrt{(2+D)^2+C^2}}\big) - 2\mu\xi_x\Big].\end{aligned} \tag{2.8}$$

The terms explicitly in ξ and η in (2.7) and (2.8) come from the Jacobian J and they cancel out in these equations. However, they play a crucial role in the boundary conditions. The boundary conditions can be read off by comparing (2.4), (2.7),

and (2.8). They are

$$\begin{aligned}\tau_{22} &= (\lambda+2\mu)D + 2(\lambda+\mu)\big(1 - \frac{2+D}{\sqrt{(2+D)^2+C^2}}\big) - 2\mu\xi_x = 0,\\ \tau_{21} &= \mu C + (\lambda+\mu)\big(C - \frac{2C}{\sqrt{(2+D)^2+C^2}}\big) + 2\mu\eta_x = 0.\end{aligned} \tag{2.9}$$

From (2.7) and (2.8) we can deduce the equations for $D(x,y,t)$ and $C(x,y,t)$, namely,

$$\begin{aligned}\rho D_{tt} &= (\lambda+2\mu)\Delta D + 2(\lambda+\mu)\Delta\big(1 - \frac{2+D}{\sqrt{(2+D)^2+C^2}}\big),\\ \rho C_{tt} &= \mu\Delta C + (\lambda+\mu)\Delta\big(C - \frac{2C}{\sqrt{(2+D)^2+C^2}}\big).\end{aligned} \tag{2.10}$$

We get the benefits of the physical interpretations of terms in C and D, as well as including the expressions for ξ and η needed in (2.9), by introducing the potential functions $P(x,y,t)$ and $S(x,y,t)$, defined by

$$\begin{aligned}\xi(x,y,t) &= P_x + S_y,\\ \eta(x,y,t) &= P_y - S_x.\end{aligned} \tag{2.11}$$

For then

$$D(x,y,t) = \Delta P(x,y,t), \quad C(x,y,t) = \Delta S(x,y,t), \tag{2.12}$$

and the derivatives of ξ and η in the boundary conditions (2.9) are written simply in terms of P and S. The equations (2.10) may then be written as

$$\begin{aligned}\rho P_{tt} &= (\lambda+2\mu)\Delta P + 2(\lambda+\mu)\big(1 - \frac{2+\Delta P}{\sqrt{(2+\Delta P)^2+(\Delta S)^2}}\big),\\ \rho S_{tt} &= \mu\Delta S + (\lambda+\mu)\big(\Delta S - \frac{2\Delta S}{\sqrt{(2+\Delta P)^2+(\Delta S)^2}}\big),\end{aligned} \tag{2.13}$$

while the boundary conditions (2.9) become

$$\begin{aligned}(\lambda+2\mu)\Delta P+2(\lambda+\mu)\big(1-\frac{2+\Delta P}{\sqrt{(2+\Delta P)^2+(\Delta S)^2}}\big)-2\mu(P_{xx}+S_{yx})=0,\\ \mu\Delta S+(\lambda+\mu)\big(\Delta S-\frac{2\Delta S}{\sqrt{(2+\Delta P)^2+(\Delta S)^2}}\big)+2\mu(P_{yx}-S_{xx})=0.\end{aligned}\tag{2.14}$$

The expressions on the right-hand sides of the differential equations (2.13) are present in the boundary conditions (2.14). Therefore, we can substitute the equivalent left-hand sides of (2.13) into (2.14), to produce the linear equations

$$\begin{aligned}\rho P_{tt}-2\mu(P_{xx}+S_{yx})=0, \quad \text{on } y=0,\\ \rho S_{tt}+2\mu(P_{yx}-S_{xx})=0, \quad \text{on } y=0.\end{aligned}\tag{2.15}$$

Thus, perhaps surprisingly, the boundary conditions are linear in this form.

From either equations (2.10) for C and D or equations (2.13) for P and S we see that in the linear theory D and P satisfy wave equations with wave speed c_1, while C and S satisfy wave equations with wave speed c_2, where

$$\begin{aligned}c_1^2=\frac{\lambda+2\mu}{\rho} \quad &\text{is the compression wave velocity,}\\ c_2^2=\frac{\mu}{\rho} \quad &\text{is the shear wave velocity.}\end{aligned}$$

These wave equations are only coupled through the boundary conditions.

We shall focus on studying the propagation of steady-profile Rayleigh waves, and, therefore, we shall make the assumption that all considered functions are of the form

$$f(x,y,t)=f(x-ct,y),$$

where c denotes the velocity of the steady-profile waves. After introducing in our equations the new variable $X=x-ct$, we reduce the Rayleigh wave problem to

two spatial dimensions, X and y.

Then equations (2.13) can be written out in the form

$$p^2 P_{XX} + P_{yy} = 2\,\frac{c_2^2 - c_1^2}{c_1^2}\left(1 - \frac{2+D}{\sqrt{(2+D)^2 + C^2}}\right), \tag{2.16}$$

$$s^2 S_{XX} + S_{yy} = \frac{c_2^2 - c_1^2}{c_2^2}\left(C - \frac{2C}{\sqrt{(2+D)^2 + C^2}}\right), \tag{2.17}$$

and the boundary conditions (2.15) reduce to

$$\begin{aligned} \sigma^2 P_X + S_y &= 0, \quad \text{on } y = 0, \\ \sigma^2 S_X - P_y &= 0, \quad \text{on } y = 0, \end{aligned} \tag{2.18}$$

after they have been integrated once with respect to X. In equations (2.16), (2.17), and (2.18) we have introduced the notation:

$$p^2 = 1 - \frac{c^2}{c_1^2}, \quad s^2 = 1 - \frac{c^2}{c_2^2}, \quad \sigma^2 = 1 - \frac{c^2}{2c_2^2}. \tag{2.19}$$

2.2 The Linear Rayleigh Wave Problem

The linear version of the steady-profile surface wave problem on an elastic half-space was first studied by Lord Rayleigh in 1885. In his honor these waves are nowadays referred to as Rayleigh waves.

In the following analysis we shall revert to using x in place of X in order to simplify our notation. We should remember, however, that now x will denote a coordinate in the moving frame of reference.

2.2.1 The Periodic Solution to the Linear Rayleigh Wave Problem

In the linear case, the differential equations (2.16) and (2.17) uncouple to the stretched Laplace equations

$$\begin{aligned} p^2 P_{xx} + P_{yy} &= 0, \\ s^2 S_{xx} + S_{yy} &= 0, \end{aligned} \tag{2.20}$$

along with the coupled boundary conditions

$$\begin{aligned} \sigma^2 P_x + S_y &= 0, \quad \text{on } y = 0, \\ \sigma^2 S_x - P_y &= 0, \quad \text{on } y = 0. \end{aligned} \tag{2.21}$$

The differential equations (2.20) have periodic, bounded solutions of the form

$$P(x,y) = A\, e^{-kpy} \cos kx, \quad S(x,y) = B\, e^{-ksy} \sin kx. \tag{2.22}$$

Substituting the above expressions for P and S in the boundary conditions (2.21), we obtain from the first equation

$$B = \frac{-\sigma^2}{s} A, \text{ where } A \text{ is an arbitrary constant,} \tag{2.23}$$

and then from the second equation

$$\sigma^4 = ps. \tag{2.24}$$

Equation (2.24) can be rewritten in the form

$$\left(1 - \frac{c^2}{2c_2^2}\right)^4 = \left(1 - \frac{c^2}{c_1^2}\right)\left(1 - \frac{c^2}{c_2^2}\right), \tag{2.25}$$

which prescribes the velocity of propagation of linear Rayleigh waves. This equation, commonly referred to as the *Rayleigh condition*, has only one real positive root $c = c_R$, which is physically acceptable. Since the Rayleigh velocity c_R does not depend on the wavenumber k, Rayleigh waves are non-dispersive in the linear case.

General Fourier series solutions for $P(x, y)$ and $S(x, y)$, and the corresponding $\xi(x, y)$ and $\eta(x, y)$, are easily developed by linear superpositions of the form:

$$P(x,y) = \sum_{1}^{\infty} (A_k \cos kx + B_k \sin kx)\, e^{-kpy},$$
$$S(x,y) = \sum_{1}^{\infty} (C_k \cos nx + D_k \sin kx)\, e^{-ksy}.$$

2.2.2 The Complex Variable Solution to the Linear Rayleigh Wave Problem

An alternate approach to deriving the solutions of the linear Rayleigh wave problem is to use complex variable theory. The equations (2.20) and the boundary conditions (2.21) with p, s, $\sigma = 1$ are essentially Laplace equations and the Cauchy-Riemann equations (with the sign of S in (2.21) changed). Accordingly, we introduce the analytic function $f(x, y) + ig(x, y)$, where f and g are solutions to the Laplace equation, and satisfy the Cauchy-Riemann equations

$$f_1(x,y) = g_2(x,y),$$
$$f_2(x,y) = -g_1(x,y),$$

for all y. (In this section the subscripts $j = 1, 2$ will denote differentiation with respect to the j-th argument of a given function.)

We then take

$$P(x,y) = f(x,py), \quad S(x,y) = -\frac{\sigma^2}{s} g(x,sy), \tag{2.26}$$

as the solutions of the linear Rayleigh wave problem. The scaling factors p, s, and σ in (2.26) are related through the Rayleigh condition (2.24). Since

$$f(x,y)+ig(x,y)=\frac{1}{i\pi}\int_{-\infty}^{\infty}\frac{f(w,0)}{w-(x+iy)}\,dw=\frac{1}{i\pi}\int_{-\infty}^{\infty}\frac{P(w,0)}{w-(x+iy)}\,dw, \tag{2.27}$$

then $P(x,y)$ and $S(x,y)$ in (2.26) are fully determined in terms of $P(x,0)$, the value on the surface.

The displacements are then

$$\begin{aligned}\xi &= P_x+S_y=f_1(x,py)-\sigma^2 g_2(x,sy)=f_1(x,py)-\sigma^2 f_1(x,sy),\\ \eta &= P_y-S_x=pf_2(x,py)+\frac{\sigma^2}{s}g_1(x,sy)=-pg_1(x,py)+\frac{\sigma^2}{s}g_1(x,sy).\end{aligned} \tag{2.28}$$

For these it is convenient to introduce an equation similar to (2.27), but with $f_1(x,0)$ replacing $f(x,0)$. i.e.,

$$f_1(x,y)+ig_1(x,y)=\frac{1}{i\pi}\int_{-\infty}^{\infty}\frac{f_1(w,0)}{w-(x+iy)}\,dw. \tag{2.29}$$

Since acccording to (2.28) the value of $\xi(x,y)$ on the surface is

$$\xi_0(x)=\xi(x,0)=(1-\sigma^2)f_1(x,0)=(1-\sigma^2)P_1(x,0), \tag{2.30}$$

we introduce the functions

$$E(x,y)=(1-\sigma^2)f_1(x,y),\quad N(x,y)=(1-\sigma^2)g_1(x,y). \tag{2.31}$$

Then (2.28) become

$$\begin{aligned}\xi(x,y) &= \frac{1}{1-\sigma^2}\big\{E(x,py)-\sigma^2E(x,sy)\big\},\\ \eta(x,y) &= \frac{1}{1-\sigma^2}\big\{-pN(x,py)+\frac{\sigma^2}{s}N(x,sy)\big\},\end{aligned} \tag{2.32}$$

and (2.29) is equivalent to

$$E(x,y) + iN(x,y) = \frac{1}{i\pi} \int_{-\infty}^{\infty} \frac{\xi_0(w)}{w - (x+iy)}\, dw. \tag{2.33}$$

Using (2.32) the curl and divergence are

$$D(x,y) = \xi_x + \eta_y = \frac{2c_2^2}{c_1^2}\, E_1(x,py), \tag{2.34}$$

$$C(x,y) = \xi_y - \eta_x = -\frac{2\sigma^2}{s}\, N_1(x,sy). \tag{2.35}$$

If we differentiate equation (2.33) with respect to x, and introduce the functions $U(x,y)$ and $V(x,y)$, defined as

$$U(x,y) + iV(x,y) = E_1(x,y) + iN_1(x,y) = \frac{1}{\pi i} \int_{-\infty}^{\infty} \frac{\xi_0'(w)}{w - (x+iy)}\, dw, \tag{2.36}$$

the relations in (2.34) and (2.35) can be recast as

$$\begin{aligned} D(x,y) &= \frac{2c_2^2}{c_1^2}\, U(x,py), \\ C(x,y) &= -\frac{2\sigma^2}{s}\, V(x,sy). \end{aligned} \tag{2.37}$$

The Delta Function Solution

A particular solution which will be used later is found by taking $P(x,0) = \pi\delta(x - x_0)$ in (2.27). Then,

$$P(x,y) = \frac{py}{(x-x_0)^2 + p^2y^2}, \quad S(x,y) = -\frac{\sigma^2}{s}\, \frac{x - x_0}{(x-x_0)^2 + s^2y^2}. \tag{2.38}$$

2.3 The Solvability Condition

The linear theory imposes no restrictions on the shape of the Rayleigh wave displacement profiles. Fourier modes, such as (2.22), can be superposed to produce general profiles moving with the speed c_R, as given by (2.25). We can determine a restriction on the expected wave profiles when we consider the full nonlinear Rayleigh wave problem

$$p^2 P_{xx} + P_{yy} = 2\,\frac{c_2^2 - c_1^2}{c_1^2}\left(1 - \frac{2+D}{\sqrt{(2+D)^2 + C^2}}\right) = F(x,y), \tag{2.39}$$

$$s^2 S_{xx} + S_{yy} = \frac{c_2^2 - c_1^2}{c_2^2}\left(C - \frac{2C}{\sqrt{(2+D)^2 + C^2}}\right) = G(x,y), \tag{2.40}$$

$$\sigma^2 P_x + S_y = 0, \quad \text{on } y = 0, \tag{2.41}$$

$$\sigma^2 S_x - P_y = 0, \quad \text{on } y = 0. \tag{2.42}$$

The differential operator which corresponds to the equations (2.39) and (2.40) is

$$L = \begin{pmatrix} p^2 \frac{\partial^2}{\partial x^2} & \frac{\partial^2}{\partial y^2} \\ s^2 \frac{\partial^2}{\partial x^2} & \frac{\partial^2}{\partial y^2} \end{pmatrix}. \tag{2.43}$$

It can easily be shown that the operator L and the boundary conditions (2.41) and (2.42) are self-adjoint. Therefore, a Fredholm alternative type consistency condition has to be imposed on the forcing terms $F(x,y)$ and $G(x,y)$ of equations (2.39) and (2.40) to ensure that they have non-trivial solutions. The proposed solvability condition restricts the shapes which can be assumed by a steady-profile Rayleigh wave.

We shall obtain the "orthogonality" or "solvability" condition by forming the inner product of the P, S problem with families of test functions based on the linear Rayleigh wave solutions. First, we consider the infinite interval case $-\infty < x < \infty$,

using the following family of test functions:

$$\widetilde{P}(x,y) = \frac{py}{(x-x_0)^2+p^2y^2}, \tag{2.44}$$

$$\widetilde{S}(x,y) = -\frac{\sigma^2}{s}\,\frac{x-x_0}{(x-x_0)^2+s^2y^2}, \tag{2.45}$$

with $-\infty < x_0 < \infty$. These test functions are solutions of the linear Rayleigh wave equations (2.20) and they also satisfy the boundary conditions

$$\sigma^2\widetilde{P}_x + \widetilde{S}_y = 0, \tag{2.46}$$

$$\sigma^2\widetilde{S}_x - \widetilde{P}_y = \frac{\sigma^4 - ps}{s\,(x-x_0)^2}, \tag{2.47}$$

along with $\widetilde{P}(x,0) = \pi\delta(x-x_0)$.

If we take $c = c_R$ in the test functions $\widetilde{P}(x,y)$ and $\widetilde{S}(x,y)$, the expression $\sigma^4 - ps$ on the right-hand side of equation (2.47) becomes zero. The boundary conditions (2.46) and (2.47) then coincide with the boundary conditions (2.21) of the linear Rayleigh problem. Therefore, to require that $c = c_R$ in $\widetilde{P}(x,y)$ and $\widetilde{S}(x,y)$ is equivalent to taking a linear Rayleigh wave solution as a test function in the orthogonality condition. However, at this point of the analysis we do not want to restrict the value of c, so the set of test functions which we shall consider is broader than the set of linear Rayleigh wave solutions.

The solvability condition, corresponding to the nonlinear problem in (2.39) to (2.42), is determined by considering the inner product

$$(L\mathcal{P}, \widetilde{\mathcal{P}}) = \int_{-\infty}^{\infty}\int_{0}^{\infty}\left\{(p^2P_{xx}+P_{yy})\widetilde{P} + (s^2S_{xx}+S_{yy})\widetilde{S}\right\}dxdy, \tag{2.48}$$

where $\mathcal{P} = (P,S)$ is the solution to the full Rayleigh wave problem, and $\widetilde{\mathcal{P}} = (\widetilde{P},\widetilde{S})$ is any of the test functions pairs given in (2.44) and (2.45). We integrate equation (2.48) by parts using the boundary conditions (2.41), (2.42), (2.46), and (2.47),

as well as the fact that $\widetilde{\mathcal{P}}$ satisfies $L\widetilde{\mathcal{P}} = 0$. The resulting orthogonality condition is

$$\int_{-\infty}^{\infty}\int_{0}^{\infty}\left\{F(x,y)\,\widetilde{P} + G(x,y)\,\widetilde{S}\right\}dxdy = -\frac{\sigma^4 - ps}{s}\int_{-\infty}^{\infty}\frac{P(x,0)}{(x-x_0)^2}\,dx, \tag{2.49}$$

for any choice of x_0 in $-\infty < x_0 < \infty$. Here, $\widetilde{P}$ and $\widetilde{S}$ are given by (2.44) and (2.45), and $F(x,y)$ and $G(x,y)$ are the forcing terms of the full non-linear Rayleigh wave equations (2.39) and (2.40).

Following the same idea, we shall derive an orthogonality condition for the Rayleigh wave problem in the periodic case. Here, the following choice of test functions is made:

$$\widetilde{P}(x,y) = e^{-npy}\cos nx, \tag{2.50}$$

$$\widetilde{S}(x,y) = -\frac{\sigma^2}{s}\,e^{-nsy}\sin nx, \tag{2.51}$$

with $n = 1,\ldots,\infty$. Each of these test function pairs satisfy the linear Rayleigh wave equations as well as the coupled boundary conditions

$$\sigma^2\widetilde{P}_x + \widetilde{S}_y = 0, \tag{2.52}$$

$$\sigma^2\widetilde{S}_x - \widetilde{P}_y = -\frac{\sigma^4 - ps}{s}n\cos nx, \tag{2.53}$$

for $n = 1,\ldots,\infty$. Once again, the value of c is not restricted.

The inner product $(L\mathcal{P}, \widetilde{\mathcal{P}})$, where $\mathcal{P} = (P,S)$ is the solution to the full Rayleigh wave problem and $\widetilde{\mathcal{P}} = (\widetilde{P},\widetilde{S})$ is any of the test function pairs given in (2.50) and (2.51), is integrated by parts using the boundary conditions and the periodicity requirements on $\mathcal{P}^{(2)}$ and $\widetilde{\mathcal{P}}$. The resulting solvablity condition is

$$\int_{0}^{2\pi}\int_{0}^{\infty}\left\{F(x,y)\,\widetilde{P} + G(x,y)\,\widetilde{S}\right\}dxdy = \frac{\sigma^4 - ps}{s}\int_{0}^{2\pi} nP(x,0)\cos nx\,dx, \tag{2.54}$$

where $\widetilde{P}$ and $\widetilde{S}$ are given by (2.50) and (2.51) for any choice of $n = 1, \ldots, \infty$. This is the solvability condition corresponding to the periodic formulation of the full nonlinear Rayleigh wave problem.

2.4 The Second-Order Theory

In the previous section we derived the solvability conditions corresponding to the full Rayleigh wave equations. Here, we shall focus on the second-order problem in the small amplitude aproximation.

We shall study nonlinear Rayleigh wave solutions of the following form:

$$\begin{aligned}
D(x,y) &= \varepsilon D^{(1)}(x,y) + \varepsilon^2 D^{(2)}(x,y) + O(\varepsilon^3),\\
C(x,y) &= \varepsilon C^{(1)}(x,y) + \varepsilon^2 C^{(2)}(x,y) + O(\varepsilon^3),\\
P(x,y) &= \varepsilon P^{(1)}(x,y) + \varepsilon^2 P^{(2)}(x,y) + O(\varepsilon^3),\\
S(x,y) &= \varepsilon S^{(1)}(x,y) + \varepsilon^2 S^{(2)}(x,y) + O(\varepsilon^3).
\end{aligned}$$

Substituting these expansions into the full nonlinear differential equations (2.39) and (2.40) and the boundary conditions (2.41) and (2.42), we see that the leading-order terms $P^{(1)}(x,y)$ and $S^{(1)}(x,y)$ are solutions of the linear Rayleigh wave problem discussed in Section 2.2.

When the forcing terms $F(x,y)$ and $G(x,y)$ are expanded out in powers of ε, we get

$$F(x,y) = \varepsilon^2 \frac{(c_2^2 - c_1^2)}{4c_1^2} C^{(1)}C^{(1)} + O(\varepsilon^3), \tag{2.55}$$

$$G(x,y) = \varepsilon^2 \frac{(c_2^2 - c_1^2)}{2c_2^2} C^{(1)}D^{(1)} + O(\varepsilon^3), \tag{2.56}$$

where $D^{(1)}(x,y) = \Delta P^{(1)}(x,y)$ and $C^{(1)}(x,y) = \Delta S^{(1)}(x,y)$. Then the second-order

equations are

$$p^2 P_{xx}^{(2)} + P_{yy}^{(2)} = \frac{(c_2^2 - c_1^2)}{4c_1^2} C^{(1)} C^{(1)}, \tag{2.57}$$

$$s^2 S_{xx}^{(2)} + S_{yy}^{(2)} = \frac{(c_2^2 - c_1^2)}{2c_2^2} C^{(1)} D^{(1)}. \tag{2.58}$$

When solutions with $c = c_R$ are considered, the second-order boundary conditions are simply

$$\begin{aligned} \sigma^2 P_x^{(2)} + S_y^{(2)} &= 0, \quad \text{on } y = 0, \\ \sigma^2 S_x^{(2)} - P_y^{(2)} &= 0, \quad \text{on } y = 0. \end{aligned} \tag{2.59}$$

When solutions with $c \neq c_R$ are considered, we bear in mind that p, s, and σ are defined in terms in c. In the first-order solutions $P^{(1)}(x, y)$ and $S^{(1)}(x, y)$ we want to take $c = c_R$. Therefore, terms from small changes $c = c_R + \varepsilon\gamma$ could appear in the second order boundary conditions.

In accordance with the notation introduced in [16] by Parker and Talbot, we define the quantity

$$K(c) = \frac{\sigma^4}{ps}. \tag{2.60}$$

In the linear theory, $c = c_R$ is defined through $K(c_R) = 1$. Parker and Talbot allow small changes of order ε in the wave speed c, i.e., $c = c_R + \varepsilon\gamma$, which will also be included here. It is important to note that this change γ is specified in advance to broaden the class of solutions; γ is not required nor determined from the equations of the problem. Changes $O(\varepsilon)$ in c will correspond to $K(c) - 1 = O(\varepsilon)$. We introduce

$$K(c) - 1 = \varepsilon\kappa, \tag{2.61}$$

following the notation of Parker and Talbot in [16]. The precise relation between

$$c = c_R + \varepsilon\gamma \quad \text{and} \quad K(c) - 1 = \varepsilon\kappa$$
$$\text{is} \quad \kappa = \gamma K'(c_R).$$

The boundary conditions (2.59) are then be modified to

$$\sigma_R^2 P_x^{(2)} + S_y^{(2)} = \frac{-\sigma_R^2 \kappa}{2} P_x^{(1)}, \quad \text{on } y = 0,$$
$$\sigma_R^2 S_x^{(2)} - P_y^{(2)} = \frac{-\sigma_R^2 \kappa}{2} S_x^{(1)}, \quad \text{on } y = 0.$$

However, we no longer need to solve the second-order boundary value problems in detail. To find the linear shapes that are acceptable to generate a nonlinear steady shape, we need only refer to the solvability conditions (2.49) and (2.54).

We substitute the expansions (2.55) for $F(x, y)$ and (2.56) for $G(x, y)$ in the solvability condition (2.49). Picking up the first-order component of the resulting expansion of the orthogonality condition in powers of ε, we get

$$\frac{(c_1^2 - c_2^2)}{4c_1^2 c_2^2} \int_{-\infty}^{\infty} \int_{0}^{\infty} \left\{ c_2^2 C^{(1)} C^{(1)} \widetilde{P} + 2c_1^2 C^{(1)} D^{(1)} \widetilde{S} \right\} dxdy = \frac{\sigma^4 - ps}{s\varepsilon} \int_{-\infty}^{\infty} \frac{P^{(1)}(x, 0)}{(x - x_0)^2} dx, \tag{2.62}$$

for any choice of x_0 in $-\infty < x_0 < \infty$ with $\widetilde{P}$ and $\widetilde{S}$ given by (2.44) and (2.45).

The factor $(\sigma^4 - ps)/s$, found on the right-hand side of (2.62), can also be expanded out in powers of ε to produce

$$\frac{\sigma^4 - ps}{s} = \varepsilon\kappa p_R + O(\varepsilon^2), \tag{2.63}$$

where $p_R = p(c_R)$.

Substituting the expansion (2.63) in (2.62), and then integrating by parts the

single integral on the right-hand side, we finally obtain

$$\frac{(c_1^2-c_2^2)}{4c_1^2c_2^2}\int_{-\infty}^{\infty}\int_{0}^{\infty}\{c_2^2C^{(1)}C^{(1)}\widetilde{P}+2c_1^2C^{(1)}D^{(1)}\widetilde{S}\}\,dxdy=\kappa p_R\int_{-\infty}^{\infty}\frac{P_x^{(1)}(x,0)}{(x-x_0)}\,dx, \quad (2.64)$$

for any choice of x_0 in $-\infty < x_0 < \infty$ with $\widetilde{P}$ and $\widetilde{S}$ given by (2.44) and (2.45). The condition (2.64), which corresponds to the infinite interval formulation of the second-order Rayleigh wave problem, will be used in Chapter 4 to perfom a local study of the surface singularities of steady-profile linear Rayleigh waves.

Similarly, we can substitute the expansions (2.55) and (2.56) in the solvability condition for the periodic case (2.54) to produce

$$\frac{(c_2^2-c_1^2)}{4c_1^2c_2^2}\int_{0}^{2\pi}\int_{0}^{\infty}\{c_2^2C^{(1)}C^{(1)}\widetilde{P}+2c_1^2C^{(1)}D^{(1)}\widetilde{S}\}\,dxdy=\frac{\sigma^4-ps}{s\varepsilon}\int_{0}^{2\pi}nP^{(1)}(x,0)\cos nx\,dx, \quad (2.65)$$

for every choice of $n = 1, \ldots, \infty$. The right-hand side of equation (2.65) can be rewritten in terms of κ using (2.63) to yield the final form of the periodic solvability condition

$$\frac{(c_2^2-c_1^2)}{4c_1^2c_2^2}\int_{0}^{2\pi}\int_{0}^{\infty}\{c_2^2C^{(1)}C^{(1)}\widetilde{P}+2c_1^2C^{(1)}D^{(1)}\widetilde{S}\}\,dxdy=\kappa p_R\int_{0}^{2\pi}nP^{(1)}(x,0)\cos nx\,dx, \quad (2.66)$$

where $\widetilde{P}$ and $\widetilde{S}$ are given by (2.50) and (2.51) for all possible choices of $n = 1, \ldots, \infty$.

It is important to note that for both the periodic and the infinite interval orthogonality conditions, a shift from the linear velocity of propagation changes the nature of the equations in a non-trivial manner. When the velocity shift is equal to zero, i.e., when $\kappa = 0$, the right-hand sides of equations (2.64) and (2.66) are also equal to zero. However, when $\kappa \neq 0$, the single integral components in either of the

solvability conditions must be included.

2.4.1 The Solvability Condition in the Fourier Series Case with $c = c_R$

In both this and the next section, the p, s and σ coefficients will actually denote the values of these scaling factors at $c = c_R$. Normally, we would refer to these as p_R, s_R, and σ_R. However, since the equations examined here are quite long, we shall drop the subscripts $_R$ to simplify notation.

When the nonlinear wave velocity c is equal to the linear Rayleigh velocity c_R, the solvability condition (2.66) simplifies down to

$$\int_0^{2\pi}\int_0^{\infty} \{c_2^2 C^{(1)} C^{(1)} \widetilde{P} + 2c_1^2 C^{(1)} D^{(1)} \widetilde{S}\}\, dxdy = 0. \tag{2.67}$$

We will use the solvability condition (2.67) to determine the set of linear wave profiles which are acceptable within the second-order formulation of the Rayleigh wave problem with $c = c_R$.

The Fourier series of the linear profiles are taken to be of the following form:

$$D^{(1)}(x,y) = \frac{2c_2^2}{c_1^2} \sum_{k=1}^{\infty} Q_k\, e^{-kpy} \cos kx, \tag{2.68}$$

$$C^{(1)}(x,y) = \frac{-2\sigma^2}{s} \sum_{k=1}^{\infty} Q_k\, e^{-ksy} \sin kx. \tag{2.69}$$

Substituting the expansions for $D^{(1)}(x,y)$ and $C^{(1)}(x,y)$, as well as the expressions (2.50) and (2.51) for $\widetilde{P}(x,y)$ and $\widetilde{S}(x,y)$ in equation (2.67), we get

$$\int_0^{2\pi}\int_0^{\infty} \left\{ \sum_{k=1}^{\infty}\sum_{j=1}^{\infty} Q_k Q_j\, e^{-[(k+j)s+np]y} \sin kx \sin jx \cos nx \right\} dxdy +$$

$$+2\int_0^{2\pi}\int_0^{\infty}\left\{\sum_{k=1}^{\infty}\sum_{m=1}^{\infty}Q_kQ_m\,e^{-[(k+n)s+mp]y}\,\sin kx\cos mx\sin nx\right\}dxdy=0, \quad (2.70)$$

for all choices of n with $n=1,\ldots,\infty$. We expand the products of sines and cosines using trigonometric identities, and then we integrate with respect to x to produce

$$\int_0^{\infty}\Bigg\{\sum_{\substack{k=1\\k-j=n}}^{\infty}\sum_{j=1}^{\infty}Q_kQ_j\,e^{-[(k+j)s+np]y}+\sum_{\substack{k=1\\k-j=-n}}^{\infty}\sum_{j=1}^{\infty}Q_kQ_j\,e^{-[(k+j)s+np]y}+$$
$$-\sum_{\substack{k=1\\k+j=n}}^{\infty}\sum_{j=1}^{\infty}Q_kQ_j\,e^{-n(s+p)y}+2\sum_{\substack{k=1\\k+m=n}}^{\infty}\sum_{m=1}^{\infty}Q_kQ_m\,e^{-[(k+n)s+mp]y}+$$
$$+2\sum_{\substack{k=1\\k-m=n}}^{\infty}\sum_{m=1}^{\infty}Q_kQ_m\,e^{-[(k+n)s+mp]y}-2\sum_{\substack{k=1\\k-m=-n}}^{\infty}\sum_{m=1}^{\infty}Q_kQ_m\,e^{-[(k+n)s+mp]y}\Bigg\}dy=0,$$

for all $n=1,\ldots,\infty$. We now integrate with respect to y, and introduce a uniform notation for all of the summation indices. This results in the infinite system of equations,

$$\sum_{k=1}^{\infty}Q_kQ_{n+k}\left[\frac{1}{(2k+n)s+np}+\frac{1}{(2n+k)s+kp}-\frac{1}{(n+k)(p+s)}\right]+$$
$$+\sum_{k=1}^{n-1}Q_kQ_{n-k}\left[\frac{1}{(k+n)s+(n-k)p}-\frac{1}{2n(p+s)}\right]=0,\ n=1,\ldots,\infty, \quad (2.71)$$

which is equivalent to the solvability condition for the case of $c=c_R$. It is convenient to multiply the coefficients of the system above by $2n(p+s)$, and to introduce the following notation:

$$\begin{aligned}\alpha_{k,n}&=\frac{2n(p+s)}{(k+n)s+(n-k)p}-1,\\ \beta_{k,n}&=\frac{2n(p+s)}{(2k+n)s+np}+\frac{2n(p+s)}{(2n+k)s+kp}-\frac{2n}{n+k}.\end{aligned} \quad (2.72)$$

The coefficients $\alpha_{k,n}$ and $\beta_{k,n}$ differ by a minus sign from the Q system coefficients

introduced by Parker and Talbot in [16]. As defined in (2.72) the α's and β's are always positive; Parker and Talbot worked with negative values.

The final form of the infinite system (2.71) for the Fourier coefficients of the steady-profile Rayleigh profiles is

$$\sum_{k=1}^{n-1} \alpha_{k,n}\, Q_k Q_{n-k} + \sum_{k=1}^{\infty} \beta_{k,n}\, Q_k Q_{n+k} = 0, \quad n = 1, \ldots, \infty. \tag{2.73}$$

This system prescribes the linear Rayleigh wave profiles, which can be used as first-order terms in a small-amplitude expansion of a nonlinear Rayleigh wave solution moving with velocity c_R.

2.4.2 The Solvability Condition in the Fourier Series Case with $\mathbf{c \neq c_R}$

In the case of $c \neq c_R$, we get a slightly more complicated system of equations due to the presence of the single integral on the right-hand side of equation (2.66). The Fourier series for $P^{(1)}(x, y)$, corresponding to the choice of $D^{(1)}(x, y)$ and $C^{(1)}(x, y)$ in (2.68) and (2.69), is

$$P^{(1)}(x, y) = -\frac{2c_2^2}{c^2} \sum_{k=1}^{\infty} \frac{Q_k}{k^2}\, e^{-kpy} \cos kx. \tag{2.74}$$

Upon substitution of this Fourier series into the integral on the right-hand side of (2.66), we obtain the expression

$$-\frac{2c_2^2}{c^2}\, \kappa p \sum_{k=1}^{\infty} \frac{Q_k}{k^2} \int_0^{2\pi} n \cos nx \cos kx\, dx,$$

which further simplifies to

$$-\pi \frac{2c_2^2}{c^2}\, \kappa p\, \frac{Q_n}{n}. \tag{2.75}$$

Substituting the result in (2.75) into equation (2.66), we obtain the infinite system of equations for the coefficients Q_n, corresponding to the case of $c \neq c_R$:

$$\sum_{k=1}^{n-1} \alpha_{k,n}\, Q_k Q_{n-k} + \sum_{k=1}^{\infty} \beta_{k,n}\, Q_k Q_{n+k} = \frac{4\kappa s}{p-s}\, Q_n, \quad n = 1, \ldots, \infty. \tag{2.76}$$

The system (2.76) reduces to the system (2.73) for the special case of $c = c_R, \kappa = 0$.

We can further simplify the equations (2.76) by rescaling the Q_n in the following manner:

$$Q_n = \frac{4s}{p-s} \widehat{Q}_n, \quad n = 1, \ldots, \infty. \tag{2.77}$$

This produces the final form of the system for the case of $c \neq c_R$:

$$\sum_{k=1}^{n-1} \alpha_{k,n}\, \widehat{Q}_k \widehat{Q}_{n-k} + \sum_{k=1}^{\infty} \beta_{k,n}\, \widehat{Q}_k \widehat{Q}_{n+k} = \kappa\, \widehat{Q}_n, \quad n = 1, \ldots, \infty. \tag{2.78}$$

In all subsequent analysis of the system above, we shall drop the hats from the coefficients $\widehat{Q}_k$ in order to simplify notation.

An alternative approach to deriving the infinite systems (2.73) and (2.78) is to substitute the Fourier series directly into the equations and the boundary conditions, and examine the resulting set of algebraic equations for the Fourier coefficients. The left-hand side of these equations is linear with a singular matrix, and the right-hand side is a nonlinear correction. Since the matrix is singular, the right-hand side must satisfy an orthogonality condition. Thus, the solvability requirement occurs at a later stage.

It appears that Parker and Talbot, who were the first to derive the systems (2.73) and (2.78), used a similar approach in [16]. Parker rederived these systems in [17] based on an orthogonality condition type of argument along with Fourier transforms. Later in [15], Parker et al. described a generalized "projection method," which produces the evolution equations for electro-elastic surface waves, of which

the systems (2.73) and (2.78) can be considered as a special case.

We derived the systems (2.73) and (2.78) from the forcing terms $F(x,y)$ and $G(x,y)$ in (2.55) and (2.56). In our formulation, they have a particularly simple form in terms of $C(x,y)$ and $D(x,y)$. Accordingly, this form of the boundary value problem is easy to use, and the resulting solvability condition is produced using a straightforward application of the Fredholm alternative orthogonality requirement.

2.5 Remarks on the Infinite Systems for the Linear Rayleigh Wave Fourier Coefficients

So far no analytic solutions of the solvability condition systems (2.73) and (2.78) have been determined. The application of familiar analytical methods to these equations is obstructed by the complicated structure of the $\alpha_{k,n}$ and the $\beta_{k,n}$ coefficients, and their non-trivial dependence on the scaling factors p and s.

2.5.1 The Constant Coefficient Systems

G.B. Whitham proposed looking at two simpler systems related to the systems (2.73) and (2.78). For both of those systems, terms in the first sum can be combined, e.g., $\alpha_{k,n}\,Q_kQ_{n-k}$ and $\alpha_{n-k,n}\,Q_{n-k}Q_k$ are products of the same Q's. In this case, the coefficients $\alpha_{k,n}+\alpha_{n-k,n}$ are roughly constant and, therefore, the following constant coefficient systems are suggested:

$$\begin{aligned} A\sum_{k=1}^{\frac{n-1}{2}} Q_kQ_{n-k} + A\sum_{k=1}^{\infty} Q_kQ_{n+k} &= \kappa\, Q_n, \quad n \text{ odd}, \\ A\sum_{k=1}^{\frac{n-1}{2}} Q_kQ_{n-k} + \frac{1}{2}AQ_{\frac{n}{2}}^2 + A\sum_{k=1}^{\infty} Q_kQ_{n+k} &= \kappa\, Q_n, \quad n \text{ even}. \end{aligned} \tag{2.79}$$

The goal is to obtain an overall view of the behavior of such systems, with the hope of gaining some understanding of their underlying structure, even if there may be considerable differences in the detailed behavior and numerical values of the constant coefficient and the real Q systems solutions. It was found that (2.79) can be solved analytically. The results turned out to be extremely useful, including getting a good initial guess for the numerical treatment of the real Q systems.

A reasonable choice for A in (2.79) ranges between $2(s+3p)/(p+3s)$ and $(p+s)/s$. For an elastic material of Poisson ratio $\nu = 1/4$, the scaling factors p and s are $p = 0.8475$ and $s = 0.3933$. Therefore, A is in the range between

$$2(s+3p)/(p+3s) = 2.8961 \quad \text{and} \quad (p+s)/s = 3.1548.$$

Also, the factor A can be scaled out of the equations using a transformation of the form $Q_k = \widehat{Q}_k/A$.

If the velocity of propagation c does not equal the Rayleigh velocity c_R, then $\kappa \neq 0$ and the linear terms in the right-hand side of the equations (2.79) must be retained. However, for $c = c_R$ we have $\kappa = 0$, and so the constant coefficient approximation reduces to

$$\begin{aligned} &\sum_{k=1}^{\frac{n-1}{2}} Q_k Q_{n-k} + \sum_{k=1}^{\infty} Q_k Q_{n+k} = 0, \quad n \text{ odd}, \\ &\sum_{k=1}^{\frac{n-1}{2}} Q_k Q_{n-k} + \frac{1}{2} Q_{\frac{n}{2}}^2 + \sum_{k=1}^{\infty} Q_k Q_{n+k} = 0, \quad n \text{ even}. \end{aligned} \tag{2.80}$$

We shall refer to either one of (2.79) and (2.80) as the constant coefficient systems, or in shorthand - the CQ systems.

The analytical solutions of the CQ systems were determined by G.B. Whitham.

He proved that when the generating function,

$$q(\theta) = \sum_{k=1}^{\infty} Q_k \cos k\theta, \tag{2.81}$$

is introduced, the system (2.79) reduces to the equation

$$Aq^2(\theta) - \kappa q(\theta) = \frac{B}{2}, \text{ where } B = \sum_{k=1}^{\infty} Q_k^2 \text{ is a constant, } A > 0, \tag{2.82}$$

while the system (2.80), which already has the A normalized out, reduces to

$$q^2(\theta) = \frac{B}{2}, \text{ where once again } B = \sum_{k=1}^{\infty} Q_k^2. \tag{2.83}$$

The solutions to either one of the $q(\theta)$ equations are pure constants which we shall denote by r_1 and r_2. The corresponding surface horizontal displacements $\xi(x,0)$ are piecewise linear with slopes given by the constants r_1 and r_2.

The solutions of the simpler equation (2.83), corresponding to the $c = c_R$ case, are $r_1 = -r_2 = \sqrt{B/2}$. This implies that the corresponding surface horizontal displacement singularities are symmetric corners. There is no restriction on the number of singularities that the CQ system solutions can have, as long as they have the prescribed symmetric form. Therefore, the set of solutions to the CQ system with $c = c_R$ is infinite. Two of these solutions are shown in Figures 2.1 and 2.2.

For the case of $c \neq c_R$, the horizontal displacement singularities are also corners; however, this time they are non-symmetric. As determined by G.B. Whitham, the slopes of the piece-wise linear sections of the solutions to (2.82) are related through the relation $r_1 r_2 = -B/(2A)$, and the special "shock-like" condition $r_1 + r_2 = \kappa/A$.

In analogy to shock dynamics, a positive shift in the velocity of propagation, i.e., $\kappa > 0$, implies that the positive non-symmetric corners in $\xi(x,0)$ steepen forward, as illustrated in Figure 2.3. Similarly, when $\kappa < 0$, the solution profiles move at speeds slower than the Rayleigh velocity c_R, and so the positive corners of $\xi(x,0)$

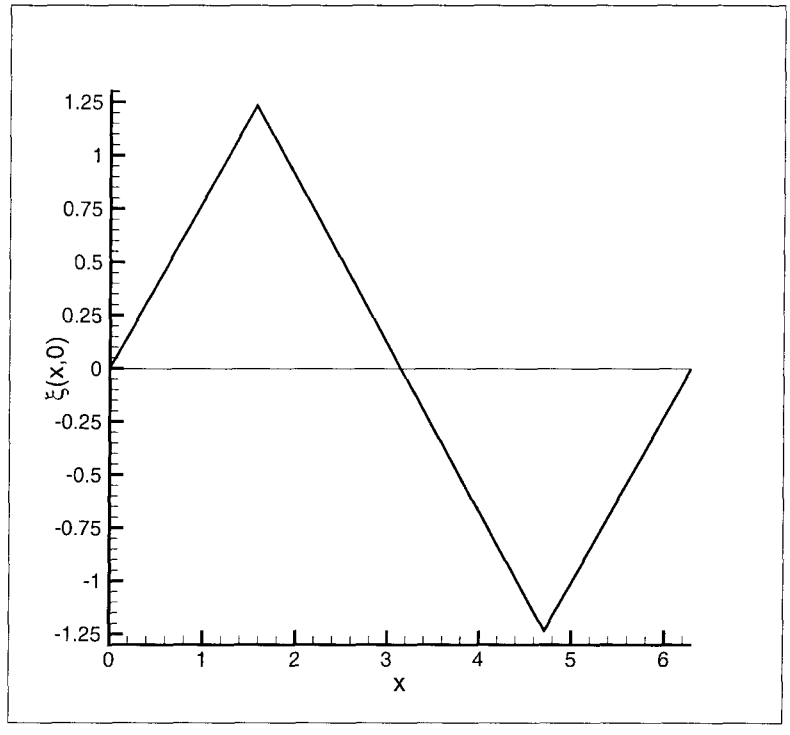

Figure 2.1: A solution to the constant coefficient system for $c = c_R$ with 2 symmetric corners.

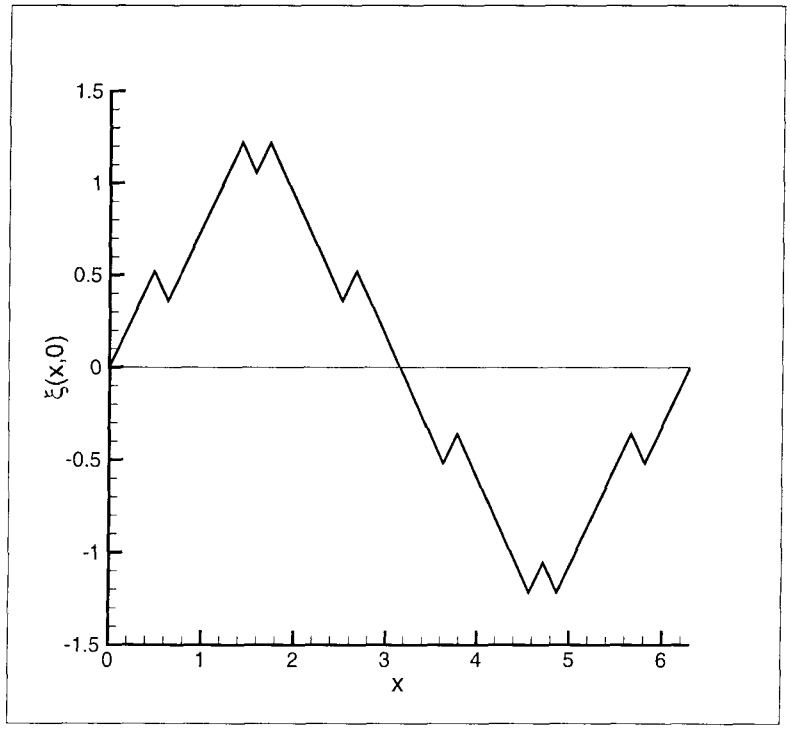

Figure 2.2: A solution to the constant coefficient system for $c = c_R$ with 8 symmetric corners.

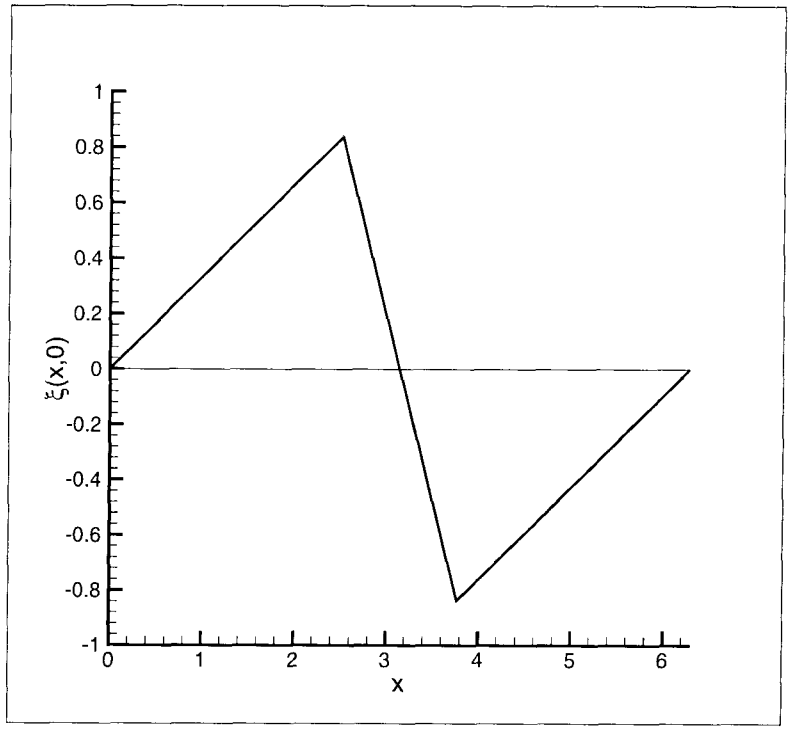

Figure 2.3: A solution to the constant coefficient system for $c \neq c_R$, $\kappa = 1$ with 2 non-symmetric corners.

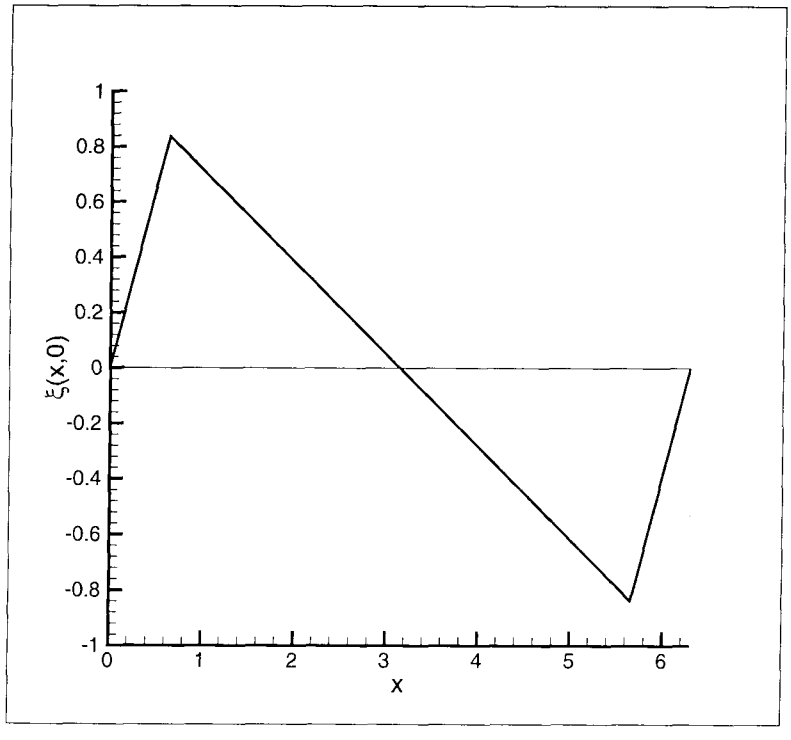

Figure 2.4: A solution to the constant coefficient system for $c \neq c_R$, $\kappa = -1$ with 2 non-symmetric corners.

steepen backward, as in Figure 2.4. Once again, there is no restriction on the number of singularities in the solutions to the CQ system for $c \neq c_R$. Thus, the CQ system system (2.79) has an infinite family of solutions, just as was the case with the solutions of (2.80).

The analytical solutions to the constant coefficient systems were employed in a numerical procedure designed to compute solutions to the Rayleigh wave equations (2.73) and (2.78). The details of the computational approach which was used are described in Chapter 3. Without loss of generality we rescaled the Q_k in (2.78) and (2.79) to take A out of (2.79), and κ out of both equations (2.78) and (2.79). Thus, the numerical results presented in Chapter 3 correspond to $\kappa = 1$, and because of that choice of κ, the $c \neq c_R$ numerical solutions presented there steepen forward, as in Figure 2.3. However, the $\kappa \neq 1$ solutions can be easily produced from the $\kappa = 1$ solutions through an appropriate rescaling.

2.5.2 The Ad Hoc Systems

The second set of equations proposed by G.B. Whitham to approximate (2.73) and (2.78) are the ad hoc systems whose coefficients are chosen to have the same asymptotic behavior for $n \to \infty$ and $k \to \infty$ as the $\alpha_{k,n}$ and $\beta_{k,n}$ in (2.72). Therefore, the ad hoc systems are expected to be very good approximations to the actual Q systems (2.73) and (2.78).

The ad hoc system corresponding to $c \neq c_R$ is

$$\begin{aligned} A\sum_{k=1}^{\frac{n-1}{2}} Q_k Q_{n-k} + A\sum_{k=1}^{\infty} \frac{n}{n+k} Q_k Q_{n+k} &= \kappa Q_n, \quad n \text{ odd}, \\ A\sum_{k=1}^{\frac{n-1}{2}} Q_k Q_{n-k} + \frac{1}{2} A Q_{\frac{n}{2}}^2 + A\sum_{k=1}^{\infty} \frac{n}{n+k} Q_k Q_{n+k} &= \kappa Q_n, \quad n \text{ even}, \end{aligned} \tag{2.84}$$

and for $c = c_R$, $\kappa = 0$ the ad hoc equations reduce to

$$\begin{aligned} &\sum_{k=1}^{\frac{n-1}{2}} Q_k Q_{n-k} + \sum_{k=1}^{\infty} \frac{n}{n+k} Q_k Q_{n+k} = 0, \quad n \text{ odd}, \\ &\sum_{k=1}^{\frac{n-1}{2}} Q_k Q_{n-k} + \frac{1}{2} Q_{\frac{n}{2}}^2 + \sum_{k=1}^{\infty} \frac{n}{n+k} Q_k Q_{n+k} = 0, \quad n \text{ even}. \end{aligned} \tag{2.85}$$

As in the case of the system (2.79), for an elastic material with a Poisson ratio of $\nu = 1/4$ a reasonable range for A is $2.8961 < A < 3.1548$.

In Chapter 3 both of the ad hoc systems (2.84) and (2.85) are solved numerically for an elastic material with $\nu = 1/4$, $p = 0.8475$, $s = 0.3933$. We show that the resulting numerical solutions are very close to the numerical solutions of the actual Rayleigh systems (2.73) and (2.78).

We experimented by solving the real and the ad hoc systems for other values of p and s, and those studies showed that the behavior of the numerical solutions does not change significantly as p and s are varied. Since changes in the scaling factors do not affect the numerical solutions significantly, then the ad hoc systems, which do not include the p and s scalings, must be appropriate approximations for the real Q equations (2.73) and (2.78).

At present there are no available exact solutions to the ad hoc systems (2.84) or (2.85). However, they appear to be more amenable to analysis since the p and s factors are not present in their equations. Our numerical studies provide empirical evidence that if analytic solutions to the ad hoc equations are found, they can be used as accurate approximations of steady-profile periodic Rayleigh waves in many practical applications.

Chapter 3 Numerical Results

Because of the inherent difficulty in solving the infinite systems (2.73) and (2.78) for the Fourier coefficients of the Rayleigh wave solutions exactly, we shall now proceed to study them numerically using the Newton-Raphson method for nonlinear equations.

First we shall describe in detail our numerical approach for the case of $c = c_R$, and then shall go on to discuss issues specific to the systems with $c \neq c_R$. This particular order of presentation was chosen because the solutions to the systems with $c = c_R$ have a simpler structure than those of the systems with $c \neq c_R$.

The predominant part of the numerical results presented in this chapter will be concerned with the behavior of the solution profiles on the surface of the elastic half-space, i.e., on $y = 0$. As discussed in Chapter 1, in relation to equations (1.1) and (1.2), the surface horizontal displacement $\xi(x, 0)$ uniquely determines the corresponding Rayleigh wave solutions for all x and y.

In the context of the periodic formulation of the problem, once we solve the systems (2.73) and (2.78) for the coefficients Q_k, we can construct the linear Rayleigh wave profiles using the following formulas:

$$\xi(x,y) = \frac{1}{1-\sigma^2}\sum_{k=1}^{\infty}\frac{Q_k}{k}\sin kx\big(e^{-kpy} - \sigma^2 e^{-ksy}\big), \tag{3.1}$$

$$\eta(x,y) = \frac{\sigma^2}{(1-\sigma^2)s}\sum_{k=1}^{\infty}\frac{Q_k}{k}\cos kx\big(\sigma^2 e^{-kpy} - e^{-ksy}\big), \tag{3.2}$$

$$D(x,y) = \frac{2c_2^2}{c_1^2}\sum_{k=1}^{\infty}Q_k\, e^{-kpy}\cos kx, \tag{3.3}$$

$$C(x,y) = \frac{-2\sigma^2}{s}\sum_{k=1}^{\infty}Q_k\, e^{-ksy}\sin kx. \tag{3.4}$$

Judging by the form of these expansions, the most singular type of behavior of the periodic wave profiles occurs when $y = 0$. For $y > 0$, the exponentials in the Fourier series smooth out the Rayleigh wave surface discontinuities. Therefore, the most challenging aspect of our numerical studies is to accurately resolve the Rayleigh wave solutions on the surface of the elastic half-space.

The Fourier series in (3.1) through (3.4) correspond to steady-profile linear Rayleigh wave solutions with surface horizontal displacements which are antisymmetric about the point $x = \pi$. This seems to illustrate all essential features and simplifies the details somewhat. In fact, we also take the surface horizontal displacements to be symmetric about the point $x = \pi/2$. This results in a further simplification of the Q equations since it reduces all even-numbered Fourier coefficients Q_{2m} to zero. These choices of symmetry are made in accordance with the Parker and Talbot original work in [16].

3.1 Computational Treatment of the Q Systems with $\mathbf{c = c_R}$

The first step we need to take in solving the Q system (2.73) numerically is to simplify the problem by truncating it to N equations with N unknowns. The truncation number N has to be significantly large for a number of reasons. Due to the special structure of the solutions to the constant coefficient system (2.80), their Fourier coefficients behave like $1/k$. Comparing the real Q system with the CQ system, we can argue that the Q_k of the former will decay slower than the Q_k of the latter. The coefficients $\beta_{k,n}$ already decay with k; therefore, the combined term $\beta_{k,n}Q_kQ_{n+k}$ can only match the order of the term Q_kQ_{n-k} in the constant coefficient case with a smaller decay in the Q_k. Therefore, we expect the Q system coefficients to decay slower than $1/k$ with k.

On the other hand, the numerically determined Q_k will be used to generate the

Fourier series of the curl and the divergence of the Rayleigh wave solutions. Since the Q_k have a very slow rate of decay, we need to employ a very large number of Fourier modes to reproduce the divergence and the curl within a reasonable level of accuracy. Thus, we need to consider a trucation number N which is quite large.

We shall iteratively generate a numerical solution of the form

$$Q_k^{(i+1)} = Q_k^{(i)} + \delta Q_k^{(i+1)}, \tag{3.5}$$

where $Q_k^{(i)}$ is the value of the coefficient Q_k at the i-th iteration step, and $\delta Q_k^{(i+1)}$ is the correction generated at the $i+1$ step. The numerical method we shall use is the Newton-Raphson method for systems of nonlinear equations. However, this method does not converge unless the initial guess for $Q_k^{(0)}$ is close enough to the solution we are looking to determine. We can now make use of the family of exact solutions to the constant coefficient system.

In fact, each one of the constant coefficient profiles can be successfully employed as an initial guess in the application of the Newton-Raphson method to the real Q system. The particular choice of a constant coefficient initial guess will be based on the expected properties of the horizontal displacement $\xi(x,0)$ for the profile to be determined. For example, if we want to produce a Rayleigh wave solution which has a $\xi(x,0)$ with two humps per period, located at specified positions along the x axis, we shall choose as an initial guess a solution to the constant coefficient system which has two corner singularities located exactly at the prescribed points. If we attempt to solve the Q system with an initial guess which does not have a structure resembling that of the corresponding solution to the CQ system, the proposed iterative method does not converge.

At each step of the iterative procedure the expression for $Q_k^{(i+1)}$ from (3.5) is substituted in the truncated version of the Q system, which is linearized about the already known values of the $Q_k^{(i)}$. The resulting linear system of N equations for the

unknowns $\delta Q_k^{(i)}$ is given by

$$\mathbf{M}\,(Q_k^{(i)})\;\delta Q_k^{(i+1)} = R\,(Q_k^{(i)}), \quad k = 1\ldots, N, \tag{3.6}$$

where $\mathbf{M}(Q_k^{(i)})$ is a non-singular $N \times N$ real matrix and $R(Q_k^{(i)})$ is a vector in R^N. We solve the linear system (3.6) for the $\delta Q_k^{(i+1)}$ using LU-matrix decomposition with relative maximum pivoting. The numerical scheme is terminated when a fixed point of the iterative process is reached. The procedure outlined here will be referred to as the numerical method I.

3.1.1 Numerical Solutions to the CQ System with $\mathbf{c = c_R}$

Numerical Method I

The performance of the numerical method I is tested first on the truncated constant coefficient system. We shall solve the truncated CQ system numerically, and then we shall compare the determined numerical solution with the corresponding exact solution of the infinite CQ system. Our goal is to find out how many Fourier modes are needed to reproduce the exact solution profiles with reasonable accuracy, and whether truncating the infinite CQ system affects the numerical solution in any significant way.

As discussed before, for $c = c_R$ we shall work with solutions which are symmetric about $x = \pi/2$. Therefore, the even-numbered Q_k will be equal to zero and the odd-numbered equations of the constant coefficient system (2.80) drop out. Accordingly, the constant coefficient system reduces to

$$E_{2m}\colon\ \frac{1}{2}\sum_{j=0}^{m-1} Q_{2j+1}Q_{2m-2j-1} + \sum_{j=0}^{\infty} Q_{2j+1}Q_{2m+2j+1} = 0, \quad m = 1, \ldots, \infty. \tag{3.7}$$

Here E_{2m} denotes the $2m$-th equation of the original CQ system (2.80).

Solution 1

First, we shall consider the simplest exact solution to the CQ system with

$$Q_k = \frac{\sin(\frac{k\pi}{2})}{k} = \begin{cases} \frac{(-1)^j}{2j+1} & \text{if } k \text{ is odd, } k = 2j+1,\ j = 0\ldots,\infty, \\ 0 & \text{if } k \text{ is even.} \end{cases} \tag{3.8}$$

The Fourier series of the surface profiles corresponding to this particular solution to the CQ equations can be determined by substituting the formula (3.8) into the Fourier expansions (3.1) through (3.4). In this manner we obtain the following expressions for the Rayleigh wave profiles on the surface of the elastic half-space:

$$\xi(x,0) = \sum_{j=0}^{\infty} \frac{(-1)^j \sin(2j+1)x}{(2j+1)^2}, \tag{3.9}$$

$$\eta(x,0) = -\frac{\sigma^2}{s} \sum_{j=0}^{\infty} \frac{(-1)^j \cos(2j+1)x}{(2j+1)^2}, \tag{3.10}$$

$$D(x,0) = \frac{2c_2^2}{c_1^2} \sum_{j=0}^{\infty} \frac{(-1)^j \cos(2j+1)x}{2j+1}, \tag{3.11}$$

$$C(x,0) = -\frac{2\sigma^2}{s} \sum_{j=0}^{\infty} \frac{(-1)^j \sin(2j+1)x}{2j+1}. \tag{3.12}$$

We shall employ 1500 Fourier modes of the form (3.8) as an initial guess for the iterative scheme. After determining the corresponding numerical solution, we resubstitute it back into the truncated CQ equations. The equations are satisfied to the order of 10^{-12}, which confirms that the iteratively generated solution has high degree of accuracy. It is important to note that in this case only four iterations of the numerical procedure are required to reach a fixed point solution. Indeed, since we use the exact solution to the infinite CQ system as an initial guess, we expect the iterative scheme to converge very fast when applied to the truncated version of the same system.

In Figures 3.1 through 3.4 we show the $\xi(x,0)$, $\eta(x,0)$, $D(x,0)$, and $C(x,0)$

generated using the computed Q_k in the Fourier expansions (3.1) through (3.4). A direct comparison of these profiles with the corresponding profiles of the exact solution 1 to the CQ system reveals that they are extremely close. If we add plots of the exact solution profiles to those of the numerically determined profiles in Figures 3.1 through 3.4, the two sets of plots would be indistinguishable.

In the first two columns of Table 3.1, the Q_k computed via the currently discussed numerical method I are compared to their corresponding exact values. We have chosen to denote a jump in the value of the index k in Table 3.1 and all subsequent tables by a double horizontal line. The first two columns of Table 3.1 reveal some notable differences between the numerical and the exact Fourier coefficients. As evident from (3.8) the exact values for the Q_k monotonically decrease with k. However, only up to about two-thirds of the computed coefficients decrease monotonically with k. In fact, the later portion of these coefficients, as illustrated in column 2 of Table 3.1, grow in absolute value as k increases. This effect is caused by the truncation of the infinite CQ system to a finite system which excludes the higher-order modes. The later portion of the modes which are included in the computations try to accommodate for the missing higher-order modes by changing in value.

To illustrate this, let us study the equations used to compute a five mode numerical solution to the CQ system consisting of Q_1, Q_3, Q_5, Q_7, and Q_9. In this case all modes higher than the ninth are taken to be zero, so we end up with the following truncated system:

$$\underset{+}{Q_1^2}/2 + \underset{-}{Q_1 Q_3} + \underset{-}{Q_3 Q_5} + \underset{-}{Q_5 Q_7} + \underset{-}{Q_7 Q_9} + 0 = 0, \tag{3.13}$$

$$\underset{-}{Q_1 Q_3} + \underset{+}{Q_1 Q_5} + \underset{+}{Q_3 Q_7} + \underset{+}{Q_5 Q_9} + 0 + 0 = 0, \tag{3.14}$$

$$\underset{+}{Q_1 Q_5} + \underset{+}{Q_3^2}/2 + \underset{-}{Q_1 Q_7} + \underset{-}{Q_3 Q_9} + 0 + 0 + 0 = 0, \tag{3.15}$$

$$\underset{-}{Q_1 Q_7} + \underset{-}{Q_3 Q_5} + \underset{+}{Q_1 Q_9} + 0 + 0 + 0 + 0 = 0, \tag{3.16}$$

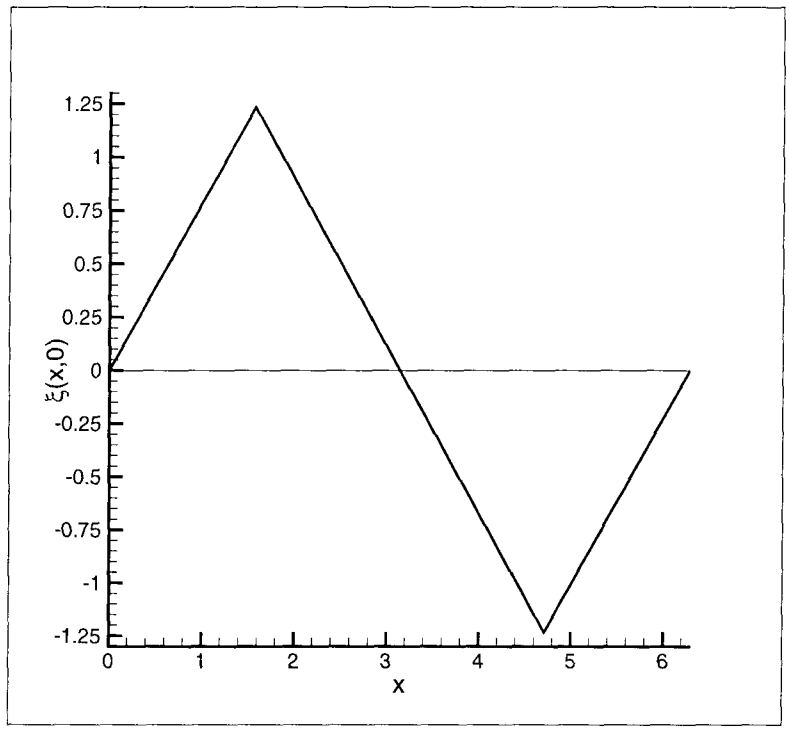

Figure 3.1: The horizontal displacement $\xi(x,0)$ of numerical solution 1 to the CQ system with $c = c_R$.

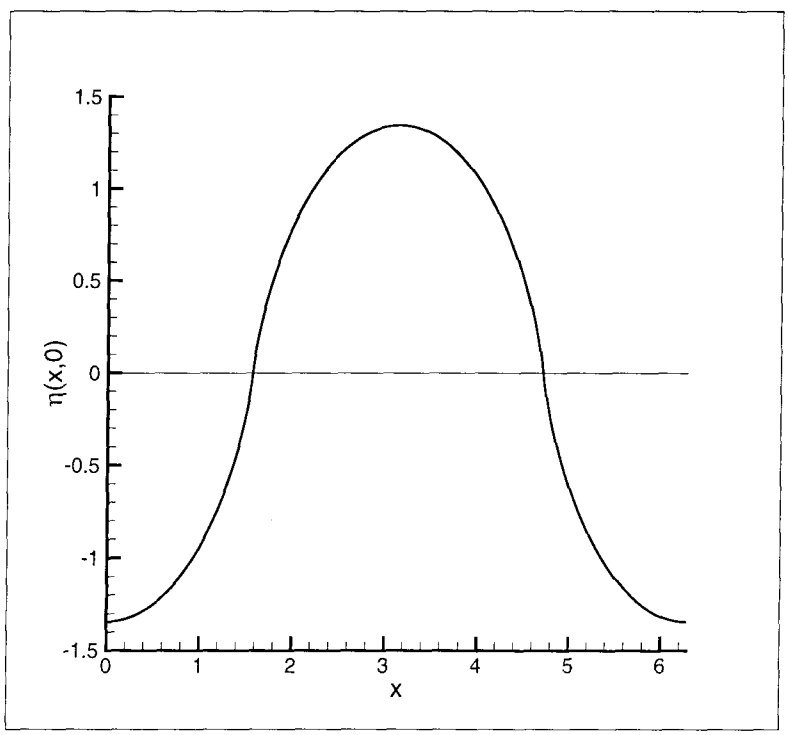

Figure 3.2: The vertical displacement $\eta(x,0)$ of numerical solution 1 to the CQ system with $c = c_R$.

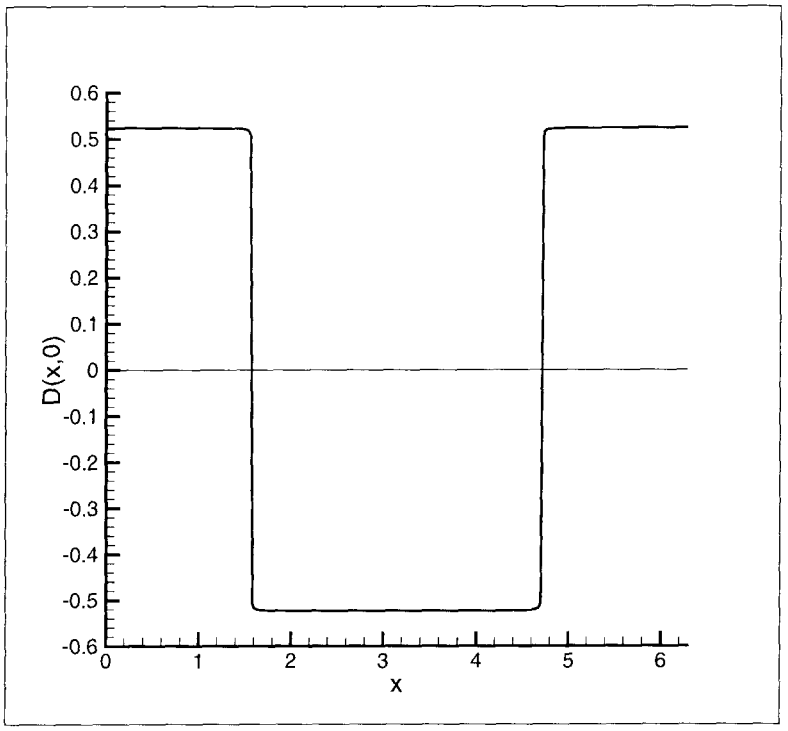

Figure 3.3: The divergence $D(x,0)$ of numerical solution 1 to the CQ system with $c = c_R$.

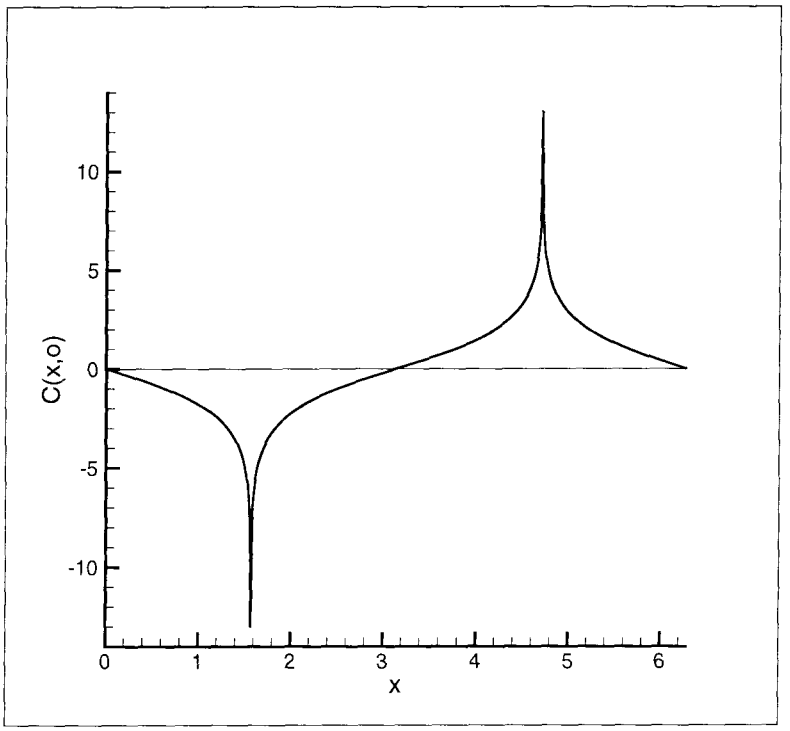

Figure 3.4: The curl $C(x,0)$ of numerical solution 1 to the CQ system with $c = c_R$.

Q_k	Q_k exact	Q_k numerical I	Q_k numerical II
Q_1	1.00000000	1.00000000	1.00000000
Q_3	-0.33333333	-0.33329642	-0.33333129
Q_5	0.20000000	0.19995578	0.19999755
Q_7	-0.14285714	-0.14280986	-0.14285453
Q_9	0.11111111	0.11106217	0.11110841
Q_{11}	-0.09090909	-0.09085913	-0.09090633
Q_{21}	0.04761905	0.04756722	0.04761622
Q_{31}	-0.03225807	-0.03220593	-0.03225527
Q_{41}	0.02439024	0.02433822	0.02438751
Q_{51}	-0.01960784	-0.01955611	-0.01960518
Q_{101}	0.00990099	0.00985151	0.00989883
Q_{199}	-0.00502513	-0.00498093	-0.00502418
Q_{501}	0.00199601	0.00196904	0.00199967
Q_{751}	-0.00133156	-0.00131949	-0.00133974
Q_{1001}	0.00099900	0.00100285	0.00101238
Q_{1251}	-0.00079936	-0.00082083	-0.00081878
Q_{1501}	0.00066622	0.00070807	0.00069283
Q_{1751}	-0.00057110	-0.00063781	-0.00060653
Q_{1997}	0.00050075	0.00059932	0.00054737
Q_{1999}	-0.00050025	-0.00059912	-0.00054697
Q_{2501}	0.00039984	0.00062398	0.00048750
Q_{2751}	-0.00036350	-0.00076845	-0.00050373
Q_{2993}	0.00033411	0.00414600	0.00130050
Q_{2995}	-0.00033389	-0.00496911	-0.00149457
Q_{2997}	0.00033367	0.00661723	0.00188259
Q_{2999}	-0.00033344	-0.01321747	-0.00343400

Table 3.1: A comparison of the exact coefficients of solution 1 to the CQ system with $c = c_R$ with the coefficients determined via the original (I) and the modified (II) numerical methods.

where Q_1 is fixed to 1 and Q_3, Q_5, Q_7 and Q_9 are the unknowns. The zeros in equations (3.13) through (3.16) denote products of one of the coefficients Q_3, Q_5, Q_7 and Q_9 with a higher-order coefficient which has been set to zero.

For the numerical solution which we are considering now, namely solution 1 as

given in Figure 3.1, the terms Q_1Q_7 and Q_3Q_5 in (3.16) are negative while $Q_1Q_9 = Q_9$ is positive; therefore, the truncation of the CQ system to five modes requires that $Q_1Q_7 + Q_3Q_5 = -Q_9$. For the exact CQ system, however, the positive sum $Q_1Q_7 + Q_3Q_5$ is balanced by the infinite negative sum

$$\sum_{j=0}^{\infty} Q_{2j+1}Q_{2j+9}, \tag{3.17}$$

of which Q_9 is just the first term. Thus when we take Q_k with $k > 9$ in (3.16) to be zero, we are forcing the numerically computed Q_9 to be considerably larger than Q_9-exact. A higher value of Q_9 in turn influences the balance of terms in (3.15) and correspondingly alters the value of $|Q_7|$. A change in the values of Q_7 and Q_9 then affects equation (3.14), which we solve for Q_5, and so the effect of "tainting" propagates from the higher-order modes to the lower-order modes. The further away we get from the last equation of the truncated system, the less perceptible the effect of tainting. The coefficient which is most significantly affected by the truncation is the highest-order one; in this case Q_9.

This brief example indicates that no matter how we truncate the infinite Q systems, we shall not be able to avoid some level of "tainting," which will be more pronounced in the case of the higher-order computed coefficients Q_k. It helps to consider a very large number of equations which confines the sizeable effects of "tainting" to the higher-order coefficients. If we include the high-order "tainted" modes in the Fourier representations of the numerical profiles, we do not produce profiles which are consistent with the known exact solutions. But if we consider only a portion of the computed coefficients, in our case the first two-thirds of the Q_k's, the numerically determined profiles check very well with the known exact profiles.

In all subsequent analysis and generation of plots, we shall disregard the last third of the determined Fourier coefficients. The higher the number of the Fourier modes we solve for, the less perceivable the impact of "tainting" for the higher-order

Fourier modes. The importance of computing a large enough number of Fourier modes is amplified by the fact that we can only retain two-thirds of the generated coefficients. As a consequence the linear systems of the form (3.6), solved as part of the iterative scheme, end up being significantly large.

The Modified Numerical Method II

One way to improve the accuracy of our scheme is to make use of the fact that we know the exact form of the Fourier coefficients for the analytic solution to the CQ system. Our ultimate goal is to produce accurate numerical solutions to the real Q system, and certainly in that case we do not have an available analytic solution. However, as will be discused in Section 3.1.4, we can get an approximate formula for the higher-order Fourier coefficients of the real Q system solutions. Thus, we can modify our numerical approach to incorporate approximate forms for the higher-order Q_k in the numerical computation of the lower-order Q_k. We shall describe the relevant modifications for the real Q system in Section 3.1.5. First, we shall focus on the modifications pertinent to the CQ system.

For simplicity, we shall describe the proposed improvement on the CQ system with five modes. When we examined the equations (3.13) through (3.16), we saw that by taking all Q_k with $k > 11$ to be equal to zero, we induce a sizable shift in the computed values for the higher-order coefficients. Now, we shall once again solve a system of four equations for four unknowns, namely Q_3, Q_5, Q_7 andQ_9, but this time we shall include the exact values for Q_{11}, Q_{13}, Q_{15} and Q_{17} in the equations we solve. We end up with the system

$$\underset{+}{Q_1^2/2} + \underset{-}{Q_1Q_3} + \underset{-}{Q_3Q_5} + \underset{-}{Q_5Q_7} + \underset{-}{Q_7Q_9} + \underset{-}{Q_9\widetilde{Q}_{11}} + \underset{-}{\widetilde{Q}_{11}\widetilde{Q}_{13}} + \underset{-}{\widetilde{Q}_{13}\widetilde{Q}_{15}} + \underset{-}{\widetilde{Q}_{15}\widetilde{Q}_{17}} = 0,$$

$$\underset{-}{Q_1Q_3} + \underset{+}{Q_1Q_5} + \underset{+}{Q_3Q_7} + \underset{+}{Q_5Q_9} + \underset{+}{Q_7\widetilde{Q}_{11}} + \underset{+}{\widetilde{Q}_9\widetilde{Q}_{13}} + \underset{+}{\widetilde{Q}_{11}\widetilde{Q}_{15}} + \underset{+}{\widetilde{Q}_{13}\widetilde{Q}_{17}} = 0,$$

$$\underset{+}{Q_1Q_5} + \underset{+}{Q_3^2/2} + \underset{-}{Q_1Q_7} + \underset{-}{Q_3Q_9} + \underset{-}{Q_5\widetilde{Q}_{11}} + \underset{-}{Q_7\widetilde{Q}_{13}} + \underset{-}{Q_9\widetilde{Q}_{15}} + \underset{-}{\widetilde{Q}_{11}\widetilde{Q}_{17}} = 0,$$

$$\underset{-}{Q_1}\underset{-}{Q_7} + \underset{-}{Q_3}\underset{-}{Q_5} + \underset{+}{Q_1}\underset{+}{Q_9} + \underset{+}{Q_3}\underset{+}{\widetilde{Q}_{11}} + \underset{+}{Q_5}\underset{+}{\widetilde{Q}_{13}} + \underset{+}{Q_7}\underset{+}{\widetilde{Q}_{15}} + \underset{+}{Q_9}\underset{+}{\widetilde{Q}_{17}} = 0,$$

where the $\widetilde{Q}_k$, $k = 11, 13, 15, 17$ denote the exact values for the solution 1 coefficients, as given by the formula (3.8). The same formula is also used to generate the initial guess Q_k, $k = 1, \ldots, 17$, where k is odd. Then the modified system is solved for Q_3, Q_5, Q_7 and Q_9 using the Newton-Raphson method. The $\widetilde{Q}_k$ with $k = 11, 13, 15, 17$ are kept fixed to their initial (and exact) values in the course of all iterations.

In summary, we intend to include in the truncated CQ equations twice as many modes as we solve for. We keep the later half of the modes fixed to the exact values prescribed by the analytic solution to the CQ system used as an initial guess. In this manner, the "tainting" of the higher order modes, though not fully eliminated, is greatly diminished. To illustrate this, in the third column of Table 3.1 we give the values of the Q_k generated using the proposed modification. Clearly, the degree of accuracy increases, and the effect of tainting goes down significantly.

The numerical results presented in this chapter were generated by solving systems of 1500 equations with 1500 unknowns, and then employing only the first 1000 of the computed coefficients. We experimented with solving systems of 100, 200, 300, 500, 750, 1000, 1500, and 2000 modes. The numerical solutions employing 1000 out of a total of 1500 generated modes seemed to provide the best resolution without becoming computationally cumbersome. We also compared the surface profiles generated with increasing numbers of modes, and made sure that the computational scheme produces consistent results at different levels of resolution.

We determined that the Fourier series of the horizontal and vertical displacements of the considered solutions do not require as many as a thousand modes to be properly resolved. In fact, adding modes higher than Q_{200} does not seem to visibly alter the surface displacement profiles. It is the divergence and the curl of the solutions to the constant coefficient system which require on the order of a thousand

modes for their Fourier representations to be accurate.

Another way to estimate the validity of using the first M Fourier modes in representing the solutions to the CQ system is to substitute the numerically determined Q_{2j+1}, $0 \leq j \leq M-1$ in the CQ equations, and to compare the resulting values with the corresponding analytical expressions for the remainders. The remainder of equation E_{2m} of the CQ system (3.7), with M Fourier modes included, has the form

$$R_{2m}^{M} = \sum_{j=M}^{\infty} Q_{2j-2m+1} Q_{2j+1} = \sum_{j=M}^{\infty} \frac{(-1)^m}{(2j-2m+1)(2j+1)}, \tag{3.18}$$

which telescopes to

$$R_{2m}^{M} = \frac{(-1)^m}{2m} \sum_{j=M-m}^{M} \frac{1}{2j+1}. \tag{3.19}$$

If we substitute the exact values for Q_{2j+1}, $0 \leq j \leq M-1$ in equation E_{2m} of the CQ system, we will get exactly $-R_{2m}^{M}$. If we substitute the numerically determined Q_{2j+1}, $0 \leq j \leq M-1$ in E_{2m}, we need to obtain a value which is very close to $-R_{2m}^{M}$.

We compared the numerically predicted with the analytical values for R_{2m}^{M} for various m and M. When the numerical computations are performed with 1500 Fourier modes, the best approximation for the remainders is provided by taking 1000 modes of the total 1500 generated modes. This is illustrated in Table 3.2. The results presented there indicate that the remainders for the CQ system are reproduced with an accuracy of 10^{-4}, except for the first 25 equations where the level of accuracy goes down to 10^{-3}. Also, the remainders computed using the modified numerical method II represent a considerable improvement over the remainders computed via the numerical method I.

The exact solution to the constant coefficient system indicates that the surface singularities in the curl are logarithmic in nature, and therefore the expected value

$2m$	$-R_{2m}^{1000}$ exact	$-R_{2m}^{1000}$ numerical I	$-R_{2m}^{1000}$ numerical II
2	-0.00025013	-0.00050748	-0.00023802
4	0.00025025	0.00047061	0.00023611
6	-0.00025038	-0.00044855	-0.00023502
8	0.00025050	0.00043285	0.00023428
10	-0.00025063	-0.00042068	-0.00023374
20	0.00025126	0.00038310	0.00023230
50	-0.00025318	-0.00033486	-0.00023157
100	0.00025647	0.00030087	0.00023299
250	-0.00026706	-0.00026422	-0.00024148
500	0.00028768	0.00025243	0.00026120
750	-0.00031334	-0.00026221	-0.00028726
1000	0.00034657	0.00028767	0.00032223
1250	-0.00039233	-0.00033264	-0.00037178
1500	0.00046210	0.00041137	0.00044915
1750	-0.00059413	-0.00057355	-0.00059796
1996	0.00155426	0.00175796	0.00166370
1998	-0.00171954	-0.00195698	-0.00184485

Table 3.2: Comparison of the exact and the numerically determined remainders for the CQ system with $c = c_R$. The numerical remainders are computed using 1000 out of 1500 generated Fourier modes.

for the curl at the singular points is infinity. From the plot of the curl on Figure 3.4, we can see that the infinite value for the curl at the singular points $\frac{\pi}{2}$ and $\frac{3\pi}{2}$ is approached. The larger the number of modes included in the Fourier expansion for the curl, the better its approximation at the singular points. There is a limit, however, on how many modes we can efficiently handle at present with the numerical iterative procedure. We feel that with 1000 Fourier coefficients the qualitative behavior of the curl at the surface singularities is captured with a satisfactory level of accuracy.

The proposed numerical scheme was tested with a variety of profiles representing solutions to the CQ system. In all of the cases examined, the numerical solutions reproduced the displacements, curl, and divergence of the exact solutions with very high levels of accuracy.

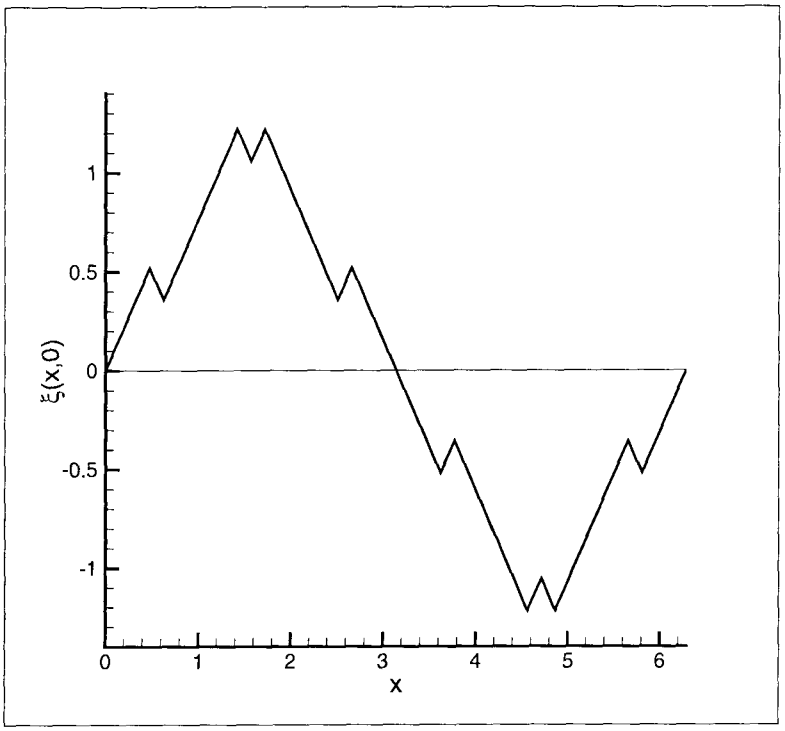

Figure 3.5: The horizontal displacement $\xi(x,0)$ of numerical solution 2 to the CQ system with $c = c_R$.

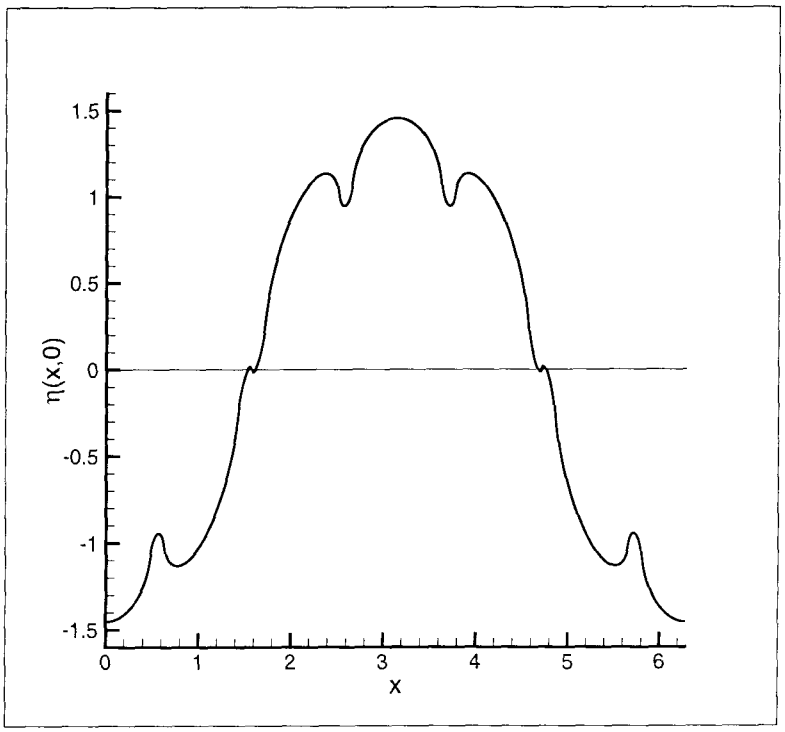

Figure 3.6: The vertical displacement $\eta(x,0)$ of numerical solution 2 to the CQ system with $c = c_R$.

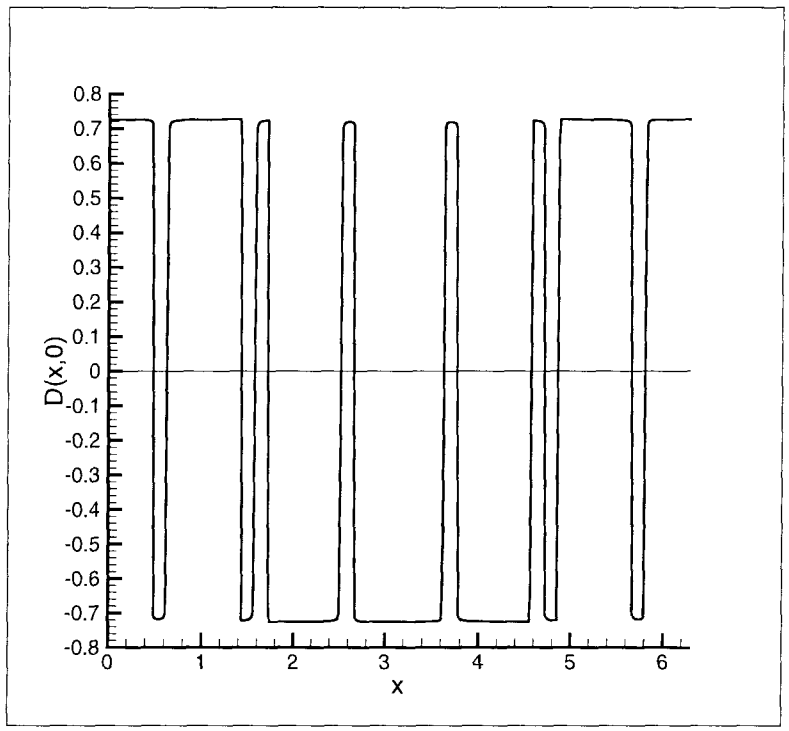

Figure 3.7: The divergence $D(x,0)$ of numerical solution 2 to the CQ system with $c = c_R$.

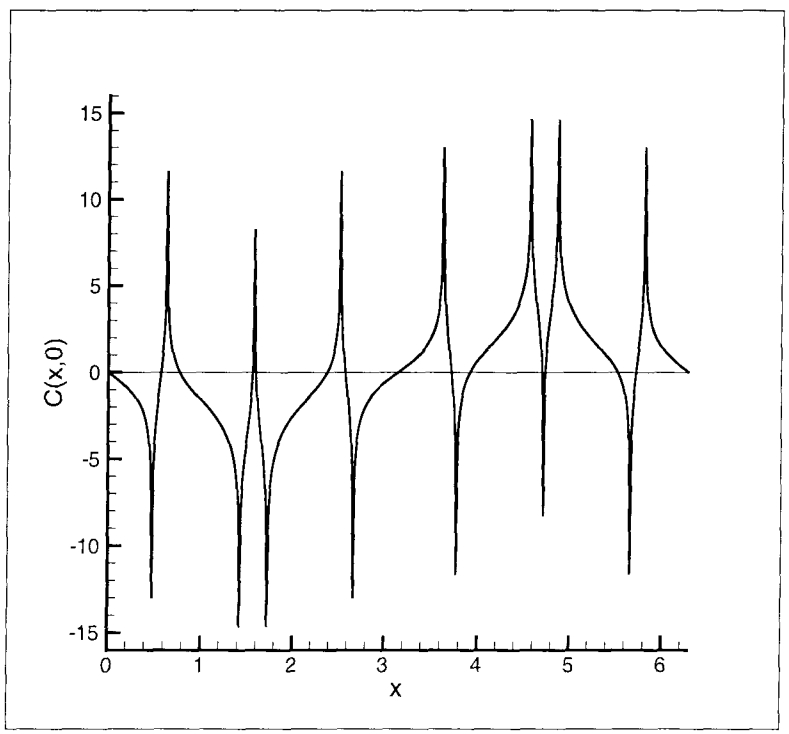

Figure 3.8: The curl $C(x,0)$ of numerical solution 2 to the CQ system with $c = c_R$.

Solution 2

As an example of a CQ system numerical solution with a more complex structure than solution 1, in Figures 3.5 through 3.8 we show the numerically determined profiles corresponding to the initial guess

$$Q_k = \frac{\sin\frac{k\pi}{2}(1-2\cos ka)+(\sin k(a+b)-\sin kb)(1-\cos k\pi)}{k\,(1-2\cos ka+2\sin k(a+b)-2\sin kb)},\ 1\le k\le 3000,$$

where $a = 0.15$ and $b = 0.48$. Since every even-numbered Q_k defined by this formula is zero, then the total number of Fourier coefficients which we consider is 1500.

Once again, if superimposed, plots of the exact and the numerical solutions cannot be distinguished. Even though the surface profiles have a reasonably complicated structure in this case, the numerical solution still captures the exact solution behavior very accurately.

3.1.2 Numerical Solutions to the Real Q System with $c = c_R$

Having established that our numerical procedure reproduces correctly the solutions to the CQ system, we now go on to find solutions to the real Q equations, as given by (2.73). We consider the case of a harmonic material of a Poisson ratio $\nu = 1/4$. The corresponding values for p and s are $p = 0.8475$ and $s = 0.3933$.

On Figures 3.9 through 3.30, we display the surface displacements, curl, and divergence for a selection of our numerical solutions to the real Q system (2.73).

Solution 1

Solution 1 was generated using as an initial guess the simplest constant coefficient periodic profile $\xi(x,0)$, as given by

$$\xi(x,0) = \sum_{k=1}^{3000} \frac{\sin\frac{k\pi}{2}\sin kx}{k^2}$$

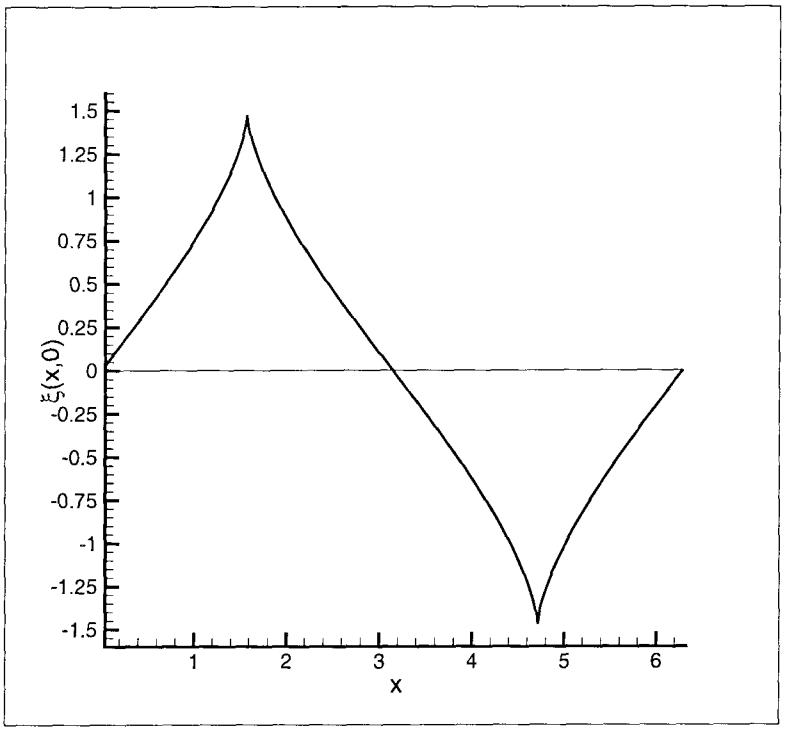

Figure 3.9: The horizontal displacement $\xi(x,0)$ of solution 1 to the Q system with $c = c_R$.

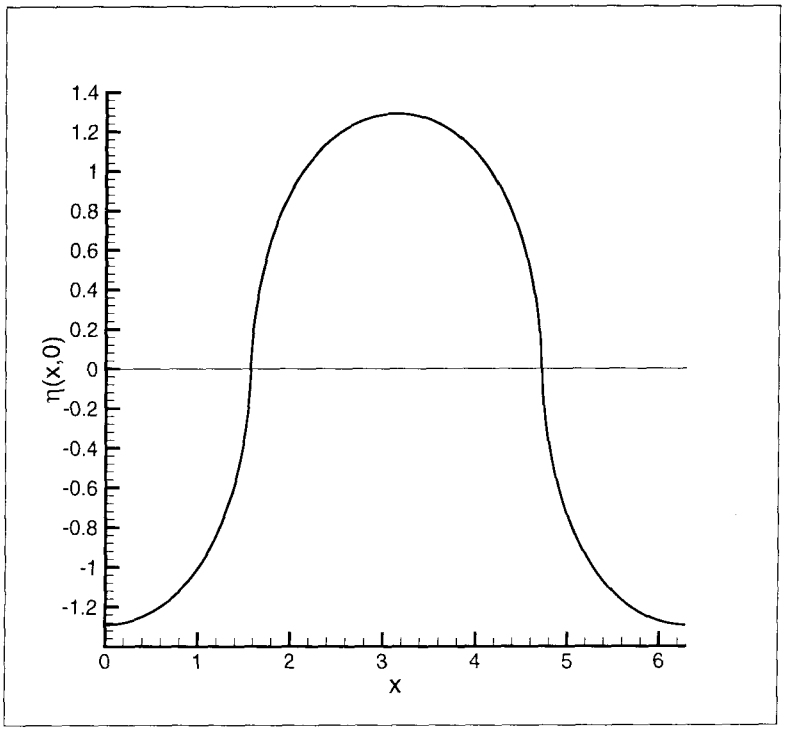

Figure 3.10: The vertical displacement $\eta(x,0)$ of solution 1 to the Q system with $c = c_R$.

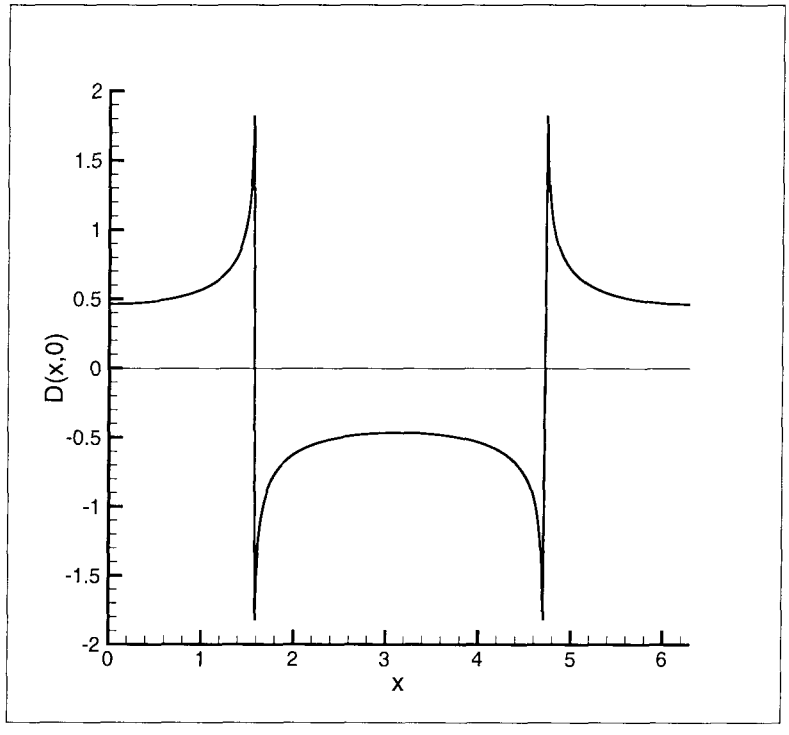

Figure 3.11: The divergence $D(x, 0)$ of solution 1 to the Q system with $c = c_R$.

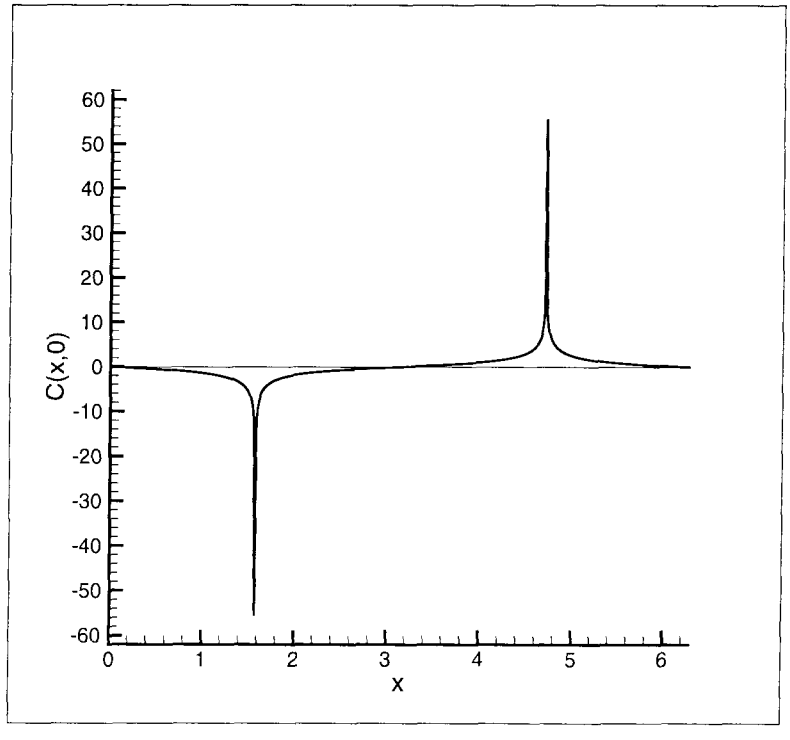

Figure 3.12: The curl $C(x, 0)$ of solution 1 to the Q system with $c = c_R$.

where

$$Q_k = \frac{\sin\frac{k\pi}{2}}{k}, \quad 1 \leq k \leq 3000. \tag{3.20}$$

In the formula above we have reverted to the k notation. Once again, all even-numbered Q_k are zero due to the $\sin\frac{k\pi}{2}$ factor, and effectively we are considering 1500 modes.

The resulting numerical solution to the real Q system displays a qualitatively new behavior at the singularities of its horizontal displacement. While the CQ system solution (3.9) has singularities which are corners, the corresponding solution to the real Q system has cusps. In fact, for all of our numerically determined solutions to the real Q system, the general features of the constant coefficient profile used as an initial guess are preserved, but the type of singularity changes from a corner to a cusp.

Since a cusp in the surface horizontal displacement translates to a higher order singularity in the curl and divergence, the need to employ a significantly large number of modes in resolving the solution profiles is further amplified.

Solutions 2 and 3

The surface horizontal displacement $\xi(x,0)$ of solution 1 has the simplest possible shape at the surface - a positive cusp at $\frac{\pi}{2}$, and a negative cusp at $\frac{3\pi}{2}$. The horizontal displacements of solutions 2 and 3 have a more complicated structure. They were chosen to correspond to the numerical solutions of the real Q system presented by Parker and Talbot in [16]. Solution 2 was generated using the initial guess

$$Q_k = \frac{\sin\frac{k\pi}{2}}{k}\,\frac{1-2\cos 0.15k}{1-2\cos 0.15}, \; 1 \leq k \leq 3000, \tag{3.21}$$

and the initial guess used to compute solution 3 is

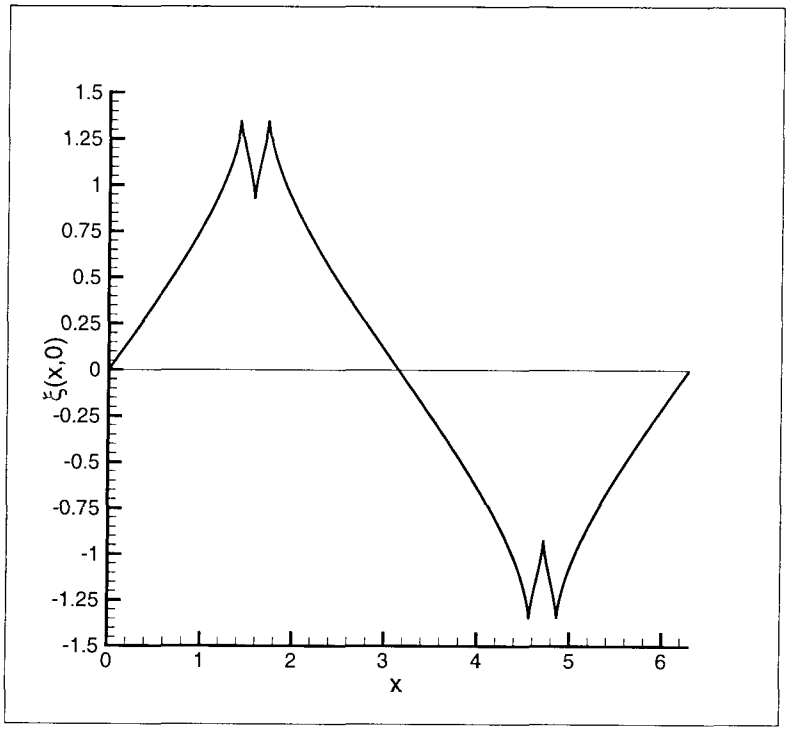

Figure 3.13: The horizontal displacement $\xi(x, 0)$ of solution 2 to the Q system with $c = c_R$.

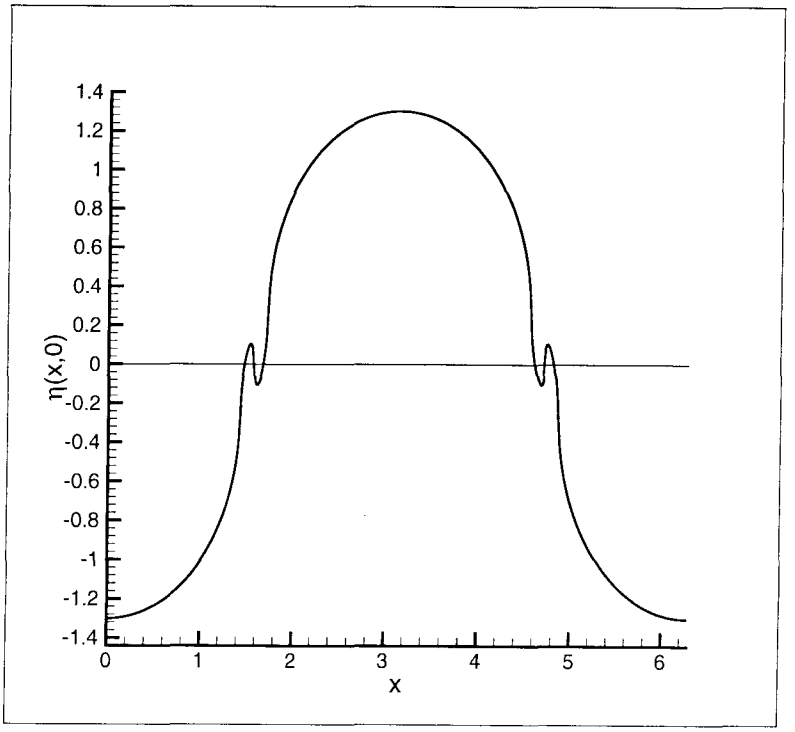

Figure 3.14: The vertical displacement $\eta(x, 0)$ of solution 2 to the Q system with $c = c_R$.

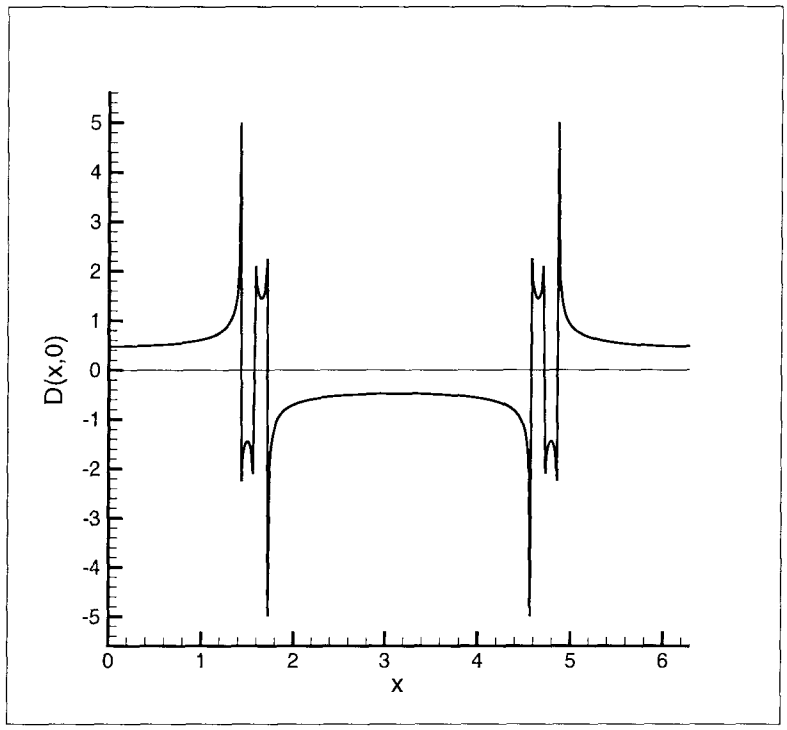

Figure 3.15: The divergence $D(x,0)$ of solution 2 to the Q system with $c = c_R$.

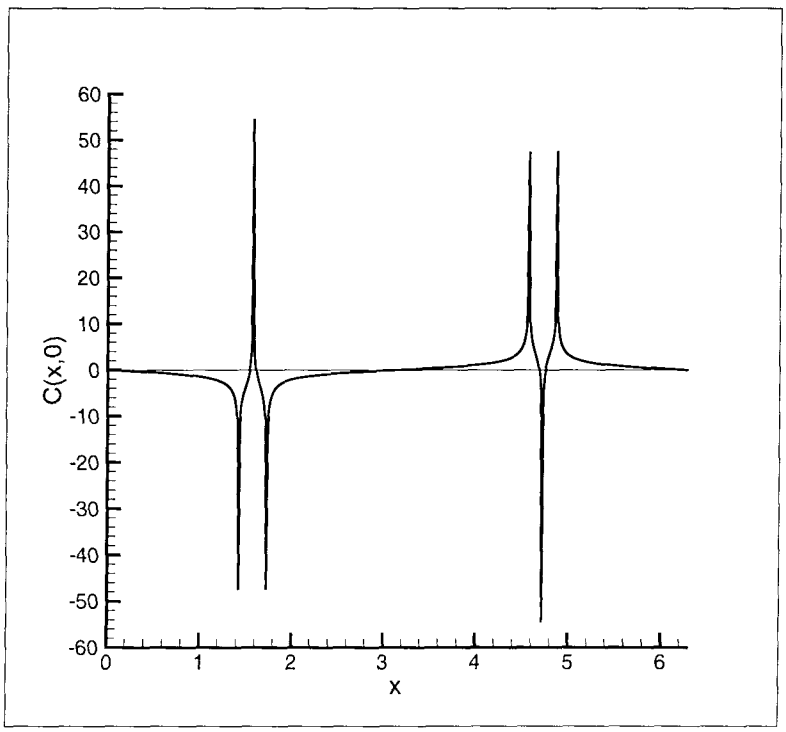

Figure 3.16: The curl $C(x,0)$ of solution 2 to the Q system with $c = c_R$.

$$Q_k = \frac{\sin\frac{k\pi}{2}(1-2\cos ka)+(\sin k(a+b)-\sin kb)(1-\cos k\pi)}{k\,(1-2\cos ka+2\sin k(a+b)-2\sin kb)},\ 1\le k\le 3000. \tag{3.22}$$

In the original work of Parker and Talbot, where a maximum of 20 non-zero Fourier modes were considered, the horizontal displacement singularities resemble finite corners, as displayed in Figures 1.1 and 1.2. The number of modes used to represent these profiles being small, some of the peaks in the computed $\xi(x,0)$ could also be interpreted as numerical instabilities. In fact, Parker and Talbot noted in [16] that their surface displacement profiles with $c = c_R$ might have inaccuracies as large as 0.02, so that the details of these profiles could possibly be erroneous.

However, when 1000 Fourier modes are used to represent the numerical solutions, the surface singularities clearly develop a cusp-like appearance. It also becomes evident that what could have been considered as numerical solution errors, or instabilities in the Parker-Talbot solutions, are actually genuine peaks in the surface horizontal displacements. As more modes are employed, the singular behavior of the surface horizontal displacements becomes more pronounced, and it increasingly exhibits fractional singularity characteristics.

The most important step in generating solutions 2 and 3 with our numerical scheme was to determine the constant coefficient system solutions to be employed as initial guesses. As discussed in Chapter 2, the solutions to the CQ system with $c = c_R$ can have any number of symmetrically shaped corners in their horizontal displacements. So in order to generate the required initial guesses, we place a symmetrically shaped corner at each location along the horizontal displacements of the Parker and Talbot solutions, where there is indication of singular behavior. To illustrate this, in Figures 3.21 through 3.26 we provide a comparison of the horizontal displacements of solutions 2 and 3 as given by Parker and Talbot, and the corresponding initial guesses for our numerical scheme. In each case we have plotted the Parker-Talbot profiles using all Fourier coefficients given in [16].

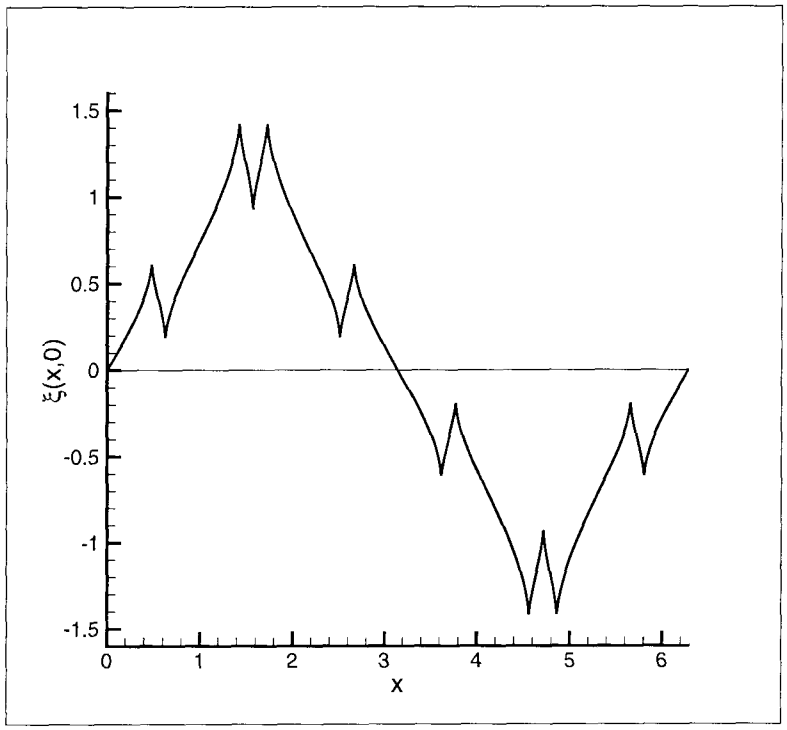

Figure 3.17: The horizontal displacement $\xi(x, 0)$ of solution 3 to the Q system with $c = c_R$.

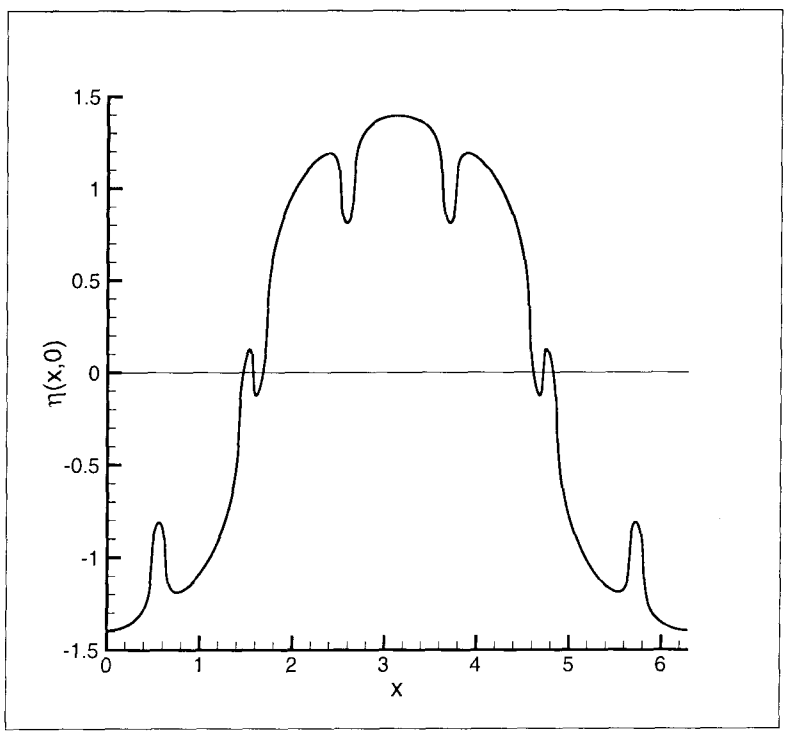

Figure 3.18: The vertical displacement $\eta(x, 0)$ of solution 3 to the Q system with $c = c_R$.

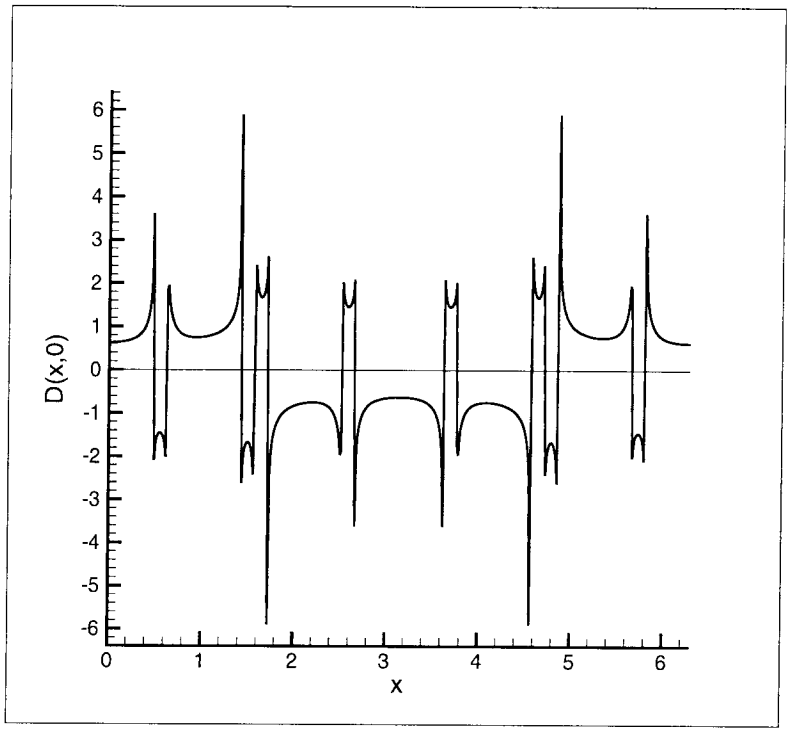

Figure 3.19: The divergence $D(x,0)$ of solution 3 to the Q system with $c = c_R$.

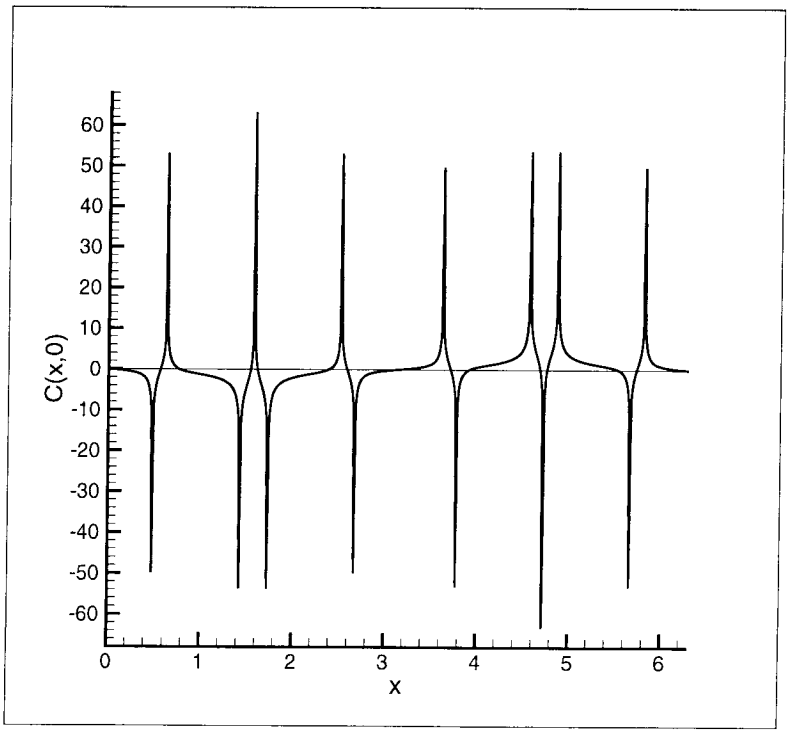

Figure 3.20: The curl $C(x,0)$ of solution 3 to the Q system with $c = c_R$.

Parker and Talbot computed their numerical solutions using an iterative procedure based on the Newton-Raphson method applied to a system of N equations with N unknowns, with N being successively increased. After the iterative procedure converges approximately for N equations, the number of unknowns is increased to $N + m$. The starting values of the additional m unknowns are taken to be zero, while the first N coefficients are set to equal the values found as a solution to the previous N equations. Parker and Talbot increased the number of unknowns by $m = 5$, since that choice of m produced an acceptable rate of convergence. The initial guess for their numerical iteration is determined by analytically solving the Q equations truncated to just three modes: $Q_1 = 1$, Q_3, and Q_5. The resulting equations can be reduced to a single quadratic equation which has two different solutions for the set of unknowns Q_3 and Q_5. Thus Parker and Talbot had two possible ways of initiating their iterative procedure, and therefore they generated two different solutions corresponding to the Q equations with $c = c_R$. However, the three mode initial guesses used by Parker and Talbot did not produce the simplest possible solution to the Q system, namely solution 1 in Figure 3.9.

In the case of our numerical procedure, there is an infinite family of possible initial guesses, namely the exact solutions to the constant coefficient system with $c = c_R$. We can start the iteration with as many modes as we wish as long as we can efficiently handle the matrices involved in the Newton-Raphson procedure. With 1500 modes it took on the order of 40 minutes to complete one iteration, and about 20 iterations were needed to reach a fixed point solution. One should also keep in mind that the more complicated the $\xi(x, 0)$ in the initial guess, the longer it takes for the iterative process to reach a fixed point solution.

It should be stressed that it is important to consider a significantly large number of Q_k in order to properly resolve the singularities in the surface displacements, curl and divergence, since the last third of the numerically determined coefficients have to be discarded due to "tainting." It appears that Parker and Talbot also encountered

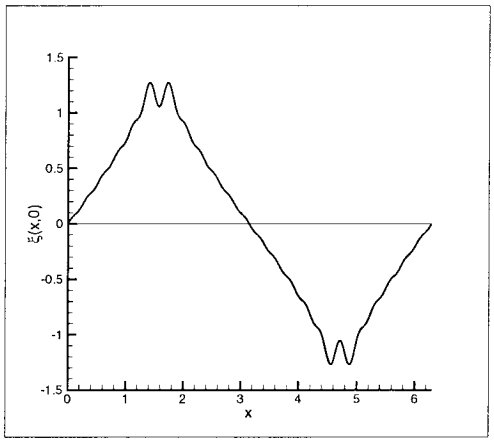

Figure 3.21: The horizontal displacement $\xi(x,0)$ of the first Parker-Talbot solution plotted using 12 Fourier modes.

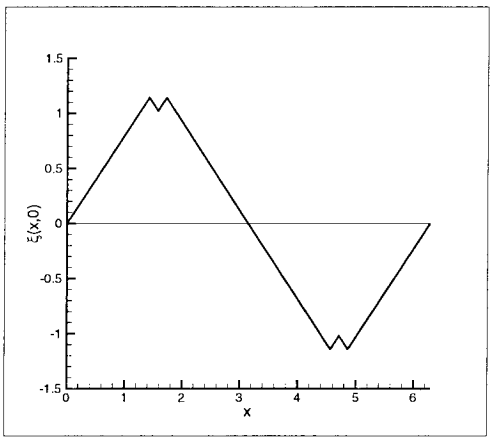

Figure 3.22: The horizontal displacement $\xi(x,0)$ of the constant coefficient profile we used as an initial guess to generate a solution corresponding to the one in Figure 3.21.

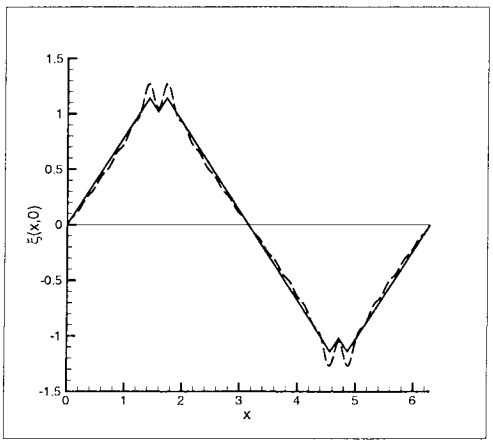

Figure 3.23: Comparison of the horizontal displacements $\xi(x,0)$ of the first Parker solution to the Q system — and the corresponding constant coefficient profile we used as an initial guess in our iterative scheme - - - .

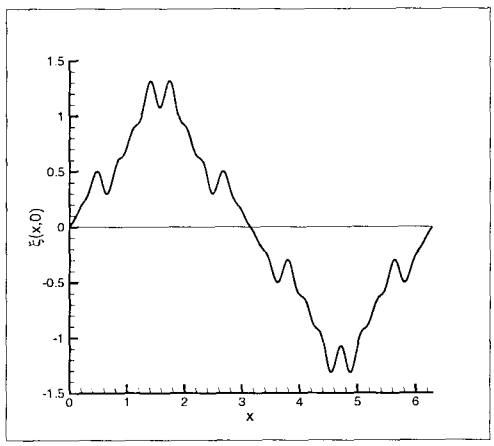

Figure 3.24: The horizontal displacement $\xi(x,0)$ of the second Parker-Talbot numerical solution plotted using 12 Fourier modes.

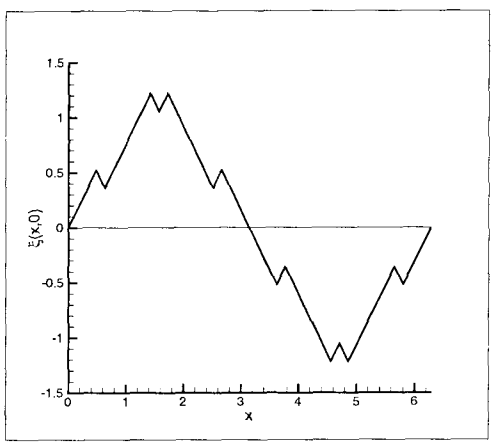

Figure 3.25: The horizontal displacement $\xi(x,0)$ of the constant coefficient profile we used as an initial guess to generate a solution corresponding to the one in Figure 3.24.

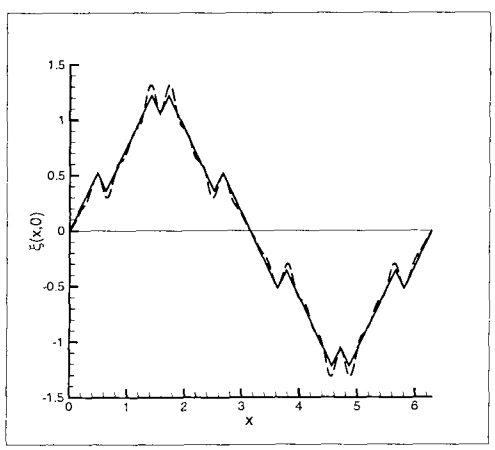

Figure 3.26: Comparison of the horizontal displacements $\xi(x,0)$ of the second Parker solution to the Q system — and the corresponding constant coefficient profile we used as an initial guess in our iterative scheme - - - .

the effect of "tainting," since they did not seem to include in their final analysis and plots the last 8 coefficients of either one of their 20-mode numerical solutions. This is why the plots of the Parker and Talbot $\xi(x,0)$ profiles, given in Figures 3.23 and 3.26, are generated using only 12 Fourier modes. From these plots one could infer that the surface singularities in the $\xi(x,0)$ are best approximated by corners. However, when a larger number of Fourier modes is considered, it becomes clear that the singularities in the horizontal displacement are in fact cusps. One should also keep in mind that the curl and divergence corresponding to these solutions are even more singular, and they require on the order of at least 500 modes to be reasonably well-resolved.

We propose that in the case of $c = c_R$ there exists an infinite family of solutions to the Q system which is directly related to the infinite family of exact solutions to the constant coefficient Q system. For every solution to the CQ system which we use as an initial guess in our numerical procedure, there exists a numerical solution to the truncated Q system. In fact, the two families of solutions appear to be related according to a simple rule of correspondence - the symmetric corners of the constant coefficient system solutions become symmetric cusps in the solutions to the truncated Q system. It is even more intriguing that this same type of transition is also observed when $c \neq c_R$, only that there we have non-symmetric corners transitioning into non-symmetric cusps.

Solution 4

To illustrate our argument for the existence of an infinite family of numerical solutions to the real Q system, on Figures 3.27 through 3.30 we show the displacement profiles, curl, and divergence of one more representative of the proposed family, chosen to have a more complicated surface structure. Once again, the general shape of this solution 4 is predetermined by the constant coefficient solution used as an initial guess to generate it. In this case, the initial guess for $\xi(x,0)$ is characterized

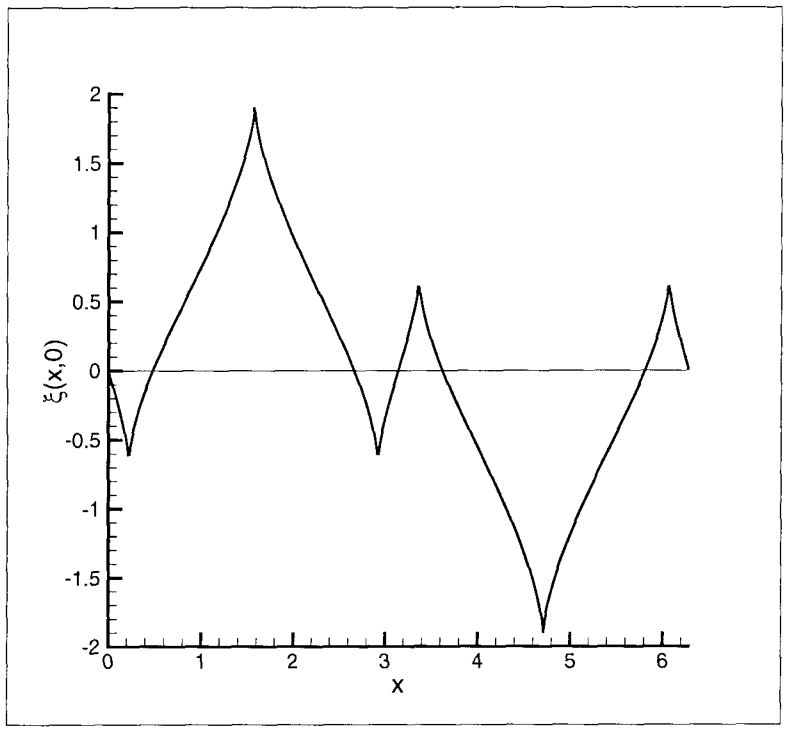

Figure 3.27: The horizontal displacement $\xi(x,0)$ of solution 4 to the Q system with $c = c_R$.

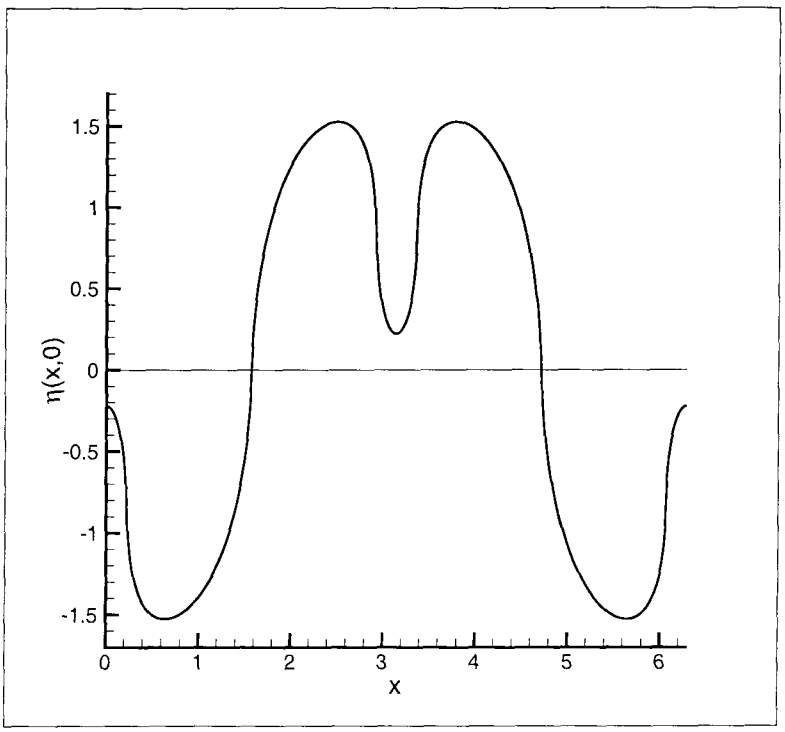

Figure 3.28: The vertical displacement $\eta(x,0)$ of solution 4 to the Q system with $c = c_R$.

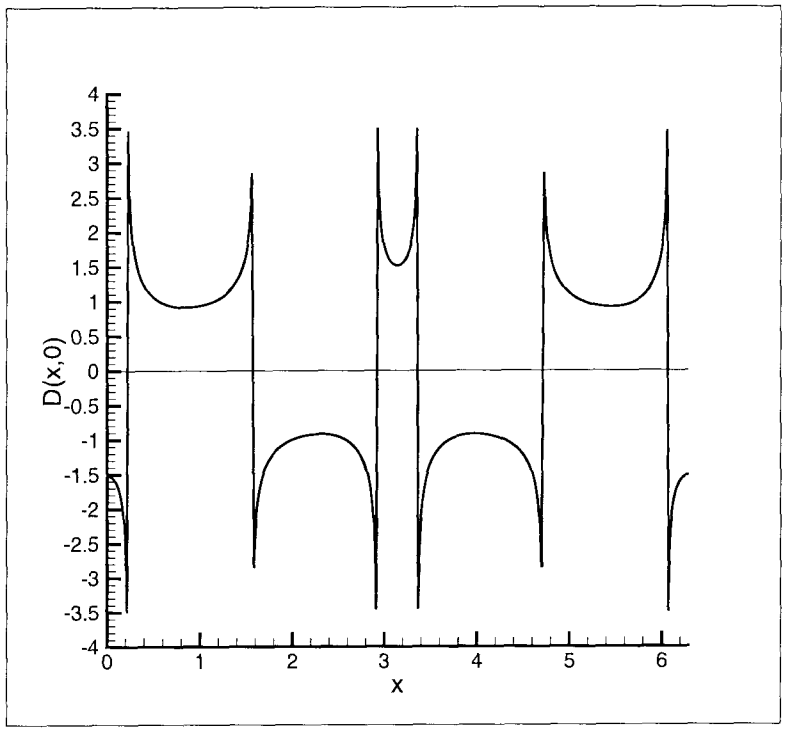

Figure 3.29: The divergence $D(x,0)$ of solution 4 to the Q system with $c = c_R$.

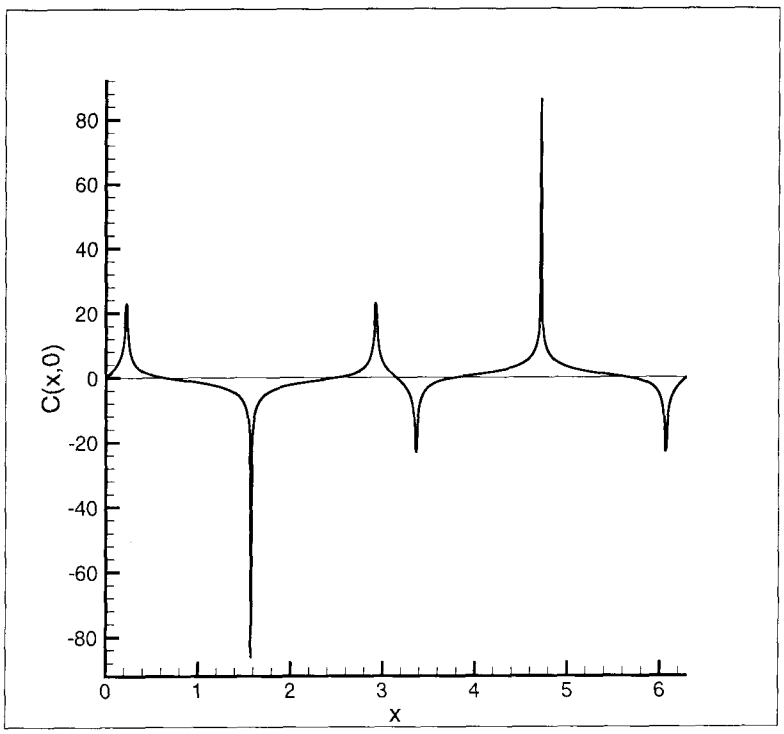

Figure 3.30: The curl $C(x,0)$ of solution 4 to the Q system with $c = c_R$.

by 3 positive and 3 negative corners of varying amplitudes. Its Fourier coefficients are given by the equation

$$Q_k = \frac{\sin\frac{k\pi}{2}}{k}\,\frac{1-2\cos 1.35k}{1-2\cos 1.35}, \quad 1 \le k \le 3000. \tag{3.23}$$

We observed that whenever the solution profiles have more surface singularities, the numerical scheme takes longer to settle to a solution. Nonetheless, it is interesting that for all of the numerical solutions presented here, including solution 4, the numerical procedure always settles to a fixed point solution. For each of the discussed numerical solutions, it took on the order of 20 iterations or less to reach a fixed point of the iteration with 1500 Fourier modes. This seems to indicate that the constant coefficient profiles represent an extremely good choice of initial guesses for the proposed numerical scheme.

The plots of the curl and the divergence of all presented numerical solutions to the Q system indicate that those quantities are infinite at the singular points of the numerical solution. This behavior is expected since the curl and the divergence are linear combinations of elastic displacement derivatives, which become infinite at the cusps.

3.1.3 Numerical Solutions to the Ad Hoc Q System with $\mathbf{c = c_R}$

The ad hoc system was proposed by G.B. Whitham as an approximation to the real Q system which retains the important features of the Q system coefficients. The ad hoc equations have a simpler structure than the actual Q equations, and we believe that an exact solution to the ad hoc system can be obtained. Since the structure of the ad hoc system resembles that of the real system very closely, the ad hoc system solutions should in turn resemble the solutions to the real Q equations. Thus, our next step is to compare numerical solutions to the ad hoc Q system with

the numerical solutions to the real Q system.

We use the Newton-Raphson iterative scheme to compute a solution to the ad hoc system (2.85), employing the horizontal displacement in (3.20) as an initial guess. The generated numerical solution satisfies the truncated ad hoc Q equations to the order of 10^{-12}. Plots of the corresponding surface displacements, curl and divergence are given in Figures 3.31 through 3.34.

By comparing these profiles to those of the numerical solution 1 to the real Q system generated with the same initial guess (3.20), we see that the two systems have almost identical surface profiles. We can also directly compare the Fourier coefficients of the two solutions, as is done in Table 3.3. The corresponding Q_k agree on the order of 10^{-3} to 10^{-2} which demonstrates that the ad hoc system is indeed a very close approximation to the actual Q system. The ad hoc system, however, does not include the p and s scalings, and that renders it more amenable to analysis.

In a similar manner, we can generate numerical solutions to the ad hoc Q system which correspond to each of the solutions 2, 3, and 4 of the real Q system. In each case, we would have to start the numerical procedure with the exact same initial guess as the one used in generating the respective solution to the real Q system. The resulting numerical solutions to the real and the ad hoc systems appear to be very closely related.

This leads us to believe that if analytic solutions to the ad hoc system are determined in the future, they will represent very good approximations for the corresponding Rayleigh wave solutions. The numerical study presented in the next section indicates that the real and the ad hoc Q systems exhibit very similar singular behavior on the surface of the elastic half-space. Consequently, any analytical results concerning the nature of the surface singularities of the ad hoc system will have direct implications for the nature of the Rayleigh wave solution singularities.

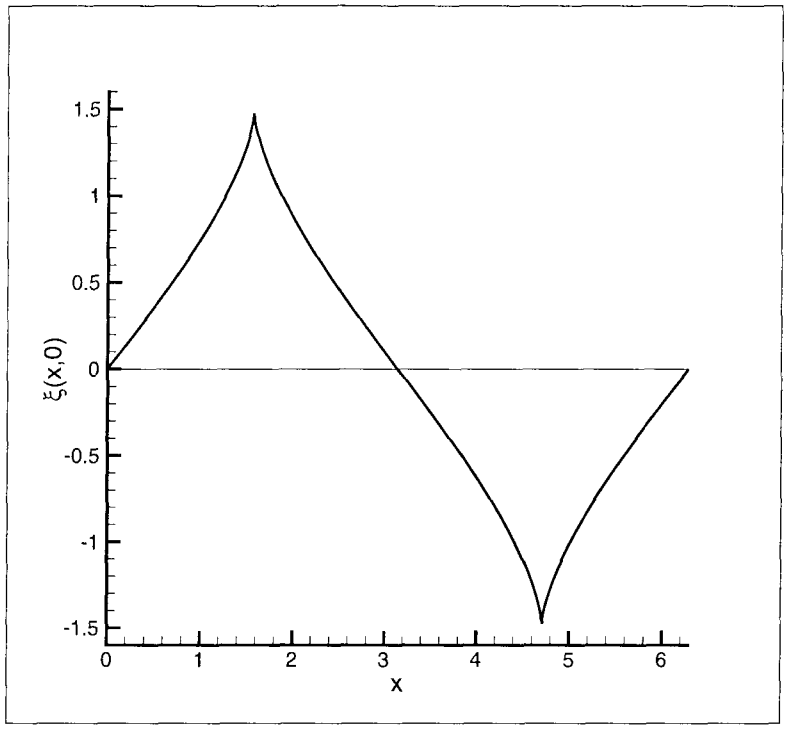

Figure 3.31: The horizontal displacement $\xi(x, 0)$ of solution 1 to the ad hoc Q system with $c = c_R$.

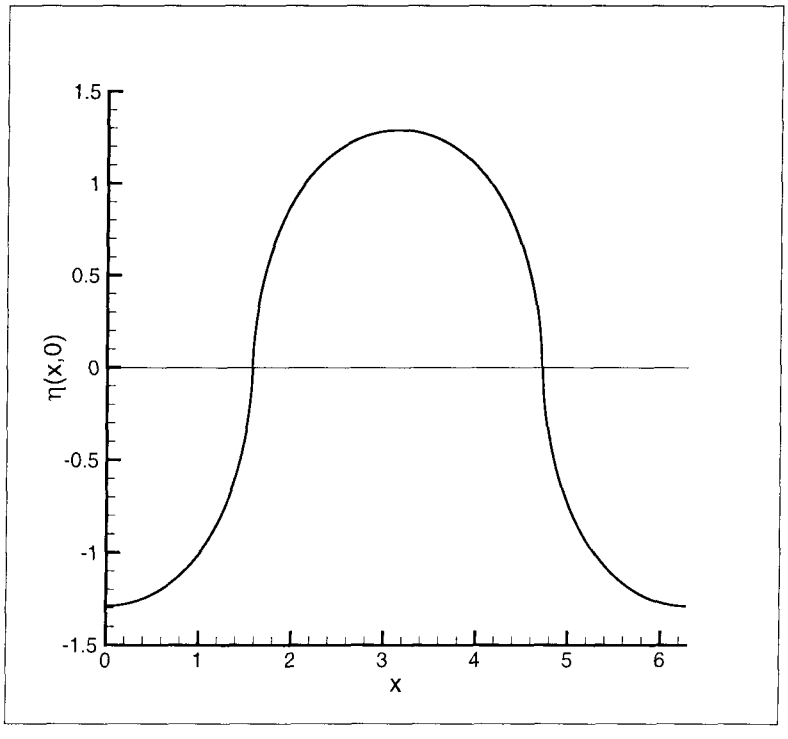

Figure 3.32: The vertical displacement $\eta(x, 0)$ of solution 1 to the ad hoc Q system with $c = c_R$.

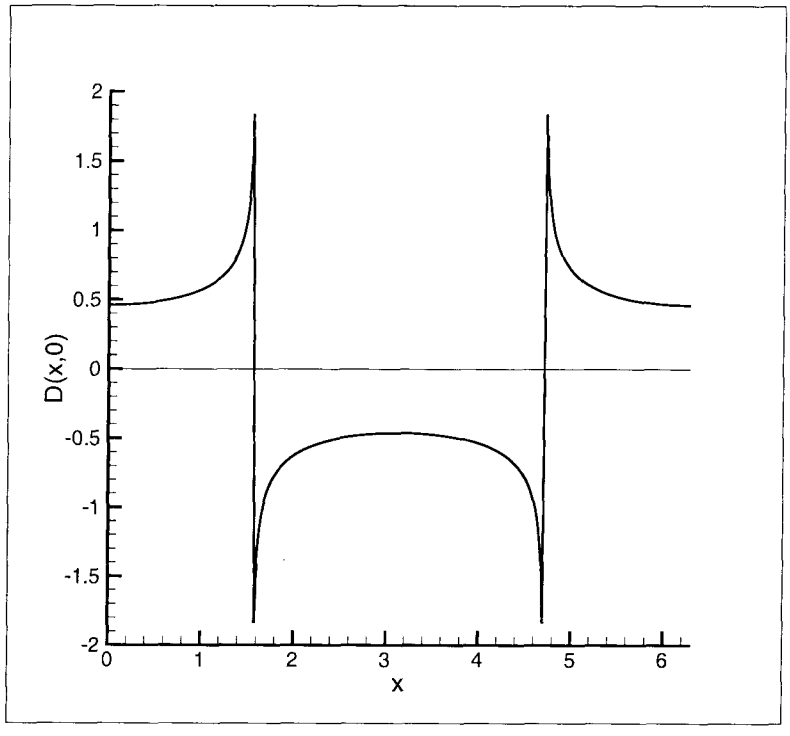

Figure 3.33: The divergence $D(x,0)$ of solution 1 to the ad hoc Q system with $c = c_R$.

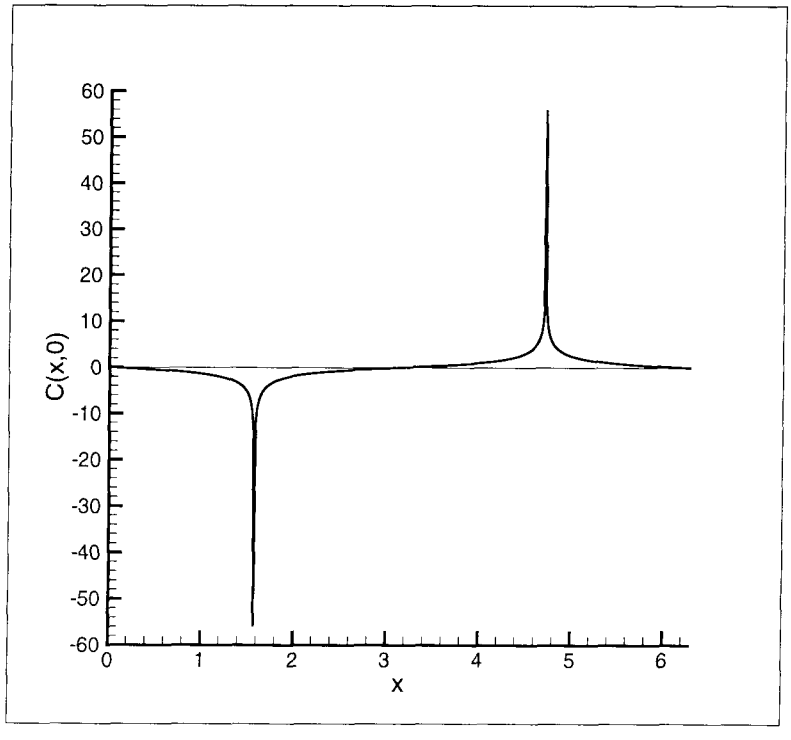

Figure 3.34: The curl $C(x,0)$ of solution 1 to the ad hoc Q system with $c = c_R$.

Q_k	Q_k ad hoc	Q_k real
Q_1	1.00000000	1.00000000
Q_3	-0.50726126	-0.50183716
Q_5	0.36249473	0.35923333
Q_7	-0.28994445	-0.28752456
Q_9	0.24529041	0.24331014
Q_{11}	-0.21459481	-0.21289011
Q_{21}	0.13942381	0.13833697
Q_{51}	-0.07709946	-0.07649897
Q_{101}	0.04881565	0.04843306
Q_{199}	-0.03097041	-0.03072239
Q_{501}	0.01662488	0.01648353
Q_{999}	-0.01052831	-0.01044834
Q_{1501}	0.00828683	0.00825419
Q_{1995}	-0.00745505	-0.00746426
Q_{1997}	0.00745392	0.00746327
Q_{1999}	-0.00745280	-0.00746229
Q_{2501}	0.00807780	0.00809829
Q_{2991}	-0.07673814	-0.07419873
Q_{2993}	0.09174870	0.08868365
Q_{2995}	-0.11742275	-0.11353972
Q_{2997}	0.17485050	0.16983723
Q_{2999}	-0.53050990	-0.50969231

Table 3.3: A comparison of the numerical solutions to the ad hoc and the real Q systems with $c = c_R$, generated using the numerical procedure I with 1500 Fourier modes.

3.1.4 Singularities in the Real and Ad Hoc Solutions with $c = c_R$

The special form of the horizontal displacements $\xi(x, 0)$ of the numerical solutions to both the real and the ad hoc Q systems seems to suggest a power law type of behavior near the singularities. This hypothesis can be tested by checking whether the numerically determined Fourier coefficients Q_k display a power law behavior. Without loss of generality, we can take the singularity to be located at $x = \pi/2$, as

is the case with our solution 1 profiles. We assume that the local behavior has the following form:

$$\xi(x,0) \backsim \widetilde{\xi}\,|x-\pi/2|^{\lambda}, \quad x \to \frac{\pi}{2}\,. \tag{3.24}$$

The leading order terms of the Fourier coefficients $\widetilde{Q}_k$ corresponding to this surface horizontal displacement are

$$\widetilde{Q}_k(\lambda) \backsim \frac{\widetilde{Q}\sin\frac{k\pi}{2}}{k^{\lambda}}, \quad k \to \infty, \tag{3.25}$$

The factors $\widetilde{\xi}$ and $\widetilde{Q}$ in formulas (3.24) and (3.25) are appropriately chosen constants and $0 < \lambda < 1$.

The Equation Fit for λ

Although (3.25) is posed initially as an asymptotic formula strictly as $k \to \infty$, it fits remarkably well for all but the first few Q_k and the first few equations. In fact, one way to proceed is to substitute (3.25) for all k into each equation and determine the λ which makes (3.25) exact for that particular equation. This parameter study for λ will be referred to as the individual equation fit.

We tested our hypothesis on equations number 2 through 10, 20, 50, 100, 1000, and 1500 using various numbers of Fourier modes of the form (3.25) with $0 < \lambda < 1$. A selection of the numerically determined values for λ providing the best fit to the respective equations of the real and the ad hoc systems are given in Table 3.4. The performed parameter study indicates that the appropriate value for λ lies in the range of $(0.63, 2/3)$ for both the real and the ad hoc systems.

Interestingly, the λ_k for small k are not drastically different from the λ_k for large k, with the maximum registered difference between them being about 0.03. Indeed, the first several λ_k increase very quickly with k, and as early as $k = 10$ the value for λ_k is greater than 0.66. The remaining values of the λ_k remain within a range

equation	λ real	λ ad hoc
2	0.6365	0.6299
4	0.6503	0.6491
6	0.6560	0.6558
8	0.6590	0.6590
10	0.6608	0.6608
20	0.6642	0.6642
50	0.6659	0.6660
100	0.6664	0.6664
1000	0.6664	0.6664
1500	0.6662	0.6662

Table 3.4: Values for λ generated using the individual equation fit and a profile with 100000 coefficients of the form (3.25).

which is very close to 0.66. This seems to indicate that there exists a unique value for λ, that is close to 0.66, which, when substituted in (3.25), approximates the Q_k of the steady profile Rayleigh waves with a high level of accuracy.

We also experimented by varying the number of coefficients $\widetilde{Q}_k$ employed in the individual equation fit for λ. This helped us verify that as the number of coefficients is increased, the respective value of λ corresponding to each of the studied equations approaches 2/3.

The Q_k Fit for λ

A different way to test whether the numerically determined coefficients Q_k have the form (3.25) is to compute the expression

$$\lambda_k = -\frac{\log|Q_k|}{\log k}, \tag{3.26}$$

using our numerically determined Q_k. The corresponding values for λ are given in Table 3.5. This test produces $(0.62, 2/3)$ as an approximate range for the appropriate values of λ. This range is indeed quite close to the λ range generated before by the

individual equation fit.

k	λ_k real	λ_k ad hoc
3	0.62759137	0.61780586
5	0.63611224	0.63049673
7	0.64054705	0.63624002
21	0.64971200	0.64714155
51	0.65376196	0.65177330
101	0.65601162	0.65430672
199	0.65795638	0.65643737
501	0.66039150	0.65901790
751	0.66091830	0.65964690
999	0.66041317	0.65930924
1251	0.65879070	0.65793523
1501	0.65588025	0.65534075
1751	0.65130209	0.65112184
1997	0.64449315	0.64465804
1999	0.64442544	0.64459288

Table 3.5: Values for λ_k determined using formula (3.26) with the numerically determined coefficients corresponding to solutions 1 of the real and ad hoc Q systems with $c = c_R$.

In the case of solution 1 to the real Q system, the λ_k grow with k up to $\lambda_{751} = 0.66091830$, then they start to decrease with k. In the case of the corresponding solution 1 to the ad hoc Q system, the maximum is reached at $\lambda_{801} = 0.65965502$. The subsequant decrease is due to "tainting" from the finite cutoff. Later, we shall demonstrate that certain modifications in the numerical procedure result in much more uniform values for λ_k.

We also determined a single value for λ which when used in (3.25) produces the best overall fit to all of the numerically computed coefficients Q_k. Comparing the first one thousand Q_k of the real system solution 1 to the proposed $\widetilde{Q}_k$, we determined that $\lambda = 0.655$ gives the the best overall fit. This is not surprising since 0.655 can be considered as an average of the λ_k given in Table 3.5. In fact, all of the

k	Q_k numerical	$\widetilde{Q}_k, \lambda = 0.655$	$\widetilde{Q}_k, \lambda = 2/3$
1	1.00000000	1.00000000	1.00000000
3	-0.50183716	-0.48695135	-0.48074986
5	0.35923333	0.34847742	0.34199519
7	-0.28752456	-0.27955083	-0.27327588
9	0.24331014	0.23712162	0.23112042
11	-0.21289011	-0.20791594	-0.20218001
21	0.13833697	0.13612765	0.13137734
51	-0.07649897	-0.07612749	-0.07271431
101	0.04843306	0.04865971	0.04610901
199	-0.03072239	-0.03120694	-0.02933805
501	0.01648353	0.01704536	0.01585288
999	-0.01044834	-0.01084637	-0.01000667
1501	0.00825419	0.00830751	0.00762803
1995	-0.00746426	-0.00689505	-0.00631013
1997	0.00746327	0.00689053	0.00630591
1999	-0.00746229	-0.00688601	-0.00630171

Table 3.6: A comparison of the numerically determined Q_k of solution 1 to the real Q system with $c = c_R$ and the approximate $\widetilde{Q}_k$ generated using formula (3.25) with $\lambda = 0.655$ and $\lambda = 2/3$.

λ-fits examined in this section are just different ways to estimate the same fractional power λ. It is reassuring that they agree to a significant degree.

In Table 3.6 we provide a comparison of the actual Q_k to their proposed approximations $\widetilde{Q}_k$ generated using formula (3.25) with $\lambda = 0.655$. To illustrate the differences of using various choices for λ, we have also included the $\widetilde{Q}_k$ computed with $\lambda = 2/3$. Although there are strong indications that the actual asymptotic value for λ might in fact be $2/3$, the numerically determined Q_k are better approximated overall using $\lambda = 0.655$.

The approximate formula for $\widetilde{Q}_k$ in (3.25) corresponds to a horizontal displacement $\xi(x, 0)$ with just two fractional singularities in the range $0 \leq x \leq 2\pi$, i.e., the simplest possible profile expected to fit the simplest numerically generated Rayleigh wave solution. The above reasoning, however, appears to also be valid for more complicated profiles, provided that the numerator of formula (3.25) is modified to

allow for the existence of additional surface singularities. It appears that the best-fit values for λ remain in the range of $0.6 \leq \lambda \leq 2/3$, no matter how complicated the considered profiles are.

3.1.5 Modification: Numerical Method II with $\mathbf{c = c_R}$

In the previous section we presented empirical evidence that the higher order Fourier coefficients of the solutions to the real and ad hoc Q systems can be approximated by a power law dependence similar to the one in (3.25) with λ in the range of $(0.63, 2/3)$.

We now propose to employ the approximate form of the Fourier coefficients in (3.25) as an initial guess for the numerical procedure applied to the truncated version of the Q systems with $c = c_R$. In this manner we account for the special structure of the Rayleigh wave solutions, as suggested by the numerical results generated so far.

In addition, we will include in the modified computations twice as many modes as we intend to solve for. The latter half of the Q_k will be fixed to the approximate values for Q_k given by formula (3.25) with $\lambda = 2/3$. The motivation for this modified approach is discussed in detail in Section 3.1.1 within the context of the CQ system. The only difference between the modified method applied to the CQ system and the modified method for the real or ad hoc Q systems is the form assumed for the higher order Fourier coefficients. While in the case of the CQ system we used the exact formula for the Q_k, here we employ an approximate formula for the Fourier coefficients $\widetilde{Q}_k$, such as the one given in (3.25).

We tested the modified method on solution 1 to the real Q system with $c = c_R$. A comparison of the Q_k coefficients computed using the original and the modified numerical procedures is given in Table 3.7. It should be noted that the more precise initial guess, employed in the modified method, reduced the number of iterations needed to reach a fixed point.

Q_k	Q_k numerical I	Q_k numerical II
Q_1	1.00000000	1.00000000
Q_3	-0.50183716	-0.50186315
Q_5	0.35923333	0.35927069
Q_7	-0.28752456	-0.28756959
Q_9	0.24331014	0.24336114
Q_{11}	-0.21289011	-0.21294605
Q_{21}	0.13833697	0.13841054
Q_{51}	-0.07649897	-0.07660302
Q_{101}	0.04843306	0.04856754
Q_{199}	-0.03072239	-0.03089191
Q_{501}	0.01648353	0.01668075
Q_{999}	-0.01044834	-0.01056441
Q_{1501}	0.00825419	0.00817068
Q_{1995}	-0.00746426	-0.00700176
Q_{1997}	0.00746327	0.00699857
Q_{1999}	-0.00746229	-0.00699539
Q_{2501}	0.00809829	0.00661144
Q_{2991}	-0.07419873	-0.02377340
Q_{2993}	0.08868365	0.02753548
Q_{2995}	-0.11353972	-0.03398364
Q_{2997}	0.16983723	0.04857040
Q_{2999}	-0.50969231	-0.13651528

Table 3.7: A comparison of the numerical solutions to the real Q system with $c = c_R$ generated using the original (I) and the modified (II) numerical methods.

More importantly, the effect of "tainting" is significantly reduced. This can be observed by comparing the higher order Q_k, documented in Table 3.7. The reduction of "tainting" also becomes evident when the Q_k from the modified method are substituted into formula (3.26). A selection of the relevant values for λ_k is given in Table 3.8. We observe that the modified λ_k are more uniformly distributed, and the higher order ones appear to be considerably less affected by "tainting" than the λ_k determined using the results of the original numerical method.

These results lead us to believe that the modified version of the numerical scheme

k	λ_k numerical I	λ_k numerical II
3	0.62759137	0.62754423
5	0.63611224	0.63604763
7	0.64054705	0.64046657
21	0.64971200	0.64953737
51	0.65376196	0.65341626
101	0.65601162	0.65541081
199	0.65795638	0.65691680
501	0.66039150	0.65847827
751	0.66091830	0.65887299
999	0.66041317	0.65881365
1251	0.65879070	0.65830199
1501	0.65588025	0.65727064
1751	0.65130209	0.65556525
1997	0.64449315	0.65295267
1999	0.64442544	0.65292642

Table 3.8: Values for λ_k computed using (3.26) and the Fourier coefficients Q_k of solution 1 to the real Q system. The values used for the Q_k coefficients were determined via the original (I) and the modified (II) numerical methods.

is an efficient approach to generating numerical solutions to the truncated versions of the infinite Q systems with $c = c_R$.

3.2 Computational Treatment of the Q Systems with $c \neq c_R$

The system (2.78) for the Fourier coefficients of a steady-profile periodic Rayleigh wave with a velocity shift is solved numerically following a procedure similar to the one outlined in the case of $c = c_R$.

The infinite system (2.78) is truncated to a finite number of equations with a finite number of unknowns. The resulting truncated system is solved numerically using the Newton-Raphson method. The only difference from the $c = c_R$ case is the choice of initial guess for the iterative procedure. This time the initial guesses are solutions to the constant coefficient Q system with $c \neq c_R$. As discussed in Chapter 2, the CQ-profiles corresponding to $c \neq c_R$ are characterized by horizontal displacements with non-symmetric finite-angle singularities. The slopes on either side of the $\xi(x, 0)$ singularities are related through the "shock-like" condition determined by G.B. Whitham.

3.2.1 Numerical Solutions to the CQ System with $c \neq c_R$

Just as we did in the case of $c = c_R$, we shall start off by testing the accuracy of the numerical method on the truncated version of the constant coefficient system

$$\frac{1}{2}\sum_{k=1}^{n-1} Q_k Q_{n-k} + \sum_{k=1}^{\infty} Q_k Q_{n+k} = Q_n, \quad n = 1, \ldots, \infty. \tag{3.27}$$

Once again, we want to estimate how strong the effect of "tainting" is, and how well the numerically determined solutions reproduce the exact solutions to the CQ system.

Solution 1

We shall consider the simplest possible exact solution to the CQ system for $c \neq c_R$ with Fourier coefficients of the following form:

$$Q_k = \frac{2}{2b - \pi} \frac{\sin kb}{k}, \quad k = 1, \ldots, \infty. \tag{3.28}$$

The corresponding surface horizontal displacement $\xi(x, 0)$ has one non-symmetric positive corner at $x = b\pi$, and a second non-symmetric negative corner at $x = (2 - b)\pi$. A choice of $b = \pi/2$ would result in the corners becoming symmetric, which is not allowed for the solutions of the CQ system with $c \neq c_R$. Therefore, the value $b = \pi/2$ is not acceptable, which is highlighted by the fact that formula (3.28) blows up when $b = \pi/2$.

We choose to consider the case $b = 0.8\pi$ since it is relevant to our later analysis. Due to this choice of b, the exact value of every fifth coefficient Q_k is equal to zero. We use 1500 Fourier modes of the form (3.28) to start the iterative procedure. Six iterations are needed before a fixed point solution is reached. The numerically determined coefficients satisfy the truncated equations to the order of 10^{-12}.

The surface profiles of numerical solution 1 to the CQ system (3.27) are shown in Figures 3.35 through 3.38. If superimposed, the surface profiles of the numerically generated solution and those of the corresponding exact solution to the CQ system are once again impossible to distinguish.

To examine the effect of "tainting" in this case, we compare the values of the computed and the exact Fourier coefficients Q_k, as given in Table 3.9. This comparison reveals that "tainting" is once again present. The highest-order computed coefficient Q_{1500} is equal to 0.01518621 – not a very good approximation for the exact value of $Q_{1500} = 0$. Moreover, in the exact solution, every coefficient of the form Q_{5m+1}, $m = 1, \ldots, \infty$ has a positive sign. The numerical solution, however, has positive Q_{5m+1} only up to Q_{856} where $m = 171$. All numerically determined

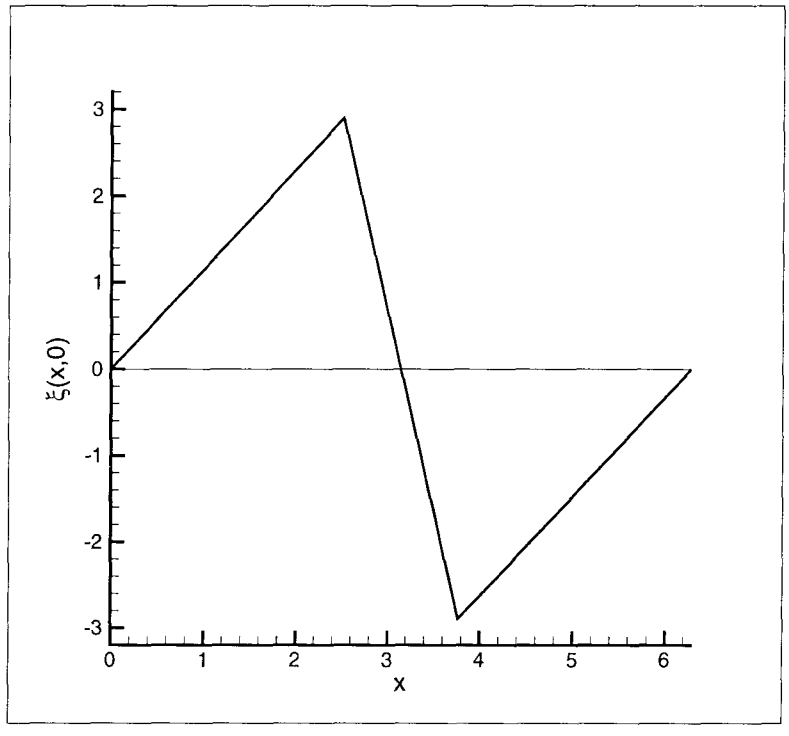

Figure 3.35: The horizontal displacement $\xi(x, 0)$ of solution 1 to the constant coefficient Q system with $c \neq c_R$.

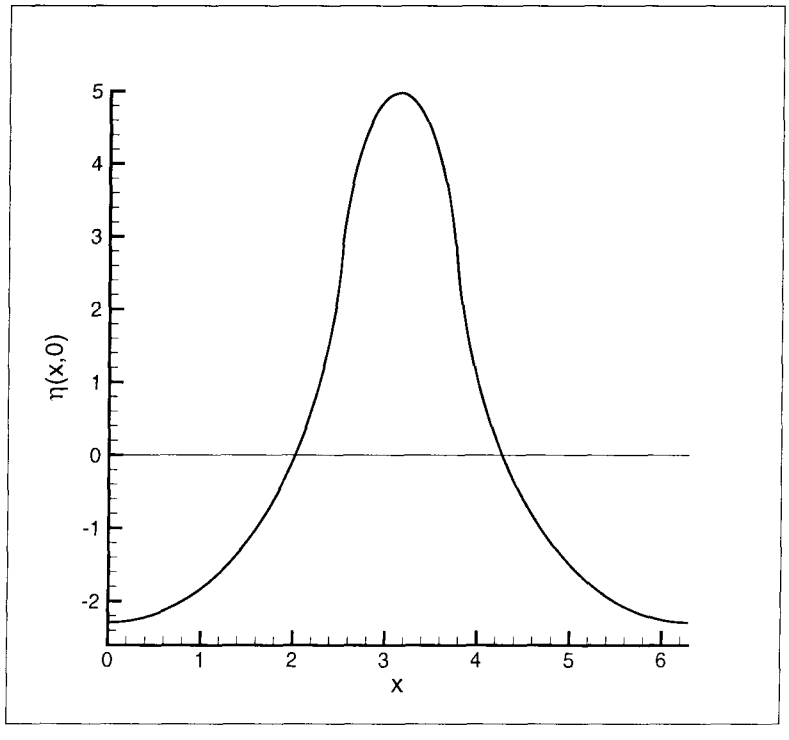

Figure 3.36: The vertical displacement $\eta(x, 0)$ of solution 1 to the constant coefficient Q system with $c \neq c_R$.

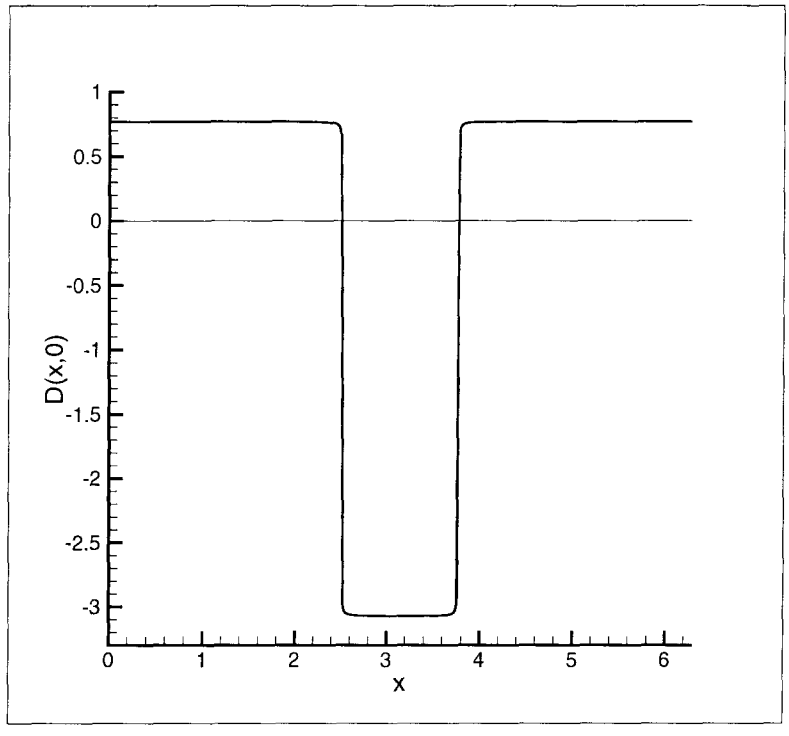

Figure 3.37: The divergence $D(x,0)$ of solution 1 to the constant coefficient Q system with $c \neq c_R$.

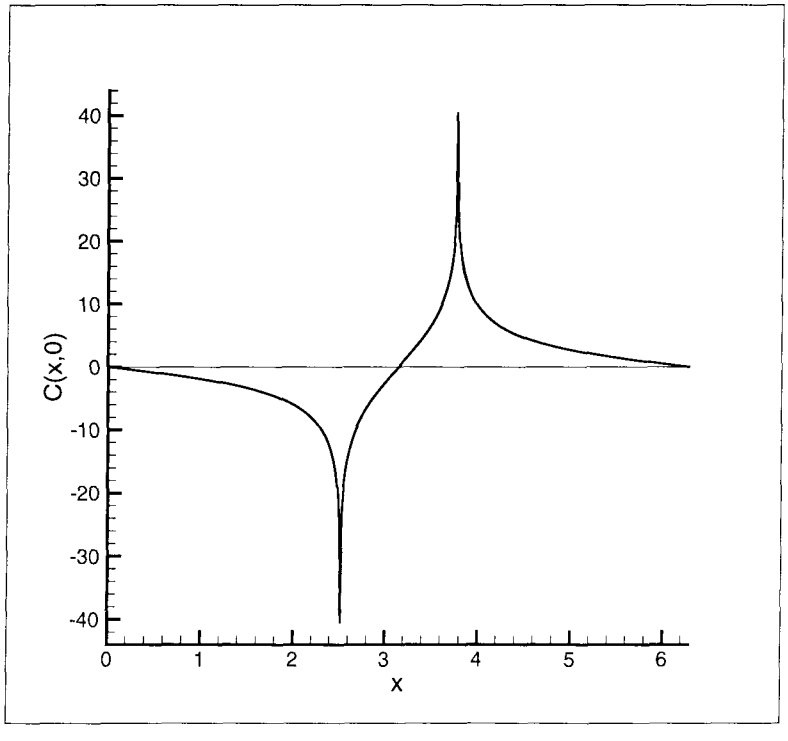

Figure 3.38: The curl $C(x,0)$ of solution 1 to the constant coefficient Q system with $c \neq c_R$.

Q_k	Q_k exact	Q_k numerical I	Q_k numerical II
Q_1	0.62365952	0.62247771	0.62336159
Q_2	-0.50455115	-0.50380724	-0.50436936
Q_3	0.33636743	0.33623390	0.33634256
Q_4	-0.15591488	-0.15635240	-0.15603324
Q_5	0.00000000	0.00077615	0.00019959
Q_6	0.10394325	0.10316523	0.10374904
Q_7	-0.14415747	-0.14369329	-0.14404764
Q_8	0.12613779	0.12616710	0.12615493
Q_9	-0.06929550	-0.06979977	-0.06943121
Q_{10}	0.00000000	0.00077571	0.00019964
Q_{11}	0.05669632	0.05595517	0.05651155
Q_{21}	0.02969807	0.02897826	0.02951874
Q_{31}	0.02011804	0.01940605	0.01994070
Q_{41}	0.01521120	0.01450340	0.01503493
Q_{51}	0.01222862	0.01152349	0.01205304
Q_{100}	0.00000000	0.00076896	0.00020095
Q_{101}	0.00617484	0.00547608	0.00600104
Q_{201}	0.00310278	0.00240866	0.00293067
Q_{301}	0.00207196	0.00137930	0.00190082
Q_{401}	0.00155526	0.00086200	0.00138453
Q_{501}	0.00124483	0.00054894	0.00107392
Q_{751}	0.00083043	0.00011735	0.00065564
Q_{998}	0.00101112	0.00116181	0.00116283
Q_{999}	-0.00062428	-0.00124197	-0.00089198
Q_{1000}	0.00000000	0.00084891	0.00028142
Q_{1001}	0.00062304	-0.00013270	0.00043560
Q_{1101}	0.00056645	-0.00022098	0.00036872
Q_{1201}	0.00051928	-0.00031762	0.00030468
Q_{1301}	0.00047937	-0.00044487	0.00023350
Q_{1401}	0.00044515	-0.00068396	0.00012191
Q_{1498}	0.00067363	0.00735094	0.00371365
Q_{1499}	-0.00041605	-0.01230829	-0.00552702
Q_{1500}	0.00000000	0.01518621	0.00632020

Table 3.9: A comparison of the exact coefficients of solution 1 to the CQ system with $c \neq c_R$ with the coefficients determined via the original (I) and the modified (II) numerical methods.

Q_{5m+1} with $m \geq 172$ are negative. Thus, the numerically determined values for the Q_{5m+1}, $m \geq 172$ are not just inaccurate in value, they also carry the wrong sign.

As in the case of $c = c_R$, we modify the numerical procedure so that the exact form for the higher-order Fourier coefficients is used in computing the lower-order Q_k. Once again, we employ twice as many Fourier coefficients as we solve for, and the second half of the considered Q_k is fixed to the exact values given by the initial guess (3.28). We include a portion of the resulting numerical solution in the third column of Table 3.9.

By comparing the Q_k computed with the two numerical approaches to the exact values for the Q_k, we observe that the modified results improve the original results by an order of accuracy. Also, the effect of "tainting" is greatly diminished. The earliest change in sign in the Q_{5m+1} coefficients computed using the modified approach occurs only after Q_{1451}. Such a change does not affect any of the analysis performed using the first two-thirds of the Q_k. The higher-order Q_k produced with the modified scheme seem to approximate the exact values for the Fourier coefficients to a much greater degree than the original Q_k.

3.2.2 Numerical Solutions to the Real Q System with $c \neq c_R$

We begin the study of the real Q equations for $c \neq c_R$ and $\kappa = 1$,

$$\sum_{k=1}^{n-1} \alpha_{k,n} Q_k Q_{n-k} + \sum_{k=1}^{\infty} \beta_{k,n} Q_k Q_{n+k} = Q_n, \quad n = 1, \ldots, \infty, \tag{3.29}$$

by using our numerical procedure to reproduce the two solutions originally determined by Parker and Talbot in [16].

Solutions 1 and 2

Plots of the horizontal displacement profiles of the Parker-Talbot numerical solutions are given in Figures 1.3 and 1.4. Our solution profiles for $\xi(x, 0)$ are shown in

Figures 3.39 and 3.43. Notice the main change is in the cusped peaks replacing what looked like corners in Figures 1.3 and 1.4. The other figures in 3.39 through 3.46 show the related quantities $\eta(x,0)$, $C(x,0)$, $D(x,0)$.

As in the case of $c = c_R$, in order to reproduce the Parker-Talbot solutions for $c \neq c_R$, we had to determine the appropriate initial guesses for our numerical procedure. For solution 1 we used the initial guess given by

$$Q_k = \frac{10}{3\pi} \frac{\sin 0.8k\pi}{k}, \quad 1 \leq k \leq 1500, \tag{3.30}$$

which is the same as (3.28) with $b = 0.8\pi$. For solution 2 we employed the constant coefficient solution with

$$Q_k = \frac{10\,(\sin 0.4k\pi - \sin 0.8k\pi)}{k\pi}, \quad 1 \leq k \leq 1500. \tag{3.31}$$

These initial guesses were generated by matching the Parker-Talbot horizontal displacements given in Figures 1.3 and 1.4 to solutions of the constant coefficient system (3.27) with similarly positioned singularities. The surface horizontal displacement of solution 1 has two singularities: one at $x = 0.8\pi$ and another at $x = 1.2\pi$. The respective $\xi(x,0)$ of solution 2 has four singularities: at 0.4π, 0.8π, 1.2π, and 1.6π. In each case, the slopes of the initial guesses on either side of the singularities have to be related through the "shock-like" condition noted earlier. The separation of the surface singularities of the considered profiles also depends on the choice of surface displacement slopes.

Our experience shows that in the case of $c \neq c_R$ we need to be very careful in the choice of initial guess, making sure that all requirements on the slopes and the location of the singularities are taken into consideration. Any failure to use the proper initial guess prevents the iterative procedure from converging. Once we have chosen the correct initial guess, however, the numerical procedure takes less iterations to reach a fixed point solution than was the case when $c = c_R$. We believe

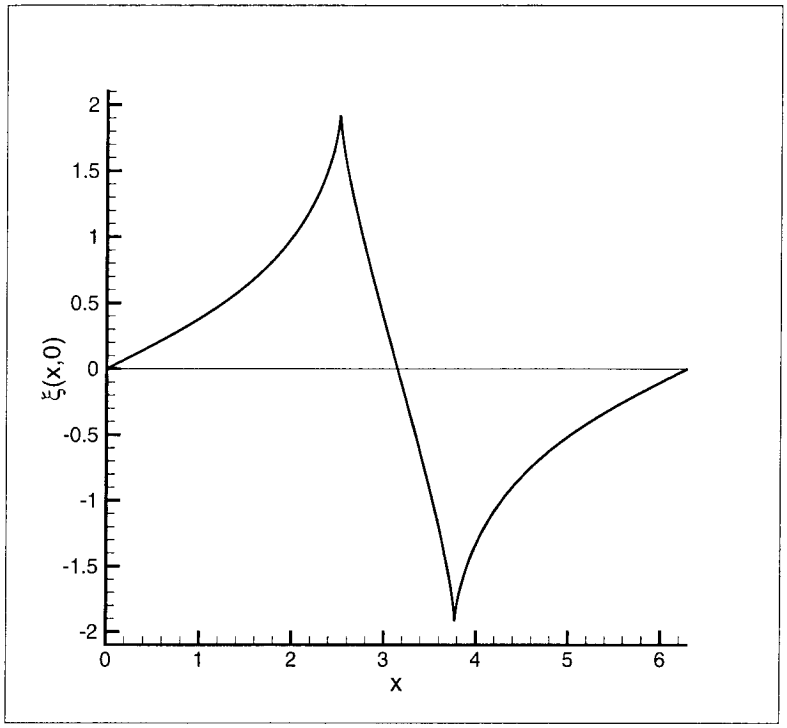

Figure 3.39: The horizontal displacement $\xi(x,0)$ of solution 1 to the Q system with $c \neq c_R$.

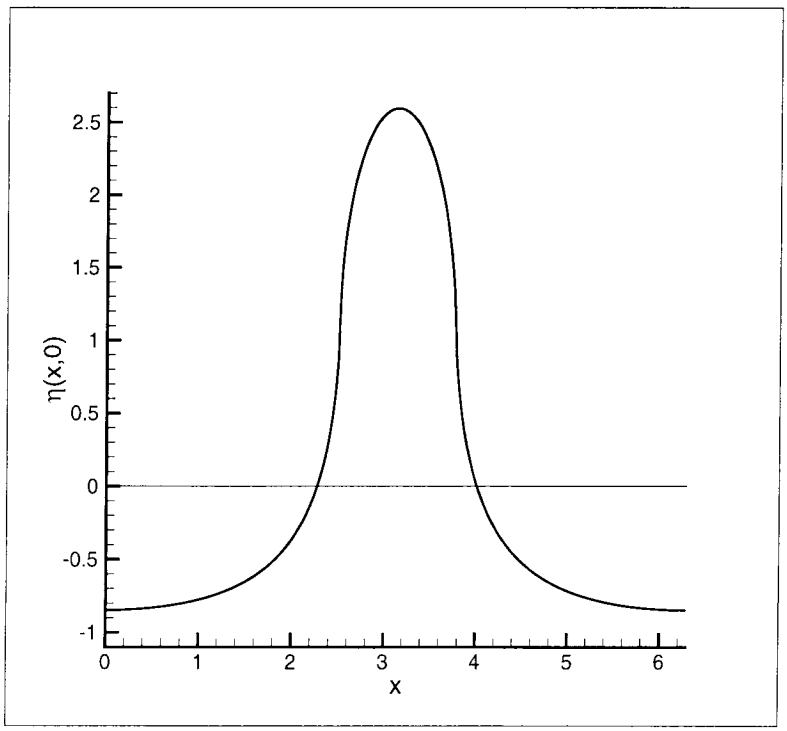

Figure 3.40: The vertical displacement $\eta(x,0)$ of solution 1 to the Q system with $c \neq c_R$.

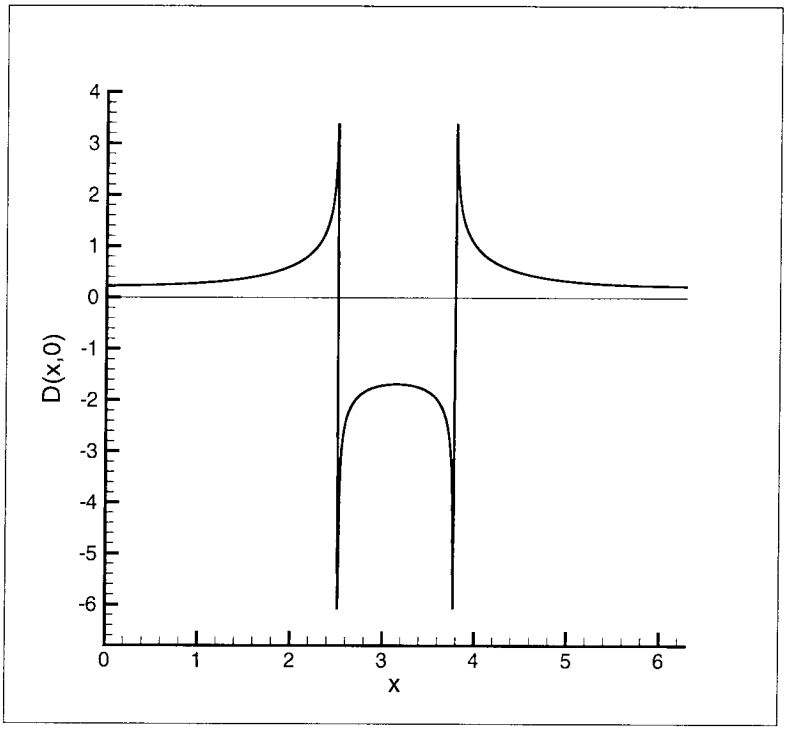

Figure 3.41: The divergence $D(x,0)$ of solution 1 to the Q system with $c \neq c_R$.

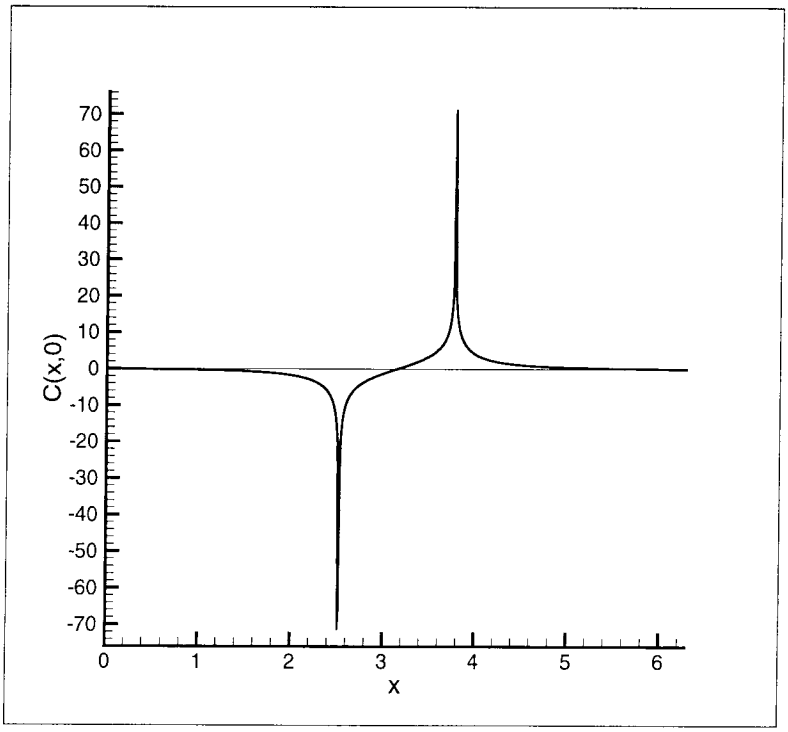

Figure 3.42: The curl $C(x,0)$ of solution 1 to the Q system with $c \neq c_R$.

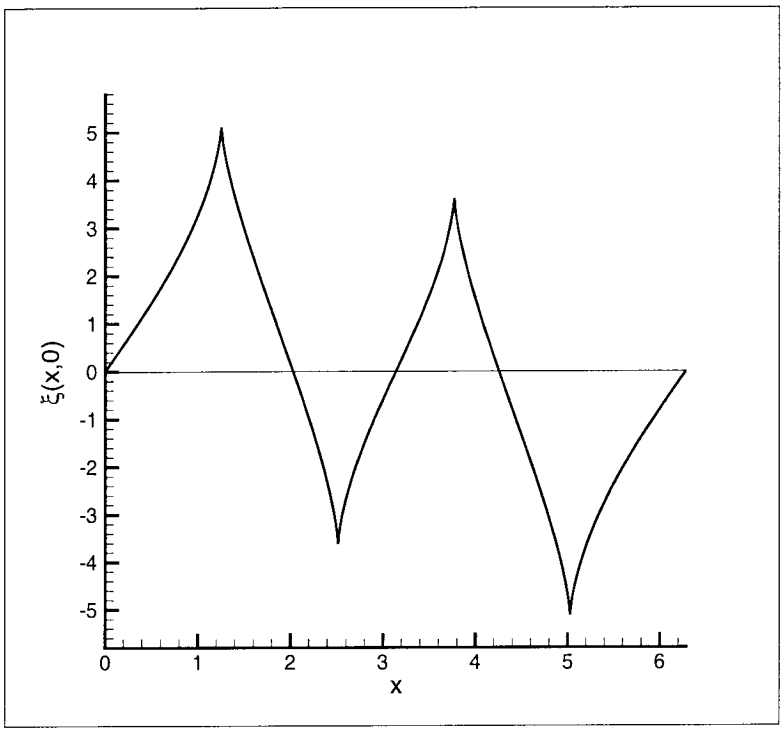

Figure 3.43: The horizontal displacement $\xi(x,0)$ of solution 2 to the Q system with $c \neq c_R$.

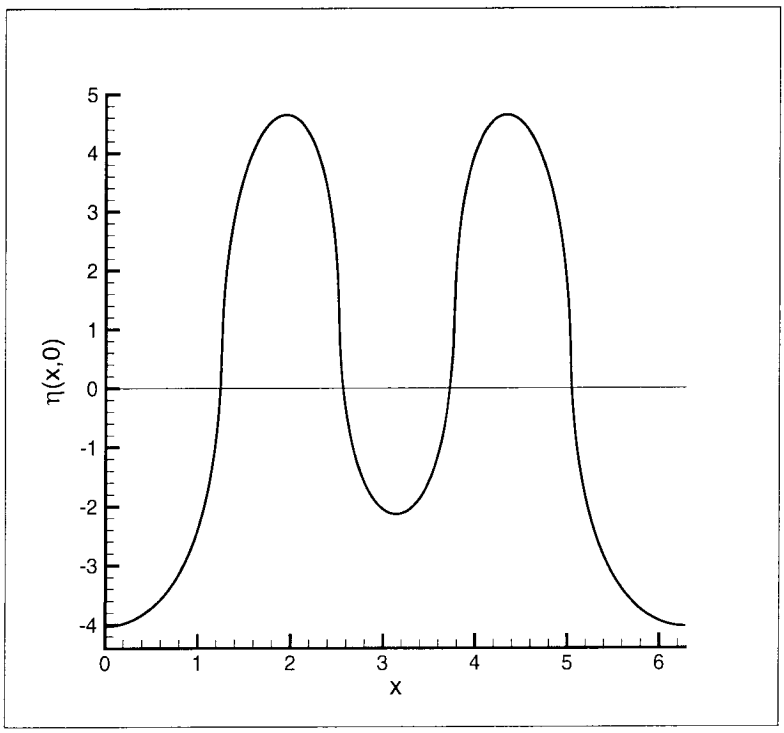

Figure 3.44: The vertical displacement $\eta(x,0)$ of solution 2 to the Q system with $c \neq c_R$.

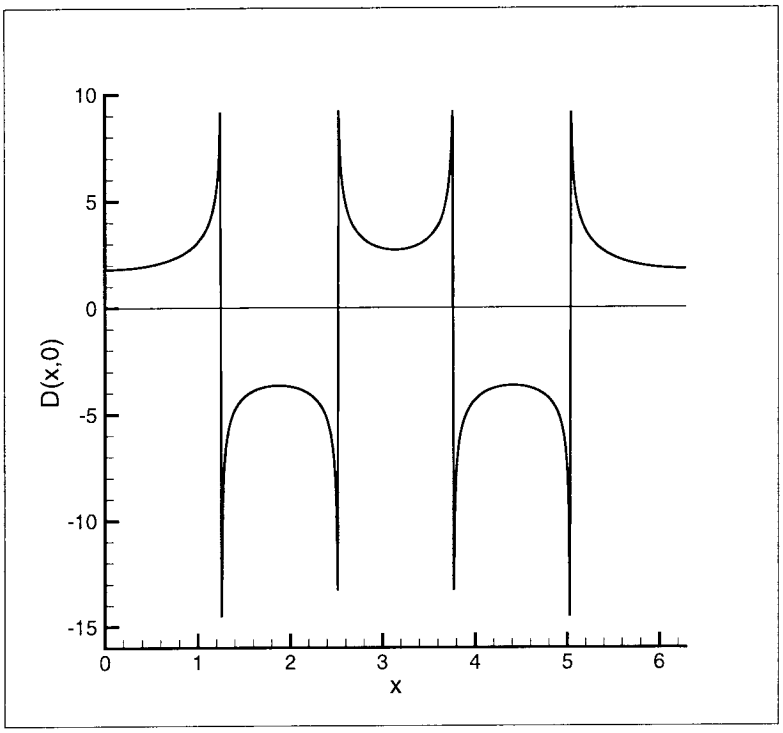

Figure 3.45: The divergence $D(x, 0)$ of solution 2 to the Q system with $c \neq c_R$.

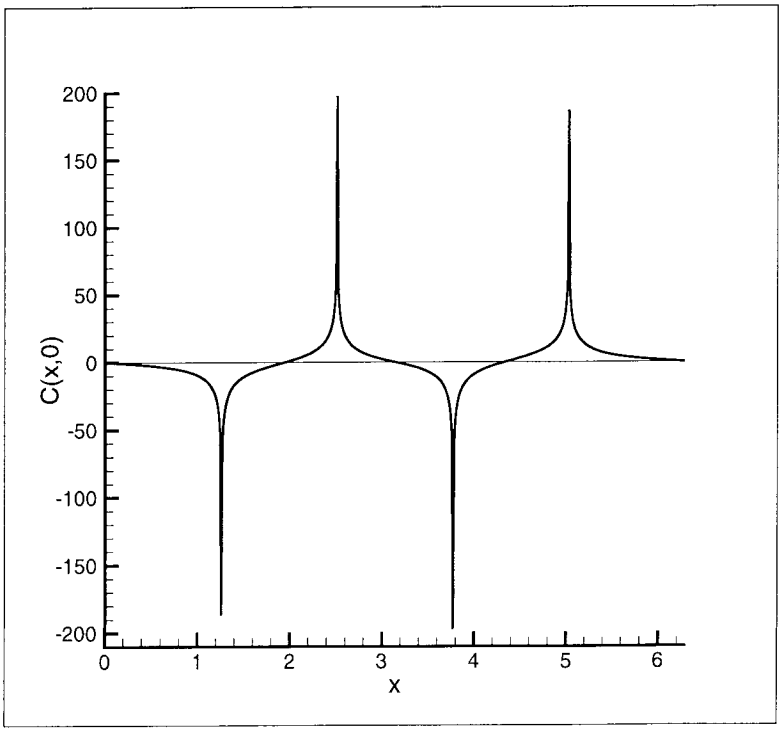

Figure 3.46: The curl $C(x, 0)$ of solution 2 to the Q system with $c \neq c_R$.

this increased sensitivity to the initial guess can be explained by the presence of the linear term on the right-hand side of system (3.29).

The surface horizontal displacement singularities of our solutions 1 and 2 turn out to be cusps, similar to the singularities in the case of the $c = c_R$ system. This finding is certainly not unexpected, and it reemphasizes the need to consider a significantly large number of Fourier coefficients in order to properly resolve the surface displacements and their derivatives. In [16], Parker and Talbot appear to have used on the order of 20 Fourier modes to produce the $\xi(x, 0)$ plots given in Figures 1.3 and 1.4. This number of modes is not enough to reproduce the cusps in the surface horizontal displacement singularities, let alone the corresponding curl and divergence. To resolve the surface profiles with a significantly higher degree of accuracy, we used 1000 out of our 1500 numerically determined Q_k. The last one-third of the computed coefficients was dropped in order to avoid "tainting."

Parker and Talbot generated their two solutions for the $c \neq c_R$ case using the same numerical approach as the one described for $c = c_R$ in Section 3.1.2. The only difference is in the choice of initial guess. For $c \neq c_R$ the initial guesses used by Parker and Talbot represent exact solutions to the system (3.29) truncated to three equations with three unknowns: Q_1, Q_2, and Q_3. Once again, the truncated system is equivalent to a quadratic equation with two different solutions, which correspond to the two numerical solutions of Parker and Talbot.

Our numerical approach entails the use of the constant coefficient system (3.27) solutions as initial guesses for the iterative procedure. Once again, since there is an infinite family of solutions to the CQ system (3.27), we expect there to be an infinite family of numerical solutions to the Rayleigh wave system (3.29). The correspondence between the two sets of solutions is described by the development of the anti-symmetric corners in the surface horizontal displacements of the CQ solutions into cusps in the solutions of the actual Q equations.

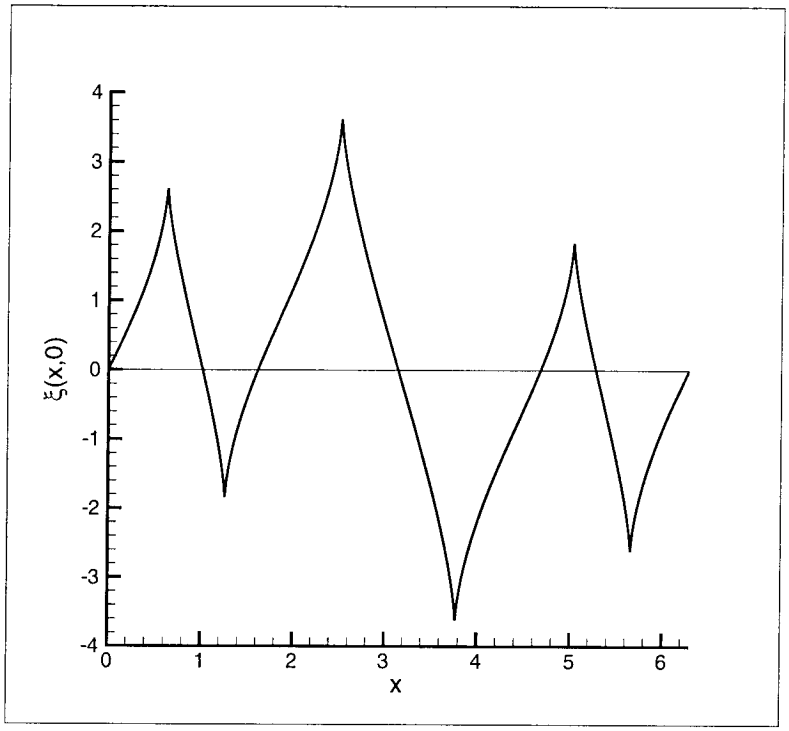

Figure 3.47: The horizontal displacement $\xi(x, 0)$ of solution 3 to the Q system with $c \neq c_R$.

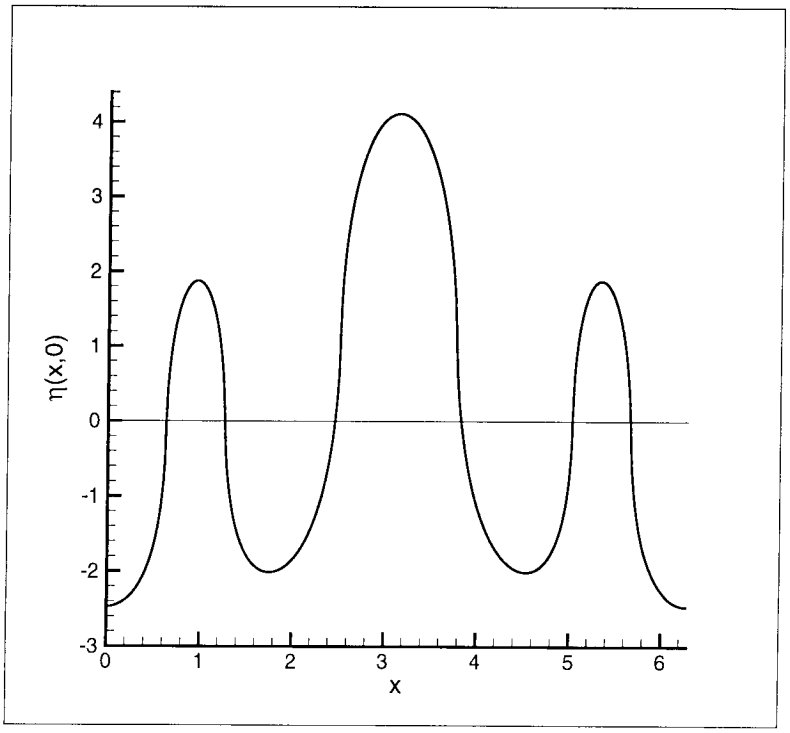

Figure 3.48: The vertical displacement $\eta(x, 0)$ of solution 3 to the Q system with $c \neq c_R$.

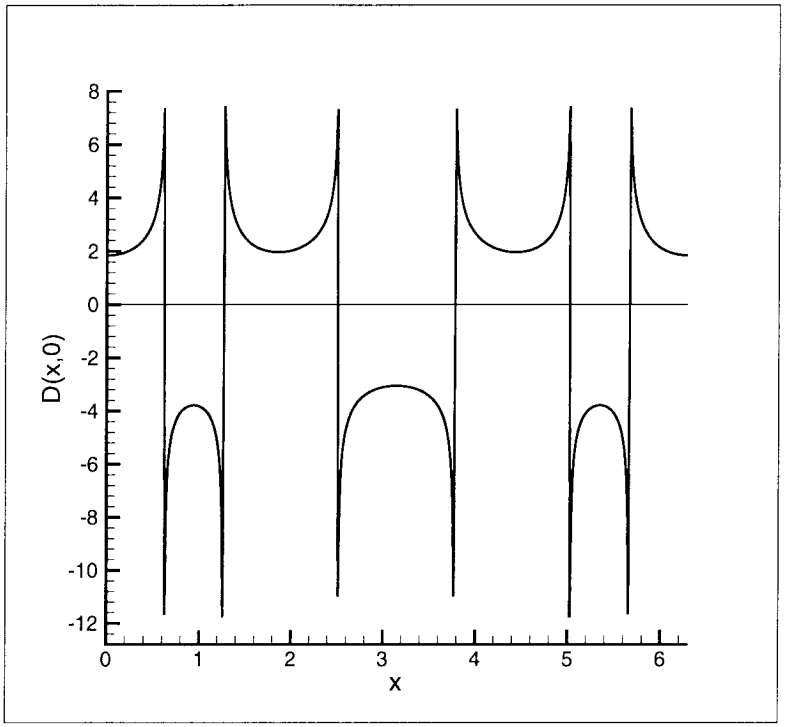

Figure 3.49: The divergence $D(x,0)$ of solution 3 to the Q system with $c \neq c_R$.

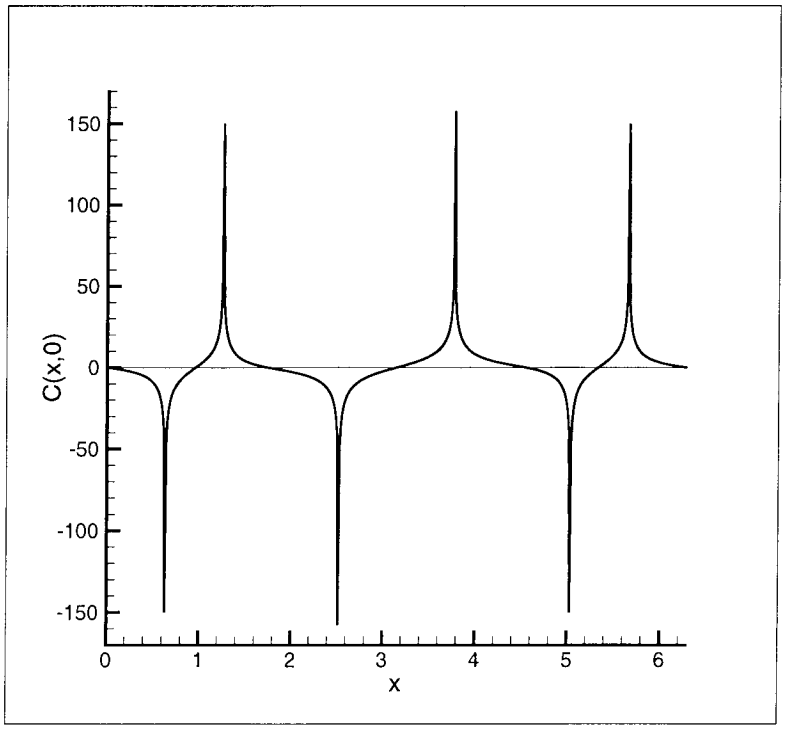

Figure 3.50: The curl $C(x,0)$ of solution 3 to the Q system with $c \neq c_R$.

Solution 3

To illustrate this point, and to show a typical new solution, we start with the initial guess

$$Q_k = \frac{10\,(\sin 0.2k\pi - \sin 0.4k\pi + \sin 0.8k\pi)}{k\pi}, \quad 1 \leq k \leq 1500. \tag{3.32}$$

The resulting solution profiles are given in Figures 3.47 through 3.50.

The structure of the surface horizontal displacement of this new solution is more complicated than that of the previous two solutions. Remarkably, it only takes 9 iterations for the numerical procedure to produce this solution - almost twice as fast as it would take for the method to converge when a comparably complicated initial guess is used in the $c = c_R$ case.

Just as expected, the surface horizontal displacement of the new solution 3 has singularities which are cusps. The solution 3 profiles display very similar features to those of numerical solutions 1 and 2. The most significant difference between solutions 1, 2, and 3 is the number and location of their surface singularities.

This, along with the study of various other numerical solutions to system (3.29), leads us to believe that the use of the constant coefficient initial guesses can potentially result in a rich infinite family of Rayleigh wave solutions.

3.2.3 Numerical Solutions to the Ad Hoc Q System with $\mathbf{c \neq c_R}$

We now turn our attention to the ad hoc system

$$\frac{1}{2}\sum_{k=1}^{n-1} A\,Q_k Q_{n-k} + \sum_{k=1}^{\infty} A\,Q_k Q_{n+k} = Q_n, \quad n = 1, \ldots, \infty, \tag{3.33}$$

where A is taken to be the average of $2(s+3p)/(p+3s) = 2.8961$ and $(p+s)/s = 3.1548$.

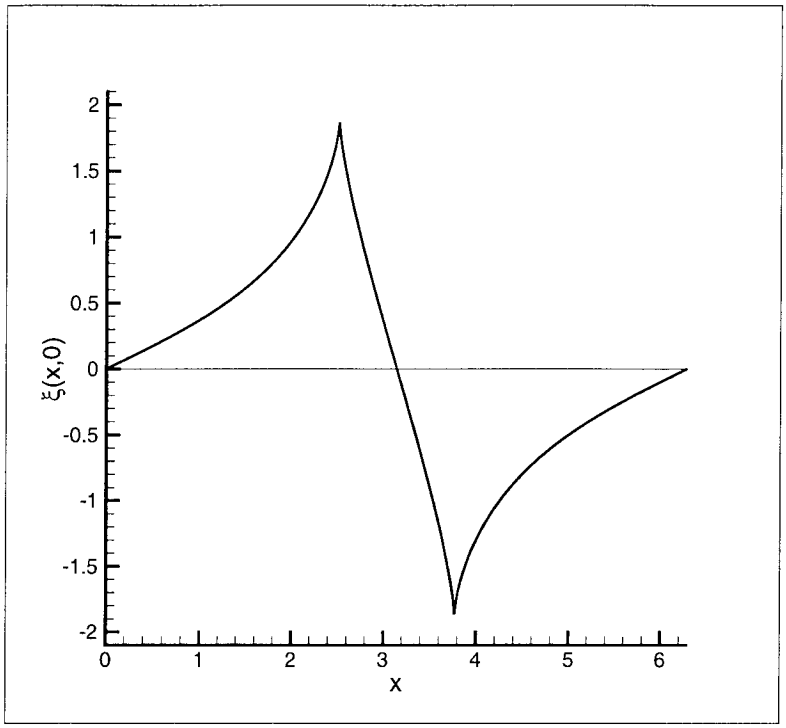

Figure 3.51: The horizontal displacement $\xi(x, 0)$ of solution 1 to the ad hoc Q system with $c \neq c_R$.

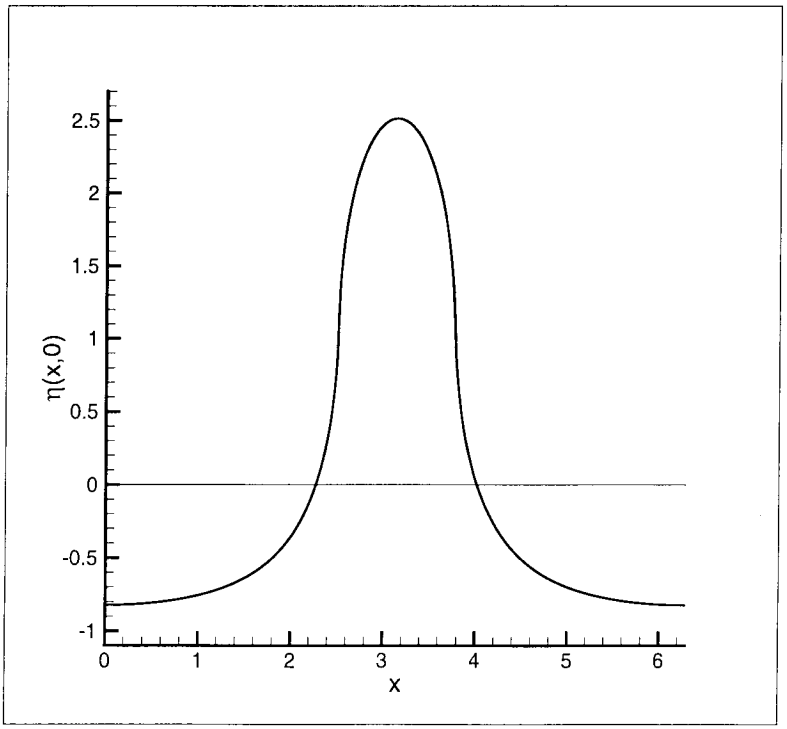

Figure 3.52: The vertical displacement $\eta(x, 0)$ of solution 1 to the ad hoc Q system with $c \neq c_R$.

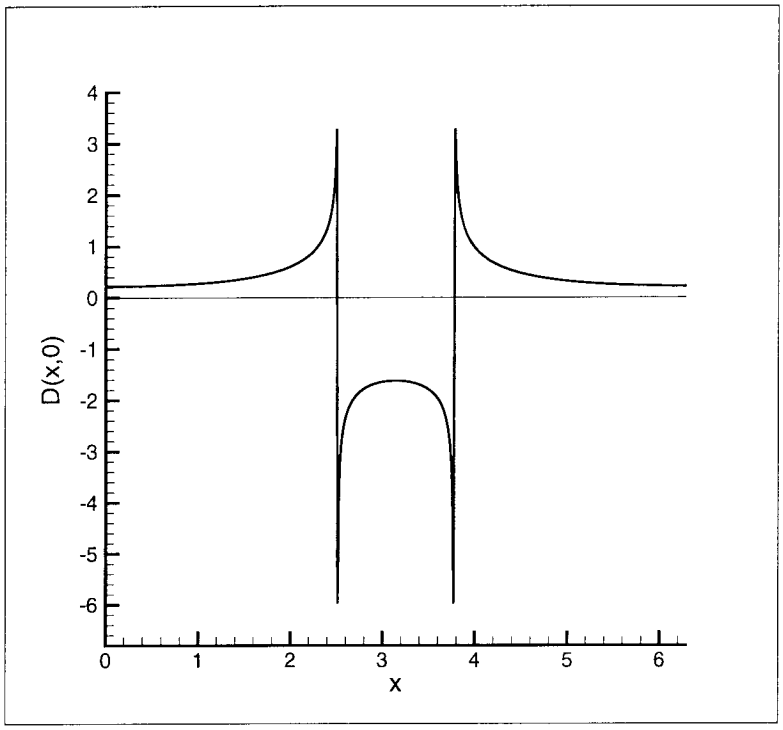

Figure 3.53: The divergence $D(x,0)$ of solution 1 to the ad hoc Q system with $c \neq c_R$.

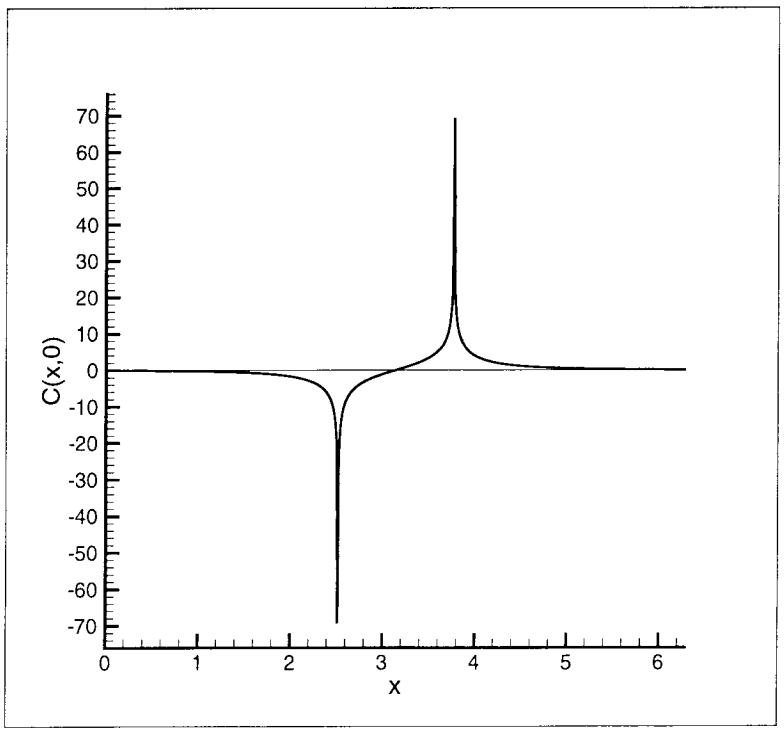

Figure 3.54: The curl $C(x,0)$ of solution 1 to the ad hoc Q system with $c \neq c_R$.

Q_k	Q_k ad hoc	Q_k real
Q_1	0.26190516	0.26908696
Q_2	-0.31555745	-0.32396285
Q_3	0.25497382	0.26411294
Q_4	-0.13541201	-0.14249193
Q_5	0.00491311	0.00817393
Q_6	0.09661847	0.09723819
Q_7	-0.14435361	-0.14757356
Q_8	0.13307494	0.13700927
Q_9	-0.07631449	-0.07923769
Q_{10}	0.00009560	0.00100033
Q_{11}	0.06662186	0.06780628
Q_{21}	0.04449095	0.04557496
Q_{31}	0.03496546	0.03587782
Q_{41}	0.02950271	0.03028911
Q_{51}	0.02590571	0.02660036
Q_{100}	-0.00325934	-0.00332602
Q_{101}	0.01761013	0.01807352
Q_{201}	0.01247304	0.01278559
Q_{301}	0.01041466	0.01067008
Q_{401}	0.00921917	0.00944749
Q_{501}	0.00838334	0.00859940
Q_{751}	0.00693452	0.00715298
Q_{999}	0.00371030	0.00378575
Q_{1000}	-0.00595099	-0.00614716
Q_{1100}	-0.00613722	-0.00635844
Q_{1200}	-0.00646967	-0.00671598
Q_{1300}	-0.00719018	-0.00745988
Q_{1400}	-0.00935039	-0.00963880
Q_{1500}	-0.23244752	-0.23468195

Table 3.10: A comparison of the numerical solutions to the ad hoc and the real Q systems with $c \neq c_R$ generated using the numerical procedure I with 1500 Fourier modes.

We generate a numerical solution to the ad hoc system, which is to be compared with the corresponding solution of the real Q system (3.29). We want to examine whether the ad hoc system solutions are good approximations to the real system solutions. In Section 3.1.3 we demonstrated that the ad hoc approximation works very well in the case of $c = c_R$. Now we want to complete our study of the ad hoc systems by examining the $c \neq c_R$ case.

We employ 1500 Fourier coefficients of the form (3.28) as an initial guess for the Newton-Raphson iterative procedure applied to the ad hoc system (3.33). Plots of the resulting surface profiles are given in Figures 3.51 through 3.54. Comparing the computed ad hoc solution with solution 1 of the real Q system, we observe that on the surface of the elastic material the real and the ad hoc solution profiles are impossible to distinguish.

A different way to estimate how close the two solutions are is to directly compare their Fourier coefficients Q_k, as is done in Table 3.10. It can be seen that the respective Q_k agree up to an order of 10^{-3} to 10^{-2}, which implies that the considered numerical solutions are indeed quite close.

Based on the presented comparison, we can suggest that, in general, the solutions of the ad hoc system (3.33) very closely resemble the solutions of the real Q system (3.29). This, along with our findings outlined in Section 3.1.3, implies that the ad hoc systems for $c = c_R$ and $c \neq c_R$ are indeed very accurate and useful models for the Rayleigh wave equations considered here.

3.2.4 Singularities in the Real and Ad Hoc Solutions with $c \neq c_R$

The numerical solutions with $c \neq c_R$ seem to display fractional singularity behavior on the surface $y = 0$ similarly to the $c = c_R$ case. Therefore, we shall try to match the computed Fourier coefficients to an asymptotic relation corresponding to the proposed singular behavior, just as we did in the $c = c_R$ case. If we assume that

the horizontal dispacement $\xi(x,0)$ has a cusp at the point $x = b$, then near the singularity we have

$$\xi(x,0) \backsim \widetilde{\xi}\,|x-b|^{\lambda}, \quad x \to b\,. \tag{3.34}$$

The leading order terms of the Fourier coefficients corresponding to this $\xi(x,0)$ are

$$\widetilde{Q}_k(\lambda) \backsim \frac{\widetilde{Q}\sin kb}{k^{\lambda}}, \quad k \to \infty\,. \tag{3.35}$$

Once again, $\widetilde{\xi}$ and $\widetilde{Q}$ are appropriately chosen constants, and $0 < \lambda < 1$.

In the following analysis we shall match the asymptotic formula (3.35) to the Fourier coefficients of each of the numerical solutions 1 of the real and the ad hoc systems with $c \neq c_R$. Since these two solutions have surface singularities at 0.8π and 1.2π, the value of b in equation (3.35) will be fixed to 0.8π. The process of matching the numerically determined Q_k to the asymptotic relation (3.35) is somewhat more complicated in this case, since the expression

$$\lambda_k = -\log\left|Q_k/(\widetilde{Q}\sin 0.8k\pi)\right|/\log k, \quad k \to \infty, \tag{3.36}$$

becomes infinite when $\sin 0.8k\pi$ is equal to zero. This occurs whenever k is a multiple of 5, i.e., $k = 5m$, $m = 1, \ldots, \infty$. Since formula (3.36) is not applicable in this case, we shall not attempt to use it to evaluate the λ_{5m}.

A selection of the λ_k values computed by substituting the numerically determined Q_k in formula (3.36) is given in Table 3.11. The oscillations in $\sin 0.8k\pi$ seem to induce oscillations in the λ_k computed using (3.36). The predominant part of the λ's given in (3.11) were chosen to correspond to values of k for which $|\sin 0.8k\pi|$ is close to 1.

The formula (3.36) is an asymptotic relation valid only when $k \to \infty$; therefore, it is only expected to predict correctly the values of λ_k for sufficiently large k.

k	λ_k real	λ_k ad hoc
2	0.42648602	0.42538372
3	0.45500091	0.46243196
4	0.45859616	0.47584438
7	0.55599674	0.55343172
12	0.57568857	0.57474040
22	0.59102396	0.59079040
52	0.60486579	0.60483098
102	0.61149173	0.61141812
197	0.61644510	0.61631648
257	0.61883418	0.61871747
502	0.63140808	0.63175965
752	0.65261944	0.65419184
992	0.68460979	0.68820458
997	0.68544314	0.68909192

Table 3.11: Values for λ_k determined using formula (3.36) with the numerically determined Q_k corresponding to solutions 1 of the real and ad hoc Q systems with $c \neq c_R$.

According to Table 3.11 the higher-order λ_k fall in the range $0.6 < \lambda_k < 0.7$, but there is far less uniformity in the computed λ values than was the case with the λ study of the $c = c_R$ numerical solutions, discussed in Section 3.1.4.

3.2.5 Modification: Numerical Method II with $\mathbf{c \neq c_R}$

Now we shall use the asymptotic formula (3.35) with $\lambda = 2/3$ and $b = 0.8\pi$ as an initial guess for the numerical procedure applied to the truncated real Q system (3.29). Also, we shall consider twice as many modes as we intend to solve for. The second half of the Fourier coefficients will be fixed to the proposed asymptotic values given by (3.35). This modification of the numerical procedure is done in order to reduce the effect of "tainting" of the higher-order modes, and to produce more accurate solutions of the $c \neq c_R$ system.

A comparison of the Q_k coefficients generated using the original and the modified

Q_k	Q_k numerical I	Q_k numerical II
Q_1	0.26908696	0.26772265
Q_2	-0.32396285	-0.32283167
Q_3	0.26411294	0.26392955
Q_4	-0.14249193	-0.14340286
Q_5	0.00817393	0.00980035
Q_6	0.09723819	0.09561084
Q_7	-0.14757356	-0.14668535
Q_8	0.13700927	0.13730819
Q_9	-0.07923769	-0.08068066
Q_{10}	0.00009560	0.00100033
Q_{11}	0.06780628	0.06595601
Q_{21}	0.04557496	0.04338588
Q_{31}	0.03587782	0.03343282
Q_{41}	0.03028911	0.02763627
Q_{51}	0.02660036	0.02377148
Q_{100}	-0.00332602	0.00107509
Q_{101}	0.01807352	0.01462169
Q_{201}	0.01278559	0.00863551
Q_{301}	0.01067008	0.00612588
Q_{401}	0.00944749	0.00466412
Q_{501}	0.00859940	0.00367247
Q_{751}	0.00715298	0.00209193
Q_{999}	0.00378575	-0.00550500
Q_{1000}	-0.00614716	0.00277831
Q_{1100}	-0.00635844	0.00309138
Q_{1200}	-0.00671598	0.00354985
Q_{1300}	-0.00745988	0.00434231
Q_{1400}	-0.00963880	0.00628283
Q_{1500}	-0.23468195	0.17568881

Table 3.12: A comparison of the numerical solutions to the real Q system with $c \neq c_R$ generated using the original (I) and the modified (II) numerical methods.

k	λ_k numerical I	λ_k numerical II
2	0.42648602	0.42419901
3	0.45500091	0.45100642
4	0.45859616	0.45033272
7	0.55599674	0.55648693
12	0.57568857	0.57703409
22	0.59102396	0.59363838
52	0.60486579	0.61033538
102	0.61149173	0.62046213
197	0.61644510	0.62974844
257	0.61883418	0.63374149
502	0.63140808	0.64576458
752	0.65261944	0.65545355
992	0.68460979	0.66374025
997	0.68544314	0.66390503

Table 3.13: Values for λ_k computed using (3.36) and the Fourier coefficients Q_k of solution 1 to the real Q system. The values used for the Q_k coefficients were determined via the original (I), and the modified (II) numerical methods.

numerical procedures is given in Table 3.12. Clearly, the effects of "tainting" in the higher-order Q_k are significantly reduced.

Table 3.13 shows a comparison of the λ_k computed using (3.36) and the Fourier coefficients Q_k determined using the original and the modified numerical methods. The λ's in the second column of Table 3.13 are more uniformly distributed, and significantly less affected by "tainting" due to the finite cutoff.

Concluding Remarks on the Modified Method II

In Section 3.2.1 the numerical scheme for the constant coefficient system (3.27) with $c \neq c_R$ was modified in a similar fashion. The numerical solution resulting from that modification had much better accuracy than the solution computed using the original procedure, as shown in Table 3.9. In Section 3.1.5 we also modified the scheme for the actual Q system with $c = c_R$, achieving what appeared to be

significant improvements in accuracy, as illustrated in Tables 3.7 and 3.8.

These two cases, along with the results presented here for the actual Q systems with $c \neq c_R$, seem to indicate that as long as the formulas used to compute the higher-order Q_k for the numerical procedure II are accurate, the proposed modifications significantly improve the accuracy of the numerical solutions of the truncated Q systems both for $c = c_R$ and $c \neq c_R$.

Chapter 4 Surface Singularities in the Infinite Interval Case

In Chapter 2 we derived the solvability condition (2.64) for the second-order Rayleigh wave equations in the infinite interval case. Now we shall use this equation to study the local behavior of the surface displacement singularities for $-\infty < x < \infty$.

In Chapter 3 we examined various numerical solutions to the periodic Rayleigh wave problem, and we found empirical evidence that the horizontal displacements of these solutions have fractional surface singularities, and locally

$$\xi(x,0) = \widetilde{\xi}\,|x|^{\lambda},$$

where x measures the distance from the singularity, $\widetilde{\xi}$ is a constant, and $0 < \lambda < 1$.

Here we shall focus on satisfying the solvability condition (2.64) using a Rayleigh wave solution which has a surface horizontal displacement with a single cusp. In an analytic approach it is presumably simpler to consider just one singularity in the infinite interval. This study should have a bearing on the periodic case even though interactions among the repeated singularities there may modify the fractional powers.

In this chapter we shall use p, s, and σ to denote the values of these factors at $c = c_R$.

4.1 The Solvability Condition

The second-order solvability condition for the infinite interval case was derived in Section 2.4 and it has the form

$$\frac{(c_1^2-c_2^2)}{4c_1^2c_2^2}\int_{-\infty}^{\infty}\int_{0}^{\infty}\left\{c_2^2C^{(1)}C^{(1)}\widetilde{P}+2c_1^2C^{(1)}D^{(1)}\widetilde{S}\right\}dxdy=\kappa p\int_{-\infty}^{\infty}\frac{P_x^{(1)}(x,0)}{(x-x_0)}\,dx, \tag{4.1}$$

where the test functions $\widetilde{P}$ and $\widetilde{S}$ are given by

$$\widetilde{P}(x,y)=\frac{py}{(x-x_0)^2+p^2y^2}, \tag{4.2}$$

$$\widetilde{S}(x,y)=-\frac{\sigma^2}{s}\,\frac{x-x_0}{(x-x_0)^2+s^2y^2}, \tag{4.3}$$

for any choice of x_0 in $-\infty < x_0 < \infty$. The functions $C^{(1)}(x,y)$, $D^{(1)}(x,y)$, and $P^{(1)}(x,y)$ are the curl, divergence, and potential P of the linear Rayleigh wave solutions, which can be used as first-order terms in small-amplitude expansions of nonlinear Rayleigh waves.

In Section 2.2.2 we showed that

$$D(x,y)=\frac{2c_2^2}{c_1^2}\,U(x,py), \tag{4.4}$$

$$C(x,y)=-\frac{2\sigma^2}{s}\,V(x,sy), \tag{4.5}$$

where the functions U and V are related to the surface horizontal displacement derivative $\xi_0'(x)=\xi_x(x,0)$ through

$$U(x,y)+iV(x,y)=\frac{1}{\pi i}\int_{-\infty}^{\infty}\frac{\xi_0'(w)}{w-(x+iy)}\,dw. \tag{4.6}$$

Also, according to equation (2.30) in Section 2.2.2, we have

$$P_x^{(1)}(x,0) = \frac{\xi_0(x)}{1-\sigma^2}. \tag{4.7}$$

When we substitute equations (4.4), (4.5) and (4.7) into the solvability condition (4.1) we get

$$\frac{\sigma^4(c_1^2-c_2^2)}{s^2\,c_1^2}\int_{-\infty}^{\infty}\int_{0}^{\infty}\left\{\frac{V^2(x,sy)\,py}{(x-x_0)^2+p^2y^2}+2\,\frac{U(x,py)\,V(x,sy)\,(x-x_0)}{(x-x_0)^2+s^2y^2}\right\}dxdy = \\ = \frac{\kappa p}{1-\sigma^2}\int_{-\infty}^{\infty}\frac{\xi_0(x)}{(x-x_0)}\,dx, \tag{4.8}$$

for any choice of x_0 in $-\infty < x_0 < \infty$. The integrals in the equation above are in a convolution form, which suggests using a Fourier transform in x. However, the multiple convolutions on the left-hand side of (4.8) show that the transformed equations will be quite complicated to solve for $\xi_0(x)$.

Based on our numerical studies, we try a singular solution $\xi_0(x) \propto |x|^\lambda$ and see whether the solvability condition (4.8) determines λ. With this form of $\xi_0(x)$, the integral on the right-hand side of (4.8) is expected to be less singular than the integral on the left-hand side. As we shall show later, this is indeed true. Since the case $\kappa = 0$, $c = c_R$ is of special interest anyway, we shall first take the right-hand side of (4.8) to be zero.

4.2 Singular First-Order Solutions in the Solvability Condition

We want to verify that a fractional singularity behavior for $\xi(x,0)$ can satisfy the solvability condition:

$$\int_{-\infty}^{\infty}\int_{0}^{\infty}\left\{\frac{V^2(x,sy)\,py}{(x-x_0)^2+p^2y^2}+2\,\frac{U(x,py)\,V(x,sy)\,(x-x_0)}{(x-x_0)^2+s^2y^2}\right\}dxdy=0, \tag{4.9}$$

and investigate whether the resulting equation fixes the fractional power λ.

We consider a surface horizontal displacement of the form

$$\xi_0(x)=\cos\frac{\lambda\pi}{2}\,\frac{|x|^\lambda}{\lambda},\quad 0<\lambda<1, \tag{4.10}$$

corresponding to a fractional singularity of power λ located at the point $x=0$. For this choice of horizontal displacement $\xi_0(x)$ the potential functions $U(x,py)$ and $V(x,sy)$ are

$$\begin{aligned} U(x,py)&=\frac{\sin\left[\nu\left(\pi/2-\theta_p\right)\right]}{(x^2+p^2y^2)^{\nu/2}},\ \theta_p=\arctan\frac{py}{x},\\ V(x,sy)&=-\frac{\cos\left[\nu\left(\pi/2-\theta_s\right)\right]}{(x^2+s^2y^2)^{\nu/2}},\ \theta_s=\arctan\frac{sy}{x}, \end{aligned} \tag{4.11}$$

according to (4.6). Here $\nu=1-\lambda$ is introduced to simplify notation.

First, we apply a Fourier transform in x to the solvability condition (4.9). The following definition of the Fourier transform

$$F(k)=\widehat{f}(k)=\int_{-\infty}^{\infty}f(x)\,e^{ikx}\,dx, \tag{4.12}$$

and its inverse

$$f(x) = \frac{1}{2\pi} \int_{-\infty}^{\infty} F(k)\, e^{-ikx}\, dk, \tag{4.13}$$

are used. The corresponding convolution relations are

$$\int_{-\infty}^{\infty} f(x-\zeta) g(\zeta)\, d\zeta \longleftrightarrow F(k)G(k), \tag{4.14}$$

$$f(x)g(x) \longleftrightarrow \frac{1}{2\pi} \int_{-\infty}^{\infty} F(k-l)G(l)\, dl. \tag{4.15}$$

When the convolution law (4.14) is applied to equation (4.9), it reduces to

$$\int_{0}^{\infty} \left\{ FT[V^2(x,sy)]\, e^{-p|k|y} - 2i\, sgn(k)\, FT[U(x,py)\, V(x,sy)]\, e^{-s|k|y} \right\} dy = 0, \tag{4.16}$$

for any choice of k in $-\infty < k < \infty$. Here, the Fourier tranforms of the following functions,

$$\int_{-\infty}^{\infty} \frac{py}{x^2 + p^2y^2}\, e^{ikx}\, dx = \pi\, e^{-p|k|y}, \tag{4.17}$$

$$\int_{-\infty}^{\infty} \frac{x}{x^2 + s^2y^2}\, e^{ikx}\, dx = \pi\, i\, sgn(k)\, e^{-s|k|y}, \tag{4.18}$$

have been used.

The main difficulty associated with equation (4.16) is in working with the Fourier transform of the product of $U(x,py)$ and $V(x,sy)$, since these two functions are scaled differently in y. Various approaches were attempted to overcome this difficulty, and ultimately equation (4.16) was solved exactly for a fractional singularity of the form (4.10) with $p = s$. The corresponding solution for λ was $\lambda = 2/3$. The

solution to the $p = s$ case helped us understand how the various components of the solvability condition (4.16) can be manipulated in order to reduce it to an algebraic equation for λ.

One possible way to proceed from the $p = s$ case to the case of general p and s was to find an approximate form for the product $U(x, py)\, V(x, sy)$ which simplifies the computation of its Fourier transform. This is the approach followed in this work. The approximate forms considered here were chosen in order to resemble the structure of the actual product $U(x, py)\, V(x, sy)$ as closely as possible. Also, we had to ensure that the approximate approach is consistent with the previously determined exact solution for the $p = s$ case.

In turn, G.B. Whitham pursued an analytic approach to this problem, and showed that a singularity of the form (4.10) satisfies the solvability condition (4.9) exactly with $\nu = 1/3$, $\lambda = 2/3$ for all values of p and s.

Determining the Fourier Transforms of $V^2(x, sy)$ and $U(x, py)\, V(x, sy)$

First, we need to find the Fourier transforms of the functions $U(x, py)$ and $V(x, sy)$. These can be evaluated using the definition in (4.6) and the convolution theorem. We get

$$\begin{aligned} \widehat{U}(k, py) &= \widehat{\xi_0'}(k)\, e^{-p|k|y} = -ik\, \widehat{\xi_0}(k)\, e^{-p|k|y}, \\ \widehat{V}(k, sy) &= \widehat{\xi_0'}(k)\, i\, sgn(k)\, e^{-s|k|y} = |k|\, \widehat{\xi_0}(k)\, e^{-s|k|y}. \end{aligned} \tag{4.19}$$

The Fourier transform of the $\xi_0(x)$ given by (4.10) is

$$\widehat{\xi_0}(k) = \frac{-\pi}{(\nu - 1)!\, |k|^{2-\nu}}. \tag{4.20}$$

Substituting (4.20) into (4.19) we obtain

$$\begin{aligned} \widehat{U}(k,py) &= \frac{i\pi\, sgn(k)}{(\nu-1)!\,|k|^{(1-\nu)}}\, e^{-p|k|y}, \\ \widehat{V}(k,sy) &= \frac{-\pi}{(\nu-1)!\,|k|^{(1-\nu)}}\, e^{-s|k|y}. \end{aligned} \tag{4.21}$$

By comparing equations (4.11) and (4.21), we establish the following Fourier transform relations:

$$\frac{\sin\left[\nu\left(\pi/2-\theta_p\right)\right]}{\left(x^2+p^2y^2\right)^{\nu/2}} \quad \xrightarrow{FT} \quad \frac{i\pi\, sgn(k)}{(\nu-1)!\,|k|^{(1-\nu)}}\, e^{-p|k|y}, \tag{4.22}$$

$$-\frac{\cos\left[\nu\left(\pi/2-\theta_s\right)\right]}{\left(x^2+s^2y^2\right)^{\nu/2}} \quad \xrightarrow{FT} \quad \frac{-\pi}{(\nu-1)!\,|k|^{(1-\nu)}}\, e^{-s|k|y}. \tag{4.23}$$

We now note that the product $V^2(x,sy)$ can be split up in the following way:

$$\begin{aligned} \frac{\cos^2\left[\nu\left(\pi/2-\theta_s\right)\right]}{\left(x^2+s^2y^2\right)^{\nu}} &= \frac{1-\cos\left[2\nu\left(\pi/2-\theta_s\right)\right]}{2\left(x^2+s^2y^2\right)^{\nu}} = \\ &= \underbrace{\frac{1}{2\left(x^2+s^2y^2\right)^{\nu}}}_{\text{term 1}} - \underbrace{\frac{\cos\left[2\nu\left(\pi/2-\theta_s\right)\right]}{2\left(x^2+s^2y^2\right)^{\nu}}}_{\text{term 2}}. \end{aligned} \tag{4.24}$$

We can use equation (4.23), with ν instead of $\nu/2$, to compute the Fourier transform of term 2 in the equation above. As for the Fourier transfrom of term 1, we can use the relation

$$FT\left[\frac{1}{2\left(x^2+s^2y^2\right)^{\nu}}\right] = \int_{-\infty}^{\infty} \frac{e^{ikx}}{2\left(x^2+s^2y^2\right)^{\nu}}\, dx = \frac{\sqrt{\pi}}{\Gamma(\nu)}\left(\frac{|k|}{2sy}\right)^{\nu-\frac{1}{2}} K_{\nu-\frac{1}{2}}(s|k|y),$$

as given in [13], where $\Gamma(\nu)$ is the Gamma function, and $K_{\nu-\frac{1}{2}}(z)$ is the modified Bessel function of order $\nu-1/2$.

The resulting closed form expression for the Fourier transform of $V^2(x, sy)$ is

$$FT\left[V^2(x,sy)\right] = \frac{\sqrt{\pi}}{\Gamma(\nu)}\left(\frac{|k|}{2sy}\right)^{\nu-\frac{1}{2}} K_{\nu-\frac{1}{2}}(s|k|y) + \frac{\pi\, e^{-s|k|y}}{2\,(2\nu-1)!\,|k|^{(1-2\nu)}}, \tag{4.25}$$

which can be conveniently substituted directly into the solvability condition (4.16). In this manner we avoid introducing a convolution integral of the form (4.15) for the Fourier transform of $V^2(x, sy)$. This simplifies the first portion of equation (4.16) to a single integral which can be integrated exactly in y.

We now examine the second product $U(x, py)\, V(x, sy)$, which has the form

$$U(x,py)\,V(x,sy) = -\frac{\sin\left[\nu\,(\pi/2-\theta_p)\right]\cos\left[\nu\,(\pi/2-\theta_s)\right]}{(x^2+p^2y^2)^{\nu/2}\,(x^2+s^2y^2)^{\nu/2}}. \tag{4.26}$$

If in this equation we had one scaling factor instead of two, we could apply to it the same kind of reasoning as in computing the Fourier transform of $V^2(x, sy)$. As one possible approximation, we now take both of the scaling factors in (4.26) to be equal to p. Then

$$U(x,py)\,V(x,sy) \approx U(x,py)V(x,py) = -\frac{\sin\left[\nu\,(\pi/2-\theta_p)\right]\cos\left[\nu\,(\pi/2-\theta_p)\right]}{(x^2+p^2y^2)^{\nu}}. \tag{4.27}$$

Using equation (4.22) with ν instead of $\nu/2$, we find that the corresponding Fourier transform is

$$FT\left[U(x,py)\,V(x,py)\right] = \frac{-i\pi\; sgn(k)\, e^{-p|k|y}}{2\,(2\nu-1)!\,|k|^{(1-2\nu)}}. \tag{4.28}$$

When (4.25) and (4.28) are substituted into the solvability condition (4.16), we obtain

$$\int_0^\infty \left\{ \frac{\sqrt{\pi}}{\Gamma(\nu)}\left(\frac{|k|}{2sy}\right)^{\nu-\frac{1}{2}} K_{\nu-\frac{1}{2}}(s|k|y)\, e^{-p|k|y} - \frac{\pi\, e^{-(p+s)|k|y}}{2\,(2\nu-1)!\,|k|^{(1-2\nu)}} \right\} dy = 0. \tag{4.29}$$

The second component of the integral above is integrated to produce

$$\frac{\sqrt{\pi}}{\Gamma(\nu)} \int_0^\infty \left(\frac{|k|}{2sy}\right)^{\nu-\frac{1}{2}} K_{\nu-\frac{1}{2}}(s|k|y)\, e^{-p|k|y} dy = \frac{\pi}{2\,(2\nu-1)!\,|k|^{(2-2\nu)}(p+s)}. \tag{4.30}$$

Making the change $s|k|y = \zeta$ on the left-hand side we get

$$\int_0^\infty \zeta^{\frac{1}{2}-\nu}\, e^{-\frac{p}{s}\zeta}\, K_{\nu-\frac{1}{2}}(\zeta)\, d\zeta = \frac{\sqrt{\pi}\, s\, 2^{\nu-\frac{3}{2}}}{p+s}\, \frac{\Gamma(\nu)}{\Gamma(2\,\nu)}. \tag{4.31}$$

Finally, we substitute the formula

$$\int_0^\infty \zeta^{\frac{1}{2}-\nu}\, e^{-\frac{p}{s}\zeta}\, K_{\nu-\frac{1}{2}}(\zeta)\, d\zeta = \frac{\sqrt{\pi}\, s\, 2^{\nu-\frac{1}{2}}}{p+s}\, \frac{\Gamma(2-2\nu)}{\Gamma(2-\nu)}\, F(1,\nu,2-\nu,\frac{p-s}{p+s}), \tag{4.32}$$

as given in [6], into equation (4.31) to produce

$$\frac{\Gamma(2-2\nu)\,\Gamma(2\nu)}{\Gamma(2-\nu)\,\Gamma(\nu)} = \frac{1}{2\,F(1,\nu,2-\nu,\frac{p-s}{p+s})}, \tag{4.33}$$

where $F(1,\nu,2-\nu,z)$ is a hypergeometric function. This equation can be further simplified to

$$\frac{(1-\nu)\cos\nu\pi}{1-2\nu} = F(1,\nu,2-\nu,\frac{p-s}{p+s}). \tag{4.34}$$

This is the final form of the solvability condition obtained with the approximation $U(x,py)\,V(x,sy) \approx U(x,py)V(x,py)$.

We can solve equation (4.34) for the same elastic material which we studied numerically in Chapter 3, i.e., for a Poisson ratio of 1/4 with $p = 0.8475$ and $s = 0.3933$. Using Maple we obtain the following solution to (4.34):

$$\nu = 0.254690, \quad \lambda = 1-\nu = 0.745310. \tag{4.35}$$

This result is reasonably close to the λ determined numerically in Section 3.1.4, where we established that in the case of numerical solution 1, an appropriate range for the numerical λ is $(0.63, 2/3)$. When we consider $p = s$, equation (4.34) reduces to

$$\frac{(1-\nu)\cos\nu\pi}{1-2\nu} = 1, \tag{4.36}$$

which has the exact solution $\nu = \frac{1}{3}$ and the corresponding λ is in fact equal to $\frac{2}{3}$.

We shall also use a second approximation for the expression $U(x,py)\,V(x,sy)$ which produces an improved estimate for the value of the fractional power λ. This time we take

$$U(x,py)\,V(x,sy) \approx \frac{s}{p}\left(\frac{p+s}{\sqrt{4ps}}\right)^{2\nu} U(x,\frac{p+s}{2}y)\,V(x,\frac{p+s}{2}y) + \\ + \frac{s}{p}\left(\frac{p-s}{\sqrt{4ps}}\right)^{2\nu} U(x,\frac{p-s}{2}y)\,V(x,\frac{p-s}{2}y). \tag{4.37}$$

This choice is made in order to reflect the structure of the product $U(x,py)\,V(x,sy)$, as given in (4.26), if it were to be expanded out as a sum of sines.

For the first component of (4.37) we have

$$FT\left[U(x,\frac{p+s}{2}y)\,V(x,\frac{p+s}{2}y)\right] = FT\left[-\frac{\sin\left[\nu\left(\pi/2-\theta_{(p+s)/2}\right)\right]\cos\left[\nu\left(\pi/2-\theta_{(p+s)/2}\right)\right]}{(x^2+(p+s)^2y^2/4)^{\nu}}\right],$$

which is equal to

$$FT\left[-\frac{\sin\left[2\,\nu\left(\pi/2-\theta_{(p+s)/2}\right)\right]}{2\,(x^2+(p+s)^2y^2/4)^{\nu}}\right].$$

The above Fourier transform can be evaluated directly using equation (4.22). We deal with the second component of (4.37) in a similar manner, and we obtain

$$FT\Big[U(x,py)\,V(x,sy)\Big] \approx$$
$$\approx \frac{-i\pi s\, sgn(k)}{2p\,(2\nu-1)!\,|k|^{(1-2\nu)}}\left[\left(\frac{p+s}{\sqrt{4ps}}\right)^{2\nu} e^{-\frac{p+s}{2}|k|y} + \left(\frac{p-s}{\sqrt{4ps}}\right)^{2\nu} e^{-\frac{p-s}{2}|k|y}\right] \quad (4.38)$$

Once again, we substitute the Fourier transforms (4.25) and (4.38) into the solvability condition (4.16) to produce

$$\int_0^\infty \left\{ \frac{\sqrt{\pi}}{\Gamma(\nu)} \left(\frac{|k|}{2sy}\right)^{\nu-\frac{1}{2}} K_{\nu-\frac{1}{2}}(s|k|y)\, e^{-p|k|y} + \frac{\pi\, e^{-(p+s)|k|y}}{2\,(2\nu-1)!\,|k|^{(1-2\nu)}} \right\} dy +$$
$$- \int_0^\infty \left\{ \frac{\pi s}{p\,(2\nu-1)!\,|k|^{(1-2\nu)}} \left[\left(\frac{p+s}{\sqrt{4ps}}\right)^{2\nu} e^{-\frac{p+3s}{2}|k|y} + \left(\frac{p-s}{\sqrt{4ps}}\right)^{2\nu} e^{-\frac{p+s}{2}|k|y} \right] \right\} dy = 0. \quad (4.39)$$

Integrating with respect to y, and then following the same steps as in deriving equation (4.34) from (4.29), we get the condition

$$\frac{(1-2\nu)\,F(1,\nu,2-\nu,\frac{p-s}{p+s})}{(1-\nu)\cos\nu\pi} + 1 = \frac{4s}{p\,(\sqrt{4ps})^{2\nu}}\left[\frac{(p+s)^{2\nu+1}}{p+3s} + (p-s)^{2\nu}\right]. \quad (4.40)$$

Solving this equation for ν numerically with $p = 0.8475$ and $s = 0.3933$, we get

$$\nu = 0.368247, \quad \lambda = 1-\nu = 0.631753, \quad (4.41)$$

which compares well with the numerically determined λ, i.e., λ in the range of $(0.63, 2/3)$. In addition, equation (4.40) reduces to equation (4.36) if we take $p = s$. Once again, the $p = s$ case is resolved exactly by $\nu = 1/3$, $\lambda = 2/3$.

We have shown that with the proposed approximations for $U(x,py)\,V(x,sy)$, the solvability condition (4.9) is indeed satisfied by a fractional singularity of the form (4.10). The required values for the fractional power are $\lambda = 0.745310$ when we take the approximate form (4.27), and $\lambda = 0.631753$ when we take (4.37).

It is significant to note that we have made no other approximations besides con-

sidering a modified form for $U(x,py)\,V(x,sy)$. Therefore, the accuracy of the determined λ increases as the quality of the approximate forms used for $U(x,py)\,V(x,sy)$ improves. This explains why the λ resulting from our second approach compares significantly better with G.B. Whitham's exact result and the numerical estimates from Chapter 3 than the λ from our first approximation.

We should also make the distinction that the solvability condition (4.9) corresponds to the infinite interval formulation of the second-order Rayleigh wave problem, while the numerical profiles given in Chapter 3 correspond to the periodic formulation of the same problem. The solvability condition analysis focused on a single-peaked fractional singularity, while the computed periodic profiles had multiple cusps, often in close proximity with each other. There is the possibility that the singularities in the periodic case will differ from the singularities in the infinite interval case due to some form of interaction between neighboring cusps. However, it is reassuring that when we compare the λ values in the periodic and the infinite interval case, they are very close.

We now turn to the case of $c \neq c_R$, $\kappa \neq 0$. Then the solvability condition is

$$\int_0^\infty \left\{ FT[V^2(x,sy)]\, e^{-p|k|y} - 2i\, sgn(k)\, FT[U(x,py)\, V(x,sy)]\, e^{-s|k|y} \right\} dy =$$

$$= \frac{2\kappa s\, c_1^2\, c_2^2}{c^2\,(c_1^2 - c_2^2)}\, i\pi sgn(k)\, \widehat{\xi}_0(k). \qquad (4.42)$$

Considering that for a fractional singularity of the type (4.10), we have

$$\widehat{\xi}_0(k) = \frac{-\pi}{(\nu-1)!\,|k|^{2-\nu}}, \qquad (4.43)$$

then the right-hand side of (4.42) is of order $O(|k|^{\nu-2})$, while, as shown in Section 4.2, the left-hand side is of order $O(|k|^{2\nu-2})$. Since we are performing local analysis of the proposed singularity, we are interested in satisfying equation (4.42) for $k \to \infty$. In that limit, the right-hand side of the solvability condition (4.42) is subdominant

to the left-hand side. Therefore, equation (4.42) reduces to (4.16) in the limit of $k \to \infty$.

Therefore, we conclude that, within the second-order theory, the horizontal displacement singularities of steady-profile Rayleigh waves are cusps, both for $c = c_R$ and $c \neq c_R$. The values for λ in each case are the same, since they are both asymptotic solutions of the solvability condition (4.9) with $\xi_0(x)$ given by (4.10). Thus, according to the second-order theory, the fractional singularities of steady-profile Rayleigh waves moving at speeds $c = c_R$ or $c \neq c_R$ have exactly the same form.

Bibliography

[1] Igor A. Beresnev, Kuo-Liang Wen. The Possibility of Observing Nonlinear Path Effect in Earthquake-Induced Seismic Wave Propagation. *Bulletin of the Seismological Society of America*, **Vol. 86, No. 4**, 1996, pp. 1028-1041.

[2] G. F. Carrier, M. Krook, C. E. Pearson. Functions of A Complex Variable. *Hod Books*, 1983.

[3] P. Chadwick. Surface and Interfacial Waves of Arbitrary Form in Isotropic Elastic Media. *Journal of Elasticity*, **6**, 1976, pp. 73-80.

[4] Arthur Erdelyi. Tables of Integral Transforms. *McGraw-Hill*, **Vol. 2**, 1954.

[5] I.M. Gelf'and, G. E. Shilov. Generalized Functions. *Academic Press*, **Vol. 1**, 1964.

[6] I.S. Gradshteyn, I.M. Ryzhik. Table of Integrals, Series and Products. *Academic Press*, 1979, p. 712.

[7] A.M. Ionov. A Space-Time Evolution Equation for Rayleigh Waves in a Nonlinear Dissipative Medium: Basic Relations. *Acoustical Physics*, **Vol. 40**, **No. 2**, 1994, pp. 237-243.

[8] A.M. Ionov. A Space-Time Evolution Equation for Rayleigh Waves in a Nonlinear Dissipative Medium: Analysis of Results. *Acoustical Physics*, **Vol. 40**, **No. 3**, 1994, pp. 363-368.

[9] F. John. Plane Strain Problems for A Perfectly Elastic Material of Harmonic Type. *Communications on Pure and Applied Mathematics*, **13**, 1960, pp. 239-296.

[10] N. Kalyanasundaram. Nonlinear Surface Acoustic Waves on an Isotropic Solid. *International Journal of Engineering Science*, **Vol. 19**, 1981, pp. 279-286.

[11] N. Kalyanasundaram, R. Ravindran, P. Prasad. Coupled Amplitude Theory of Nonlinear Surface Acoustic Waves. *Journal of the Acoustical Society of America*, **72(2)**, 1982, pp. 488-493.

[12] N. Kalyanasundaram, G.V. Anand. Periodic Rayleigh Waves of Finite Amplitude on an Isotropic Solid. *Journal of the Acoustical Society of America*, **72(5)**, 1982, pp. 1518-1523.

[13] F. Oberhettinger. Fourier Transforms of Distributions and Their Inverses. *Academic Press*, 1973, p. 106.

[14] D.F. Parker. The Nonlinear Dispersion of Rayleigh Waves. *Physica* **16D**, 1985, pp. 385-397.

[15] D.F. Parker, A.P. Mayer, A.A. Maradudin. The Projection Method for Nonlinear Surface Acoustic Waves. *Wave Motion*, **16**, 1992, pp. 151-162.

[16] D.F. Parker, F.M. Talbot. Analysis and Computation for Nonlinear Elastic Surface Waves of Permanent Form. *Journal of Elasticity*, **15**, 1985, pp. 389-426.

[17] D.F. Parker. Waveform Evolution for Nonlinear Surface Acoustic Waves. *International Journal of Engineering Science*, **Vol. 26**, **No. 1**, 1988, pp. 59-75.

[18] I.N. Sneddon. The Use of Integral Transforms. *McGraw-Hill*, 1972.

[19] G.B. Whitham. Linear and Nonlinear Waves. *John Wiley & Sons*, 1974.

[20] E.A. Zabolotskaya. Nonlinear Propagation of Plane and Circular Rayleigh Waves in Isotropic Solids. *Journal of the Acoustical Society of America*, **91(5)**, 1992, pp. 2569-2575.